

UNIVERSITA' VITA-SALUTE SAN RAFFAELE

**CORSO DI DOTTORATO DI RICERCA INTERNAZIONALE
IN MEDICINA MOLECOLARE**

CURRICULUM IN EXPERIMENTAL AND CLINICAL MEDICINE

**MICRO-MECHANICAL FINGERPRINTS OF
BLADDER IN HEALTH AND DISEASE**

DoS: Dr Massimo Alfano



Second Supervisor: Prof Dr Jochen Guck

Tesi di DOTTORATO di RICERCA di Laura Martínez Vidal

matr. 015627

Ciclo di dottorato XXXV

SSD MED/24

Anno Accademico 2021/2022

RELEASE OF PHD THESIS

Il/la sottoscritto/a / <i>I, the undersigned</i>	Laura Martínez Vidal
Matricola / <i>registration number</i>	01567
nat_ a/ <i>born in</i>	Ubeda (Spain)
il/on	08.02.1994

autore della tesi di Dottorato di ricerca dal titolo / *author of the PhD Thesis titled*
Micromechanical fingerprints of bladder in health and disease

AUTORIZZA la Consultazione della tesi / *AUTHORIZES the public release of the thesis*

NON AUTORIZZA la Consultazione della tesi per mesi / *DO NOT AUTHORIZE the public release of the thesis for months*

a partire dalla data di conseguimento del titolo e precisamente / *from the PhD thesis date, specifically*

Dal / *from*/...../..... Al / *to*/...../.....

Poiché / *because:*

l'intera ricerca o parti di essa sono potenzialmente soggette a brevettabilità/ *The whole project or parts of it may be the subject of a patent application;*

ci sono parti di tesi che sono già state sottoposte a un editore o sono in attesa di pubblicazione/ *Parts of the thesis have been or are being submitted to a publisher or are in the press;*

la tesi è finanziata da enti esterni che vantano dei diritti su di esse e sulla loro pubblicazione/ *the thesis project is financed by external bodies that have rights over it and its publication.*

E' fatto divieto di riprodurre, in tutto o in parte, quanto in essa contenuto / *reproduction of the thesis in whole or in part is forbidden*

Data /Date 17.10.2022

Firma /Signature



DECLARATION

This thesis has been:

- composed by myself and has not been used in any previous application for a degree. Throughout the text I use both ‘I’ and ‘We’ interchangeably.
- has been written according to the editing guidelines approved by the University

Permission to use images and other material covered by copyright has been sought and obtained. For the following image/s (Figure 9), it was not possible to obtain permission and is/are therefore included in thesis under the “fair use” exception (Italian legislative Decree no. 68/2003).

All the results presented here were obtained by myself, except for:

- 1) AFM-based measurements – done in collaboration with Dr. Matteo Chighizola and Prof. Alessandro Podestà at the University degli Studi di Milano, Cimina
- 2) Nanoindenter measurements – done in collaboration with Dr. Massimiliano Berardi at Optics 11, Amsterdam, The Netherlands
- 3) Brillouin measurements – done in collaboration with Dr. Claudia Testi and Prof. Giancarlo Ruocco, IIT, Rome, Italy.
- 4) Ultrasound imaging of rat bladders – performed by technician Dr. Elisa Alchera, URI, OSR, Milano, Italy
- 5) Histopathological evaluation was performed together with Dr Roberta Lucianò, URI, OSR, Milano, Italy

Part of the introduction presented in this thesis has been published in the following publication:

- Martinez-Vidal *et al.*, “Causal contributors to tissue stiffness and clinical relevance in urology”, Nature Communications Biology 2021.

All sources of information are acknowledged by means of reference.

Acknowledgements

I would like to thank to everyone who contributed to the development of this work as completion of my PhD thesis.

Firstly, I would like to thank Dr. Massimo Alfano for allowing me joining his team and working on the development of this project. Many thanks to all the present and former members of the Extracellular Microenvironment Unit and URI: Dr Irene Locatelli, Elisa Alchera, Chiara Venegoni and Dr Filippo Pederzoli, especially for supporting me with preclinical models. I also want to thank the pathologist Dr. Roberta Lucianò for teaching me the basis of pathology.

I also would like to express my gratitude to Prof Jochen Guck (MPI, Erlangen) for his assistance as a second assessor.

I am grateful to all members of Phys2BioMed consortium (Horizon 2020 Marie Curie ITN) for great scientific contributions, providing funding and great and inspiring meetings. This complex and yet greatly stimulating interdisciplinary work could not have been realized without the diverse expertise and precious experiences provided by all these scientists, both senior and early stage career researchers. Thanks for interesting discussions, fruitful feedback and fun moments during all congresses and progress meetings.

Special thanks go to Prof Alessandro Podestà and Dr Matteo Chighizola (Università degli Studi di Milano) for assisting during AFM measurements, AFM expertise, providing with the instrument and fruitful discussions and feedback on results and data analysis.

Many thanks to Dr Massimiliano Berardi (Optics11, Amsterdam) for contributing to nanoindenter measurements, discussion and data analysis.

My gratitude also goes to Prof Giancarlo Ruocco and Dr Claudia Testi (IIT, Rome) for teaching me the basis of Brillouin microscopy, assisting with measurements and data analysis and interesting and stimulating discussions.

I am also very grateful to my friends, for cheerful moments together, support and friendship.
To those at home, far but always close.

Finally, I would like to thank my family for their unconditional support, love and trust.

Abstract

Tissue mechanics determines tissue homeostasis, disease development and progression. Bladder strongly relies on its mechanical properties to perform its physiological function, but these are poorly unveiled under normal and pathological conditions. In addition, the bladder is a multilayer organ and it is thus needed to understand tissue mechanics at the microscale, spatially resolving the different bladder layers and their contribution to altered tissue mechanics. This thesis aimed to characterize the micromechanical fingerprints of the healthy bladder wall, and to identify modifications associated with the onset and progression of pathological conditions of actinic cystitis and bladder cancer. To do so I used two indentation-based instruments (an Atomic Force Microscope and a nanoindenter) and compared the micromechanical maps with a comprehensive histological analysis. I found that the healthy bladder is a mechanically inhomogeneous tissue, with a gradient of increasing stiffness (in terms of Young's modulus, YM) from the urothelium to the lamina propria, which gradually decreased when reaching the muscle layer. Stiffening in fibrotic tissues correlated with increased deposition of dense extracellular matrix in the lamina propria. An increase in tissue compliance was observed before the onset and invasion of the tumor. In addition, aiming to establish an experimental approach that would facilitate its application to the clinical environment, I here used Brillouin imaging to investigate healthy and fibrotic bladder, and confront the mechanical information from this non-contact technique to the gold-standard in nanomechanics (indentation-based mechanical tests). While Brillouin imaging reported the same mechanical trend observed by indentation-based mechanical tests when investigating intrinsic mechanical heterogeneities of the bladder wall, a decrease of Brillouin shift in fibrotic bladder was observed contrary to the increased YM measured by indentation-based mechanical tests, thus highlighting different physical phenomena detected by the different techniques and the need to further investigate correlations between both techniques. By providing high resolution micromechanical investigation of each tissue layer of the bladder, I here depicted the intrinsic mechanical heterogeneity of the layers of the healthy bladder as compared with the mechanical properties alterations associated with either actinic cystitis or bladder tumor; and provided an accurate comparison of the gold-standard technique in biomechanics to Brillouin imaging.

Table of Contents

Acronyms and abbreviations	3
List of figures and tables.....	4
1. Introduction – Mechanobiology and mechanomedicine	7
1.1. Mechanobiology relevance	7
1.2. Causal contributors to tissue stiffness and dysregulation in malignant diseases ...	10
1.2.1. Cellular contribution to tissue stiffness	10
1.2.2 ECM deposition, remodeling and topographic reconfiguration of the neoplastic stroma	13
1.2.3 Pre-metastatic niche.....	18
1.2.4 Extracellular vesicles as a novel mediator of tissue stiffness.....	19
1.3. Methods to measure tissue stiffness.....	20
1.3.1. From micro to macro scale: stiffness in clinical practice	20
1.3.2. Microindentation based techniques	22
1.3.3. Brillouin imaging to assess tissue mechanics.....	28
2. Introduction – Bladder.....	33
2.1. Bladder anatomy	33
2.2. Bladder pathologies: actinic cystitis and cancer	35
2.3. Bladder – why its biomechanics?.....	38
3. Aim of the research project	45
4. Materials and Methods	46
4.1. Ultrasound image analysis	46
4.2. Rat model of actinic cystitis.....	47
4.3. Rat model of bladder carcinogenesis (BBN model)	47
4.4. Human specimens	48
4.5. Sample preparation for mechanical analysis.....	48
4.6. Indentation techniques	49
4.6.1. AFM-based indentation measurements	49
4.6.2. Nanoindenter measurements.....	51
4.7. Brillouin microscopy.....	54

4.8.	Histological analysis pairing.....	55
4.9.	Collagen quantification.....	56
4.10.	Statistical methods.....	56
5.	Results	58
5.1.	Chapter 1. Micromechanical fingerprints of bladder in health and disease investigated by microindentation techniques.....	58
5.1.1.	Establishment of a standardized protocol for network-wide mechanical characterization of tissues.....	58
5.1.2.	The healthy bladder wall exhibits regional differences in tissue stiffness	62
5.1.3.	The healthy bladder exhibits temporal evolution in tissue elasticity (stiffening) among aging of the adult animal	65
5.1.4.	Microscale mechanics in the actinic cystitis model and during disease progression	67
5.1.5.	Bladder cancer tissue elasticity.....	72
5.2.	Chapter 2. Towards a more clinical set-up – micromechanical fingerprints of bladder in health and disease by Brillouin imaging. Indentation vs spectroscopy based techniques.....	77
5.2.1.	Brillouin imaging of the healthy bladder wall.....	78
5.2.2.	X-ray irradiation causing actinic cystitis resulted in a decrease of tissue Brillouin shift and lowered the Brillouin shift heterogeneity respect to healthy animals.....	81
6.	Discussion.....	82
7.	References	91

Acronyms and abbreviations

AFM:	atomic force microscopy
BBN:	N-(4-hydroxybutyl)nitrosamine
BCG:	Bacillus Calmette–Guérin
CAFs:	cancer-associated fibroblasts
CIS:	carcinoma in situ
CKD:	chronic kidney disease
DIC:	differential interference contrast
ECM:	extracellular matrix
EMT:	epithelial mesenchymal transition
EVs:	extracellular vesicles
LOX:	lysyl oxidase
LUTS:	lower urinary tract disorders
M':	longitudinal modulus
MIBC:	muscle invasive bladder cancer
MMPs:	matrix metalloproteases
MRE:	magnetic resonance elastography
MRI:	magnetic resonance imaging
NMIBC:	non muscle invasive bladder cancer
PCa:	prostate cancer
RAS:	renin-angiotensin system
RTE:	real time elastography
SNAP:	standardized nanomechanical atomic force microscopy
SWE:	shear wave elastography
SWS:	shear wave speed
TAMs:	tumor-associated macrophages
TGFB1:	transforming growth factor b
TNM:	tumor, node, metastasis
ν_B :	Brillouin shift
VEGF:	vascular endothelial growth factor
YM:	Young's modulus
Γ_B :	full-width at half maximum

List of figures and tables

Figure 1. Schematic overview of the major diseases in which tissue stiffness is altered.	8
Figure 2. Extracellular matrix and tumor microenvironment.....	15
Figure 3. Schematic representation of AFM.....	23
Figure 4. Indentation curve: force vs displacement.	24
Figure 5. Indentation instruments: AFM and Chiaro nanoindenter from Optics11 Life.	27
Figure 6. Brillouin Spectrum.....	29
Figure 7. Brillouin microscope scheme.....	30
Figure 8. Range of Brillouin shift values for different tissues.	31
Figure 9. Comparison between microindentation-based techniques and spectroscopy-based Brillouin microscopy.....	32
Figure 10. Bladder anatomy.....	34
Figure 11. Types and stages of bladder cancer.	37
Figure 12. Ultrasound imaging (US) for physiological volume determination.	46
Figure 13. Methodological approach for bladder stiffness characterization.	49
Figure 14. Surface roughness image of bladder tissue cryosections.....	52
Figure 15. YM's at different indentation depths obtained using the nanoindenter.....	53
Figure 16. Standardized AFM-based measurements of murine bladder tissues.....	61
Figure 17. Healthy bladder wall exhibits regional differences in tissue elasticity.....	63
Figure 18 . Representation of YM data extracted by the two instruments (AFM and nanoindenter) of each single tissue layer	64
Figure 19. Micromechanical map of healthy bladder wall and aging effect on stiffness.....	66
Figure 20. Murine model of actinic cystitis (X ray radiation).....	67
Figure 21. Representative bladder wall stiffness gradient collected with the nanoindenter at month 4.....	68
Figure 22. Micromechanics of murine bladder in a model of actinic cystitis (X ray radiation).	70
Figure 23. Animal not responding to X-ray treatment	71
Figure 24. Murine model of bladder cancer (BBN).	73
Figure 25. Micromechanics of BBN model.	75
Figure 26. Micromechanics of bladder cancer patients.....	76
Figure 27. Brillouin imaging of the healthy bladder wall.....	79

Figure 28. Brillouin imaging of healthy bladder wall at different ages of the adult rat life..	80
Figure 29. Micromechanics of murine bladder in a model of actinic cystitis (X ray radiation).	81
Figure 30. Comparison of Brillouin and YM maps of bladder in a) health and b) fibrosis.	87
Table 1. Commonly used techniques for the mechanical characterization of living tissues....	21
Table 2. Mechanical moduli of human urological tissues.....	40

Part of the introduction presented in section 1 (1.1, 1.2 and 1.3.1) and section 2 (2.3) has been published in the following publication: Martinez-Vidal *et al.*, “Causal contributors to tissue stiffness and clinical relevance in urology”, Nature Communications Biology 2021.

1. Introduction – Mechanobiology and mechanomedicine

1.1. Mechanobiology relevance

The concept that malignancies have an increased consistency and rigidity compared to the surrounding healthy parenchyma is well known in medicine, as palpation of solid masses during physical examination has been the mainstay of tumor diagnosis for centuries. While this example represents an old-fashioned and unaware use of the mechanical properties of tissues for clinical purposes, Mechanics is emerging as a pivotal hallmark for several diseases and pathologies. The extracellular matrix (ECM) is a highly dynamic matrix that, far from being a passive filler, plays important regulatory functions in health and disease. Over the years, it became clear that the ECM influences cell behavior not only by means of its chemical composition, but also by its physical and mechanical properties (Hadden *et al*, 2020; Lu *et al*, 2012). Remarkably, single cancer cells seem to be softer and more deformable than their normal counterpart, probably to favor their movement and progression within the tumor microenvironment and beyond (Alibert *et al*, 2017). Indeed, mechanomedicine is an emerging multidisciplinary field focused on understanding how physical forces and cell and tissue mechanics regulate cell behavior, development, and tissue organization in physiological and pathological conditions (Naruse, 2018). **Mechanomedicine**, at the intersection between biology, medicine, physics, engineering and material science, studies how specific diseases have particular mechanical fingerprints (Janmey & Miller, 2011) (**Figure 1**), as are cancer, fibrosis, aging, cardiovascular diseases and chronic diseases as diabetes. Therefore, quantitative cell and tissue mechanobiology potentially offers the possibility to add a new class of hallmarks of diseases by identifying the changes in their physical properties.

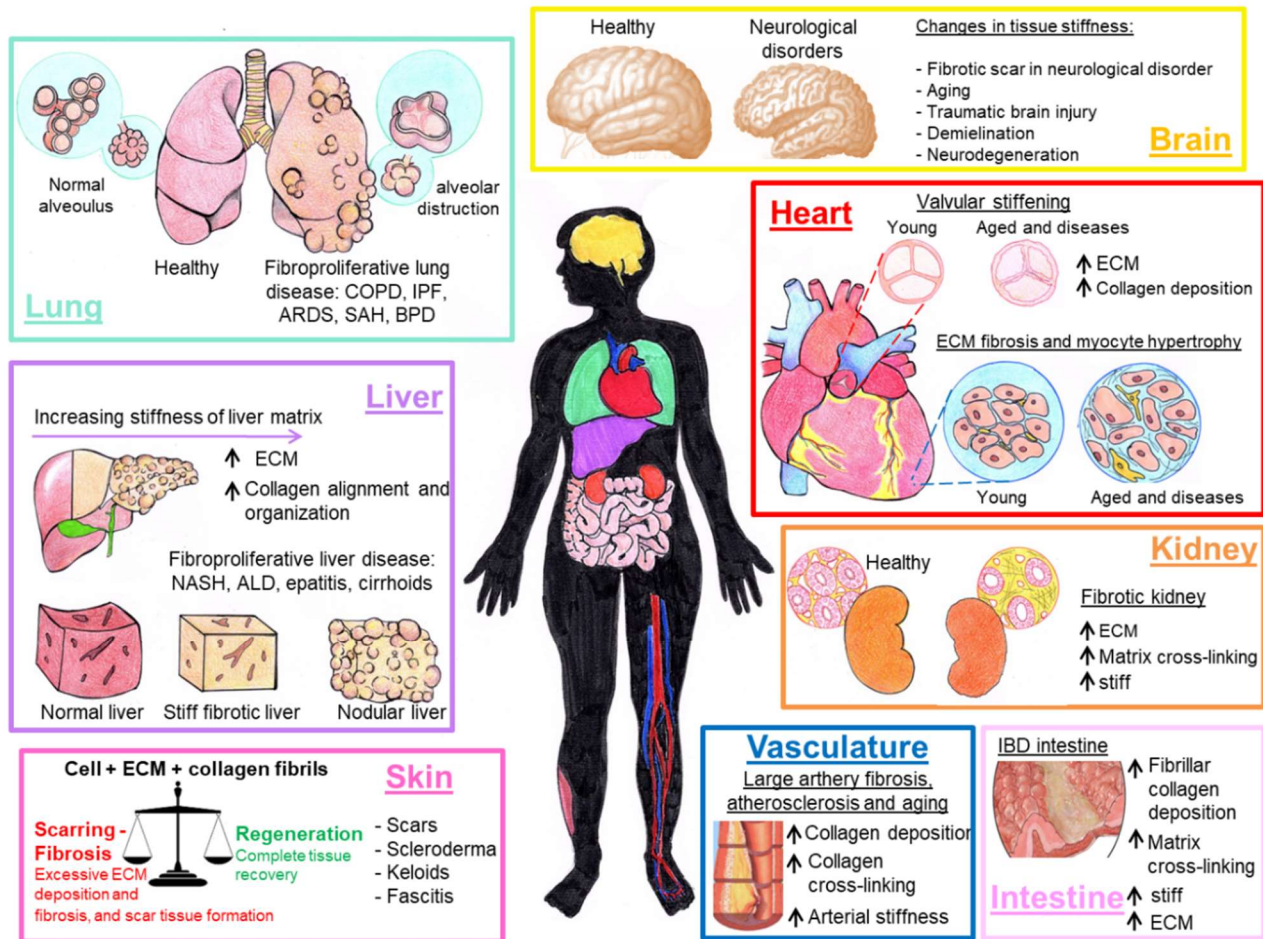


Figure 1. Schematic overview of the major diseases in which tissue stiffness is altered. The hallmark of fibrosis is excessive extracellular matrix (ECM) synthesis and deposition that improve liver matrix remodeling and stiffening. In addition to change the amount of collagen deposited in the ECM, the alignment of the collagen fibrils is also contributing significantly to the alteration of the stiffness of tissues matrix. Increased matrix stiffness is not only a pathological consequence of fibrosis in traditional view, but also recognized as a key driver in pathological progression of fibrosis and cancer. Moreover, it is very likely that significant changes in cell and tissue mechanics contribute to age-related cognitive decline and deficits in memory formation which are accelerated and magnified in neurodegenerative states, such as Alzheimer's and Parkinson's disease.

Abbreviations: COPD, chronic obstructive pulmonary disease; IPF, idiopathic pulmonary fibrosis; ARDS, acute respiratory distress syndrome; SAH, pulmonary subarachnoid haemorrhage; BPD, bronchopulmonary dysplasia; IBD, inflammatory bowel disease; NASH, non-alcoholic steatohepatitis; ALD, alcoholic liver disease (Martinez-Vidal *et al*, 2021).

Several mechanical parameters of tissues are of clinical relevance, among them **stiffness** is considered one of the most important and best described mechanical parameter of biological tissues in research (Darnell *et al*, 2018; Huang *et al*, 2019) (**Box 1**), and thus the main one this dissertation focuses on. Pathological changes in tissue stiffness can be traced to altered amounts and/or function of its two fundamental constituents: cells (number and/or phenotype) and ECM (deposition and/or degradation). Knowledge of abnormal tissue states and the mechanical changes that occur in disease are important not only for diagnosis, but also for tissue engineering and recapitulation of such diseases in *in vitro* models. These approaches are expected to generate novel therapeutic targets that allow restoration of healthy tissue mechanics and mechanotransduction responses (Guimarães *et al*, 2020; Mancini & Sonis, 2014). Therefore, it is not surprising that mechano-based therapies that target increased tissue stiffness and associated cellular responses in cancer and fibrosis-mediated diseases are emerging clinically (Tschumperlin & Lagares, 2020). For instance, targeting of the renin-angiotensin system (RAS) by anti-RAS drugs has been shown to increase the anti-angiogenic effects of bevacizumab in liver metastases of colorectal cancer by reducing the ECM deposition and remodeling operated by metastasis-associated fibroblasts (Shen *et al*, 2020).

Box 1. Mechanics of materials: basic concepts and definitions

- **Stiffness** (rigidity). Most used mechanical parameter for characterization of living tissues. It gives the resistance to undergoing (elastic) deformation in response to the application of a force, the property of being inflexible and hard to distort (Murphy *et al*, 2013). A stiff material, by definition, has a high elastic modulus (Young's modulus), i.e., a considerable stress is needed for a minor deformation. The stiffness of a material is represented by the ratio between stress and strain, being the Young's modulus the constant of proportionality between stress and strain, and one of the most common measures of intrinsic stiffness of the material. Units of Young's modulus are force unit per area, being Pascal (Pa) the most widely used.
- **Viscoelasticity**: time-dependent anelastic behavior of materials. This means that the temporary response to a stimulus is delayed, and there is a loss of energy inside the material (Friedrich-Rust *et al*, 2007). Viscoelastic behavior normally occurs at different time scales (relaxation times) in the same material. Viscoelasticity can be reported by Shear storage modulus (G') and shear loss modulus (G'').

1.2. Causal contributors to tissue stiffness and dysregulation in malignant diseases

The ECM is a general term to indicate the tissue non-cellular components that form an essential scaffold for cellular constituents. The structure of ECM differs in composition between tissues but is essentially made up of collagen fibers, proteoglycans and multiadhesive matrix proteins that are secreted by different cell types (Frantz *et al*, 2010). The ECM is a dynamic component of tissues, where there is a constant feedback loop between the ECM and the cells within it: while cells produce and remodel the different ECM components, biochemical and biomechanical features of the ECM direct cell phenotypes. This equilibrium of the ECM turnover and crosstalk with the resident cells is crucial for tissues development and homeostasis.

1.2.1. Cellular contribution to tissue stiffness

- The cellular determinants of ECM remodeling

Several cell types shape the ECM structure and composition. Among them, **fibroblasts** are the main producers of ECM components, including structural proteins (e.g., fibrillar and non-fibrillar collagens, elastin), adhesive proteins (e.g., laminin and fibronectin) and proteoglycans (Frantz *et al*, 2010). Moreover, they play a pivotal role in overseeing ECM quality and quantity, as they produce different enzymes involved in the maturation and catabolism of collagens, like lysyl oxidase (LOX), which mediates collagen fibers crosslinking (thereby strengthening the ECM), and matrix degrading enzymes, such as metalloproteinases (Alfano *et al*, 2016). Under physiological conditions, fibroblasts are generally quiescent, but they can be activated in response to a plethora of different mechanical and biochemical stimuli (Nikos K. *et al*, 2019; DeLeon-Pennell *et al*, 2020). Chronic and deregulated fibroblast activation is at the basis of the altered ECM metabolism characterizing several diseases, including cancer. Chronically activated cancer-associated fibroblasts (CAFs) represent the main source of ECM production and remodeling within the tumor microenvironment (**Figure 2, section 1**, page 15) where they promote neoangiogenesis and epithelial to mesenchymal transformation (EMT) (Goulet *et al*, 2019; Kalluri, 2016; Paolillo & Schinelli, 2019; Liu *et al*, 2019).

In addition to fibroblasts, **macrophages** express genes involved in ECM modulation, like transforming growth factor β induced protein (TGFBI) and matrix metalloproteinase 9, which ultimately lead to the release of associated proteins and factors in the stromal environment (Etich *et al*, 2019; Lim *et al*, 2018; Murray & Wynn, 2011). For instance, a subpopulation of macrophages expressing the lymphatic vessel endothelial hyaluronan receptor 1 proteins has been shown to regulate ECM composition in the arterial wall and in the lung (Lim *et al*, 2018). Moreover, macrophages can modulate fibroblast-mediated production of ECM, which contributes in turn to the regulation of fibrosis (Wynn, 2010). It is interesting to note that the mechanical status of the ECM can control the efficacy of TGF-beta activation by reparative fibroblastic cells and the release of traction-mediated latent TGF- β 1 stored in the ECM (Hinz, 2015). Macrophages play an important role also in the ECM remodeling in the tumor microenvironment. Tumor-associated macrophages (**TAMs**) may contribute to tumor progression by producing pro-inflammatory cytokines that will ultimately lead to apoptosis suppression and proliferation activation (Valilou *et al*, 2018). In addition, TAMs shape tumor ECM by secreting MMPs and matrix-associated proteins, and they organize collagen I into fibrillar bundles, as shown in a mouse model of colorectal cancer (Paolillo & Schinelli, 2019; Emon *et al*, 2018).

- **Cell stiffness, density and traction**

Not only do cells contribute to tissue stiffness by secretion of proteins and growth factors, but there is an important cellular contribution to the rigidity of their surrounding environment by means of cell stiffness, density and contractility. As previously mentioned, **cancer cells are softer** than their non-transformed counterparts (Ramos *et al*, 2014). In vitro tests have shown that increasing ECM stiffness increases both tumor cell proliferation and invasiveness (Alonso-Nocelo *et al*, 2017), although the softening of cancer cell lines was not associated with the aggressiveness of several solid neoplasia (Ramos *et al*, 2014; Faria *et al*, 2008; Lekka *et al*, 2012; Zemła *et al*, 2018). Of particular note is the fact that the elasticity of tumor cells now represents one of the markers for the recognition and isolation of circulating tumor cells (Osmulski *et al*, 2015).

It has been reported that mechanical forces played by the neoplastic cells or cancer associated fibroblasts in the in situ colon carcinoma are sufficient to remodel the basal membrane to allow for tissue invasion (Glentis *et al*, 2017). On the other hand, it has been reported in vitro that focal adhesion points of the cell with the substrate, resulting in the formation of stress fibers in the cell, mediate cell traction. When **cell density** is high enough to keep cells close to each other, this cell traction increases the local stiffness, an event that is particularly relevant when high density of tumor fibroblasts or mesenchymal stem cells are seeded on a soft substrate (Venugopal *et al*, 2018).

Tumor progression is mediated by the ability of tumor cells to invade the tissue layers to reach blood vessels and spread in secondary organs. Invasion by in situ carcinoma requires tumor cells to pass the basal membrane to reach the lamina propria located below the epithelial layer. Besides the MMP-mediated remodeling of the ECM, including the ECM composing the basal membrane (Linder *et al*, 2011), physical remodeling of the basal membrane has also been reported to be induced independently of MMPs. The basal membrane can be remodeled by a large protrusion of cancer cells that physically tears and then displaces the basal membrane (Kelley *et al*, 2019). On the other hand, cancer-associated fibroblasts have recently been reported to modify the ECM of the basal membrane independently of MMPs (Glentis *et al*, 2017), as that in the presence of MMP inhibitors, the physical contact between CAFs and the basal membrane was reported to sustain invasion (Glentis *et al*, 2017). By **applying mechanical forces** on the basal membrane, CAFs reduced the density of fibers of intermediate stiffness, creating patches of soft, inhomogeneous material sparsely interspersed with thick fibers. By exerting **contractile forces** CAFs can soften the basal membrane, thus adding a second mechanism that is proteolysis-independent to the tumor progression of in situ carcinoma (Glentis *et al*, 2017). Because this event has not been reported for fibroblasts isolated from the juxta-tumoral tissue, it would be important to unveil the tumor-derived factors (i.e., extracellular vesicles) that induce transformation of fibroblast to CAFs and that enhance their mechanical forces.

Increased local stiffness by mechanical forces due to cell traction, proteolysis-independent remodeling of the ECM adds another piece of information regarding tumor progression and why MMP inhibitors have failed in clinical trials (Herszényi *et al*, 2012).

1.2.2 ECM deposition, remodeling and topographic reconfiguration of the neoplastic stroma

The ECM plays a crucial role in the classically defined hallmarks of cancer, from tumor onset, progression and metastasis (Mohan *et al*, 2020; Cui *et al*, 2018), as its biochemical and biophysical characteristics undergo constant remodeling (Stewart *et al*, 2008; Eble & Niland, 2019). During cancer and fibrotic diseases, dysregulated matrix synthesis and remodeling takes place. Cell components of the tumor microenvironment (cancer cells, CAFs and TAMs) modulate ECM through different activities.

- ECM remodeling proteins

Stromal cells secrete a vast variety of ECM remodeling proteins, one very important example is LOX. **LOX** is an extracellular enzyme that catalyzes the crosslinking of collagen and elastin through oxidative deamination of lysine residues (Wang *et al*, 2017). Reduced LOX activity in humans has been described in two X-linked recessively inherited disorders (e.g. Menkes disease and occipital horn syndrome (Royce *et al*, 1980; Kaler *et al*, 1994)), while elevated LOX levels are clinically associated with increased systemic/organ fibrosis (Murawaki *et al*, 1991; Kagan, 2000). In cancer, LOX plays an important role within the tumor microenvironment since early stages of tumorigenesis (Li *et al*, 2018) (**Figure 2, section 2**, page 15). By upregulation of LOX, CAFs increase collagen crosslinking, altering ECM topology, directionality and mechanical properties, ultimately leading to ECM stiffening (Wei *et al*, 2017), which promotes metastasis and infiltration of tumor-supporting immune cells (Emon *et al*, 2018). A positive correlation between LOX expression and cell migration, invasion, EMT and metastasis has been observed (Emon *et al*, 2018; Mohan *et al*, 2020). Furthermore, LOX overexpression is an indicator of poor patient prognosis in several tumors (Wei *et al*, 2017; Cui *et al*, 2018; Nilsson *et al*, 2015; Stewart *et al*, 2008; Liu *et al*, 2018). Thus, there is potential application of LOX inhibitors in clinical trials to facilitate permeability of drugs and infiltration by tumor-killing immune cells (Ye *et al*, 2020), taking into consideration that LOX inhibitors can only reduce the further crosslinking of collagen fibers, but not restore the already cross-linked ECM.

Matrix metalloproteases (MMPs) are secreted by tumor cells, CAFs, TAMs and other stromal components (**Figure 2, section 3**, page 15). MMPs allow for ECM degradation, necessary for cancer cell invasion and metastasis (Paolillo & Schinelli, 2019). These proteases are implicated in almost all steps of metastasis, and an elevated level of MMPs is directly correlated with poor prognosis and high risk of relapse (Cho *et al*, 2003; Herszényi *et al*, 2012). Furthermore, MMPs release ECM-attached soluble growth factors and cytokines (Gonzalez-Avila *et al*, 2019), including vascular endothelial growth factor (VEGF), which will ultimately promote neoangiogenesis, contributing to tumor growth and potential metastatic spreading (Apte *et al*, 2019; Pupa *et al*, 2002). For example, MMP-9 and MMP-2 cleave TGF- β , promoting tumor invasion and angiogenesis (Hines, 2011; McCawley & Matrisian, 2001; Yu & Stamenkovic, 2000; Lambert *et al*, 2003; Masson *et al*, 2005). Werb and colleagues pointed out the role of proteolysis as a mechanism of altering extracellular signaling (Egeblad & Werb, 2002). For instance, they demonstrate that MMP-2 is a strong contributor to prostate carcinogenesis and that MMP-2 deficiency results in a reduction of immature blood vessel number (Littlepage *et al*, 2010). Likewise, they found that MMP-9 has both pro- and anti-tumorigenic effects, depending on the environment and stage in cancer progression (Egeblad & Werb, 2002; Littlepage *et al*, 2010). These discoveries fostered new paradigms about the role of MMPs, the microenvironment, inflammation in development and cancer and changed the way in which biomedical researchers view proteolysis, from ECM destruction to extracellular signal transduction (Kessenbrock *et al*, 2010). After several clinical trials targeting MMP inhibition led to disappointing results about 20 years ago, probably due to an insufficient knowledge of the MMP interactome and of the pharmacology of the tested compounds, novel studies are ongoing testing MMPs to activate prodrugs or facilitate drug delivery (Vartak & Gemeinhart, 2007; Fields, 2019).

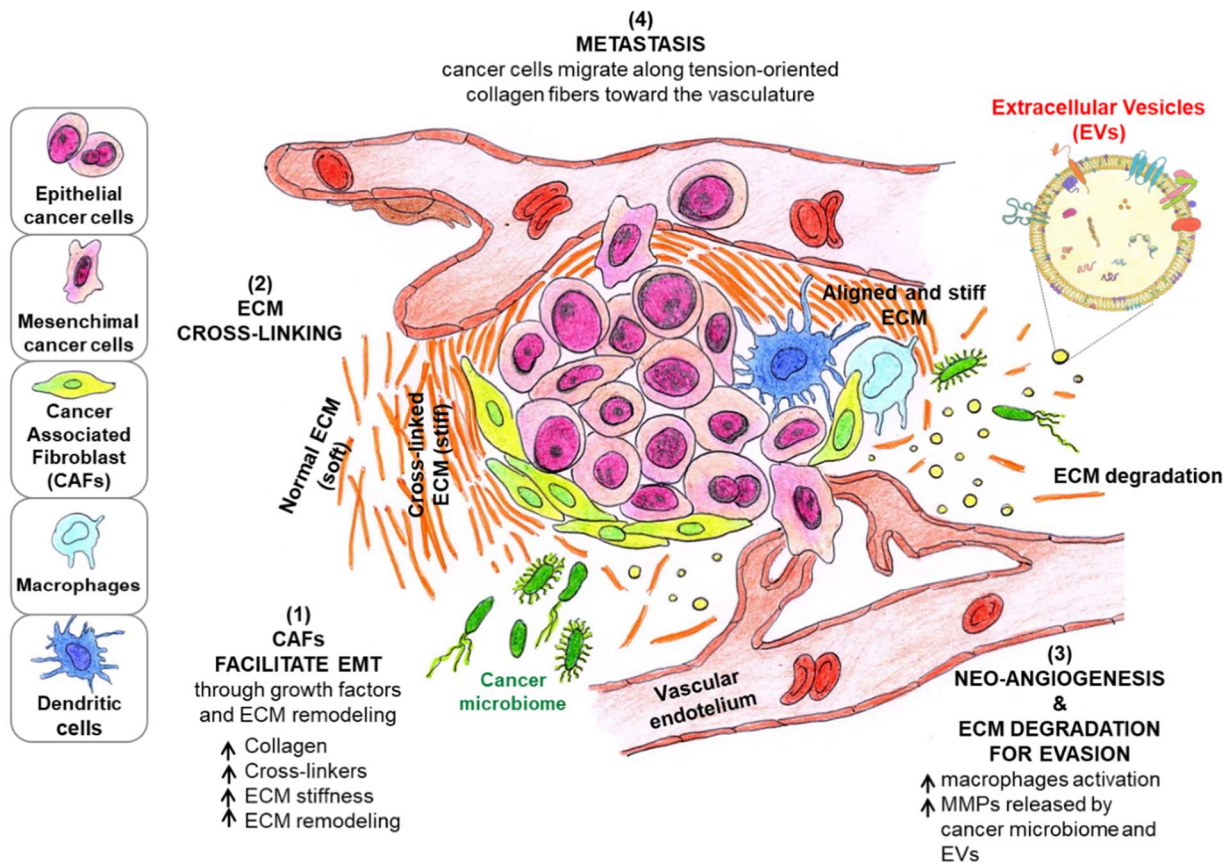


Figure 2. Extracellular matrix and tumor microenvironment. Cell components of the TME (cancer cells, CAFs and TAMs) modulate ECM through different activities. One of these modulations is the topographic reconfiguration of the stroma: ECM anisotropy. By upregulation of LOX, CAFs increase collagen crosslinking, altering ECM topology as well as directionality and mechanical properties. Increased collagen cross-linking induces stiffer microenvironment, which modulates macrophages activation (1). Cancer-associated fibroblasts (CAFs) represent the main source of ECM production and remodeling within the TME where they promote neoangiogenesis and EMT (2). Tumor-associated macrophages (TAMs), microbiome and extracellular vesicles (EVs) reshape ECM by secreting MMPs and matrix-associated proteins. MMPs release ECM-attached soluble growth factors and cytokines, which promote neoangiogenesis, contributing to tumor growth and potential metastatic spreading (3). Finally, cancer cells migrate along tension-oriented collagen fibers towards the vessels. The alignment of ECM fibers yields a rigid structure that contributes to tumor stiffness and acts as sort of highway for cancer cell migration, leading metastasis (4). Abbreviations: ECM: ExtraCellular Matrix; TME: Tumor MicroEnvironment; CAFs: Cancer Associated Fibroblasts; EMT: Epithelial-Mesenchymal Transition; TAMs: Tumor Associated Macrophage; LOX: Lysyl Oxidase enzyme; MMPs: Matrix MetalloProteinases; EVs: Extracellular Vesicles (Martinez-Vidal *et al*, 2021).

- **ECM stiffness and topographic modification**

Topographic reconfiguration of the stroma is an additional ECM modification that happens during disease establishment and progression. The alignment of ECM fibers (i.e., ECM **anisotropy** (**Box 2**)) yields a rigid structure that contributes to tumor stiffness (Shen *et al*, 2020; Liu *et al*, 2019). One example is the radial alignment of thick collagen bundles seen at the invasive front in breast cancer (Etich *et al*, 2019). Linearization of collagen fibers has been associated with an increase of tissue stiffness, and both properties are related to the presence of neoplastic tissue and poor prognosis, while non-neoplastic tissue exhibits a more random orientation of fibers and lower tissue stiffness (Liu *et al*, 2019; Lim *et al*, 2018; Murray & Wynn, 2011; Thomas A. Wynn, 2010). The anisotropic organization of biological ECM is not a clinically applied parameter, but several studies have revealed that the significant increase of alignment of collagen fibers (i.e., increase of its anisotropy) has an impact on gene expression, differentiation, proliferation and migration of cancer cells, with aligned fibers acting as sort of highway for cancer cell migration (Lim *et al*, 2018; Emon *et al*, 2018) (**Figure 2, section 4**, page 15). Interestingly, metastatic breast tumors are characterized by bundles of aligned collagen fibers oriented perpendicular to the tumor interface, highlighting the effect of ECM anisotropy as a strong regulator of directed cell migration (Wang *et al*, 2017; Kaler *et al*, 1994). Another interesting example of the effect of tissue alignment in cancer invasion regards the pattern of invasion: invading mesenchymal melanoma and sarcoma cells, which are known to typically invade as single cells, can invade collectively when three-dimensional tissue density is high and the activity of MMPs contribute to tissue alignment (Haeger *et al*, 2014; Wolf *et al*, 2007). Moreover, Friedl and coworkers demonstrated in vivo that invading cancer cells preferentially orient along aligned collagen fibers and bundles, vascular structures and nerves (Ilina *et al*, 2018; Weigelin *et al*, 2012; Wolf *et al*, 2013), while mesenchymal tumour cells move collectively along these confined trails despite their labile cell–cell junctions (Haeger *et al*, 2014, 2020). Interestingly, anisotropy remodeling of ECM would probably lead to the generation of stiffness gradients, which leads us to introduce the concept of durotaxis. Durotaxis has recently been proposed as a mechanism driving directed migration, which is the process by which cells follow gradients of extracellular mechanical stiffness, from soft to stiff substrate (Shellard & Mayor, 2021). The concept of durotaxis has also been reported for several cancer cell lines, showing that cells displayed the strongest durotactic migratory response when migrating on the softest regions of stiffness gradients (2–7 kPa), with decreased responsiveness on stiff regions of gradients (DuChez *et al*, 2019). On the other side,

a stiffer substrate promotes the proliferative capacity of cells and enhances tumor growth (Romani *et al*, 2021). Durotaxis might have an important role in facilitating the forward movement of the invasion front, where tumor cells from the tumor niche move forward following the avenues of the stiffer ECM created by the surrounding CAFs.

Box 2. Main concepts on ECM remodeling contributing to stiffness

Desmoplasia: increased matrix production with remodeling of connective tissue structures adjacent to the tumor (Taljanovic *et al*, 2017).

Cancer-associated fibroblasts (CAFs): the main source of ECM production and remodeling within the tumor microenvironment, promoting neoangiogenesis and epithelial to mesenchymal transformation (EMT) (Liu *et al*, 2019).

Lysyl oxidase (LOX): enzyme that converts lysine into high reactive aldehydes forming crosslinking between fibers of collagens and elastin(Johnston & Lopez, 2018).

Metalloproteases (MMPs): extracellular enzymes that degrade the ECM components (Jabłońska-Trypuć *et al*, 2016).

Tumor-associated macrophages (TAMs): polarized macrophages that suppress antitumor immunity and promote tumor progression (Pathria *et al*, 2019).

Anisotropy: reorganization of the topography of the ECM toward linearization of the alignment of ECM fibers (Park *et al*).

Altogether, the increase in ECM deposition and in its alignment facilitates cell proliferation, migration and tumor cell invasion. As a result, neoplastic tissues are generally stiffer than the normal tissue, due to the ECM alterations mainly induced by CAFs (Paolillo & Schinelli, 2019; Royce *et al*, 1980). For example, gradual stiffening of tumor stroma along with increasing tumor aggressiveness has been reported for several cancers, including colorectal and breast malignancies (Zhang & Reinhart-King, 2020). Another example of the association between ECM remodeling and disease is the fibrotic change in the prostate that results in an increase in the stiffness of the tissue, as a consequence of inflammatory processes (Mohan *et al*, 2020; Zhu *et al*, 2019; Kwon *et al*, 2019).

Stromal cells contribute to ECM and tissue stiffness and, at the same time, a high stiffness matrix has been suggested to be important for maintaining an invasive phenotype (Stewart *et al*, 2008), as well as favoring EMT (Noguchi *et al*, 2018) facilitating the transition from epithelial and non-motile phenotype to a mesenchymal and motile (invasive) phenotype providing cellular motility (Mierke, 2018). In the case of breast cancer, it has been shown that denser breast tissue is a risk factor for breast cancer development (Barcus *et al*, 2017; Northey *et al*, 2020). Such increased breast density is a result of increased connective tissue deposition and ECM components, mostly collagen (Barcus *et al*, 2017), which is not only increased in deposition but also more oriented, stiffer and correlated with higher epithelial cell density (Northey *et al*, 2020). Collagen alignment has also been seen to have potential as a prognostic marker for invasive breast carcinoma patients (Conklin *et al*, 2018; Esbona *et al*, 2018). This stiffer stroma increases breast cancer risk by inducing the oncogene ZNF21771. Furthermore, in breast cancer *in vivo* initiation of metastasis is promoted by a stiffer microenvironment induced by increased collagen crosslinking (Levental *et al*, 2009). Interestingly, it has been shown that collagen fibril density, which is a surrogate for tissue stiffness, modulates macrophage activation and cellular functions during tissue repair (Liu *et al*, 2018), and that cytokine secretion is enhanced with an increase of fibril density. In a different study, it was stated that immune cells such as macrophages are sensitive to the surrounding rigidity: lesions of higher stiffness from human breast cancer biopsies were populated with a higher number of macrophages, resulting in an increased cellular TGF- β signaling (Goulet *et al*, 2019).

1.2.3 Pre-metastatic niche

Tumor cells, together with CAFs, hematopoietic progenitor cells and TAMs prepare a suitable “soil” for incoming metastasis in distant tissues and organs. This abnormal, tumor growth-favoring microenvironment is the so-called pre-metastatic niche (Høye & Ertler, 2016). The ECM is closely related to tumor metastasis, and the tumor-environmental transition from softer tissue to stiff fibrous tissue goes hand in hand with metastasis progression. First, in the primary tumor site, primary tumor cells secrete soluble growth factors (as VEGF- α , TGF β and tumor necrosis factor α) and extracellular vesicles (see section 1.2.4) containing miRNAs, integrins, growth factor receptors and chemoattractants (Sergei Kusmartsev, 2006; Whiteside, 2017). These soluble growth

factors and extracellular vesicles arrive at the target tissue and prime it, as a first step of preparing a suitable microenvironment for metastasis formation (Guo *et al*, 2019). As a second step, bone marrow derived cells, CAFs, myofibroblasts and TAMs colonize the niche, resulting in an altered expression of collagens and MMPs. Finally, tumor cells that underwent EMT arrive at the target tissue as tumor circulating cells, which they colonize to form a second tumor (Karamanos *et al*, 2019; Yoshida *et al*, 2019; Lu & Kang, 2007). Collagen stabilizing enzymes are overexpressed during metastasis and hypoxic conditions, where they play a critical role hydroxylating collagen in response to hypoxia-inducible factors (Karamanos *et al*, 2019). One example of the priming of the tissue are breast cancer cells that metastasize to lung, where they secrete collagen and change the organization of ECM fibers (Alfano *et al*, 2016; Liu *et al*, 2019). Colorectal liver metastasis presents high collagen turnover together with collagen isoforms changes, contributing to the generation of a favorable tumor microenvironment (Masci *et al*, 2016; Whitehead *et al*, 2015). On the other hand, metastatic melanoma cells can re-organize the collagen matrix depending on their invasive potential: the higher the invasive potential, the greater the traction force of the cell on the ECM, resulting in a more linearized ECM where cell migration is enhanced (Weis & Chersesh, 2011).

1.2.4 Extracellular vesicles as a novel mediator of tissue stiffness

Tumor-secreted factors and extracellular vesicles (EVs) are secreted by the primary tumor which induce pre-metastatic niche formation, by remodeling the ECM, vasculature and effects on the immune system (Peinado *et al*, 2017). EVs have been recognized as key signaling mediators in regulating the tumor microenvironment by transferring several bioactive molecules involved in reprogramming and microenvironment remodeling, tumor angiogenesis, and metastasis (Peinado *et al*, 2011, 2012; Hood *et al*, 2011). They have emerged as pivotal mediators of intercellular communications in local and distant microenvironments under patho/physiological conditions. EVs contain bioactive materials such as proteins, nucleic acids, lipids and several MMPs (Raposo & Stoorvogel, 2013). These metalloproteinases are involved in altering EVs production either through the shedding of transmembrane proteins or by directly contributing to ECM remodeling. Although the nucleic acid and proteomic contents of EVs have been studied for their roles in the development of various diseases and tissue repair, information regarding the secretion and biological activities of EV-associated matrix-remodeling enzymes and their regulators is only just beginning to emerge.

1.3. Methods to measure tissue stiffness

1.3.1. From micro to macro scale: stiffness in clinical practice

With the development of new techniques that allow us to understand the mechanical properties and alterations of cells and ECM during disease, a new emerging hallmark arises: changes in mechanics of cells and tissues as a hallmark of disease onset and progression (Thiery & Sleeman, 2006; Steeg, 2006; Kalluri, 2010). Nevertheless, assessing mechanical characteristics of tissues still remains challenging. Several techniques assessing mechanical properties of tissues and cells have been developed at different scales, aiming to address these challenges. **Table 1** summarizes commonly used techniques for the mechanical characterization of biological specimens. Different available techniques to study tissue and organ stiffness vary in the resolution of the appreciable modifications: atomic force microscopy (AFM) based measurements provide the finest resolution in the micro-/nano- scale, but they are limited to *ex vivo* specimens. On the other hand, imaging-based techniques, like magnetic resonance elastography (MRE), shear wave elastography (SWE), and real time elastography (RTE), can only provide macroscale maps of tissue stiffness, thus providing an overview of the organ stiffness. How to complement different techniques with different resolutions is still a matter of research, and future studies are needed to define the framework to integrate micro- and macro-scale stiffness data.

Nanotechnology allows the manipulation and inspection of matter at the nanometer scale, and provides a new perspective to physicochemical properties of matter, including biological systems. Advances in nanotechnology, such as the emergence of AFM (Parot *et al*, 2007), magnetic and optical tweezers, super-resolution photonic microscopy, use of micro-patterns and micropillars, and microfluidics (Kollmannsberger & Fabry, 2007) have allowed probing the mechanical properties of cells and tissues showing that specific diseases have particular mechanical fingerprints. For example, cancerous cells have shown to be significantly softer than normal cells (Lekka *et al*, 2012; Prabhune *et al*, 2012) while human breast invasion and aggression correlates with extracellular matrix stiffness (Provenzano *et al*, 2008; Paszek *et al*, 2005; Acerbi *et al*, 2015). Quantitative cell and tissue mechanobiology offers therefore the possibility to add to the growing list of molecular markers a new class of markers based on physical properties. Among the several approaches that have been developed, AFM presents several advantages, such as the possibility of combining topographical and mechanical imaging with high spatial and force resolution, as well as

adding specific mapping abilities using functionalized probes (Radmacher, 2007; Alcaraz *et al*, 2003; Puricelli *et al*, 2015; Mostowy *et al*, 2011).

Table 1. Commonly used techniques for the mechanical characterization of living tissues					
Technique	Concept	Modulus	Sample	Scale	Ref
Atomic Force Microscopy (AFM)	Atomic-level indentation (nanoindentation) or shear rheology (atomic force microscopy-based rheology)	E (indentation),	Ex vivo tissue	Microscale, nanoscale	(Crichton <i>et al</i> , 2011; Cross <i>et al</i> , 2007; Uriarte <i>et al</i> , 2016)
Shear rheometry	Application of small-amplitude oscillatory shear stress and quantification of the resulting strain	G', G'' (shear, viscoelastic)	Ex vivo tissue	Macroscale	(Schachar <i>et al</i> , 2011; Yoo <i>et al</i> , 2011)
Compressive deformation	Classic stress-strain analysis. Uniaxial stress is applied to compress the material and a relationship is established with the resulting strain	E (elastic)	Ex vivo tissue	Macroscale	(Barak & Black, 2018)
Magnetic Resonance Elastography (MRE)	Magnetic resonance visualization of tissue deformation resulting from the introduction of shear waves into the tissue derived from external vibrations non-invasive, promising for clinical applications	G', G'' (shear, viscoelastic)	In vivo tissue,	Macroscale	(Shi <i>et al</i> , 2015; Murphy <i>et al</i> , 2013)
Real Time Elastography (RTE)	Sonography-based non-invasive method. It uses conventional ultrasound probes to compare echo signals before and after slight compression	E (elastic)	In vivo tissue	Macroscale	(Friedrich-Rust <i>et al</i> , 2007)
Shear Wave Elastography (SWE)	External acoustic force pulses are used to generate shear waves which propagate perpendicular to the ultrasound beam, causing transient displacements that result in an image of the distribution of the shear-wave velocities	Shear wave speed (SWS), that can be converted into E and G	In vivo tissue	Macroscale	(Taljanovic <i>et al</i> , 2017)

The following chapter describes the principles and reviews biological applications on the literature of the two microscale techniques used during my PhD project: AFM-based indenters and Brillouin imaging.

1.3.2. Microindentation based techniques

AFM is becoming a prevalent tool in cell biology and biomedical studies, especially those focusing on the mechanical properties of cells and tissues (Gavara, 2016). AFM was invented in 1986, and it belongs to the branch of scanning probe microscopy techniques. AFM can provide nanometer-resolution maps for cell topography, stiffness, viscoelasticity and cell adhesion, and it is possible to overlay such information with optical images of the probed material (Gavara, 2016). This technique gathers the information by "feeling" or "touching" the surface of the sample with a mechanical probe. The AFM probes consist in an interacting tip attached to an elastic lever (cantilever) that bends under the interaction forces between the probe and the surface of the sample (**Figure 3**). Bending of the cantilever (typically referred to as deflection) is monitored by shining a laser light onto the gold-coated backside of the cantilever, and measuring the position of its reflected light using a four quadrant photodiode that detects laser displacement. This deflection is then translated into a difference of photovoltage detected by each quadrant of the photodiode, which can discern whether the bending is caused by attractive or repulsive forces between the tip and the sample. A set of three piezoelectric positioners allows nanometer-scale movement of the tip with respect to the sample (in x, y and z).

AFM can be used in different modes to characterize different parameters of biological samples. I here used AFM in force spectroscopy mode for the mechanical characterization of biological tissues, i.e., bladder tissues. Therefore, this chapter will focus on this specific AFM application.

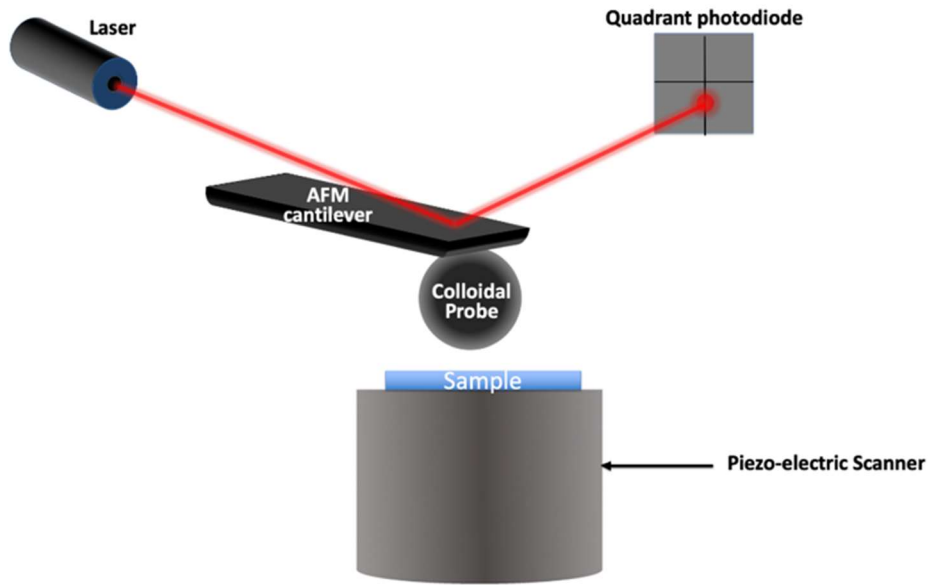


Figure 3. Schematic representation of AFM. An AFM cantilever functionalized with a colloidal probe is used to indent the sample, cantilever deflection is detected by means of a quadrant photodiode.

AFM-based mechanical characterization is based on using the AFM's tip to apply force on the sample, while tracking how the sample deforms in response to such force. By measuring the deflection of the cantilever through the extent of laser dislocation, the upward force acting on the tip can be calculated, the sample deformation can be measured and then mechanical properties of the sample can be determined. In this mode, AFM uses the tip of the cantilever as an indenter to push into the sample. The resulting forces (F) on the cantilever tip can be calculated in the following way:

$$F = k_c d$$

where k_c is the stiffness (spring constant) of the cantilever, which behaves as a hookean spring; and d is the cantilever deflection that AFM can measure with high precision. During the measurement, the vertical displacement of the cantilever and its deflection are recorded simultaneously, and then converted to force-versus-displacement curve, called force curve. In a typical force (indentation) curve or ramp, we identify two phases: approaching and retracting phase (**Figure 4**). During the approach, the cantilever is moved towards the sample, which in the curve appears as a flat line as

the tip is still too far away from the sample and does not experience any interaction force (A). When the tip reaches the surface of the sample and starts interacting the sample surface, is the so called the contact point (B), from which the load starts increasing and the tip moves deeper into the sample until a maximum force is reached (C). During the retraction/withdraw phase the piezo is retracted (D) until the tip gets out of contact (E).

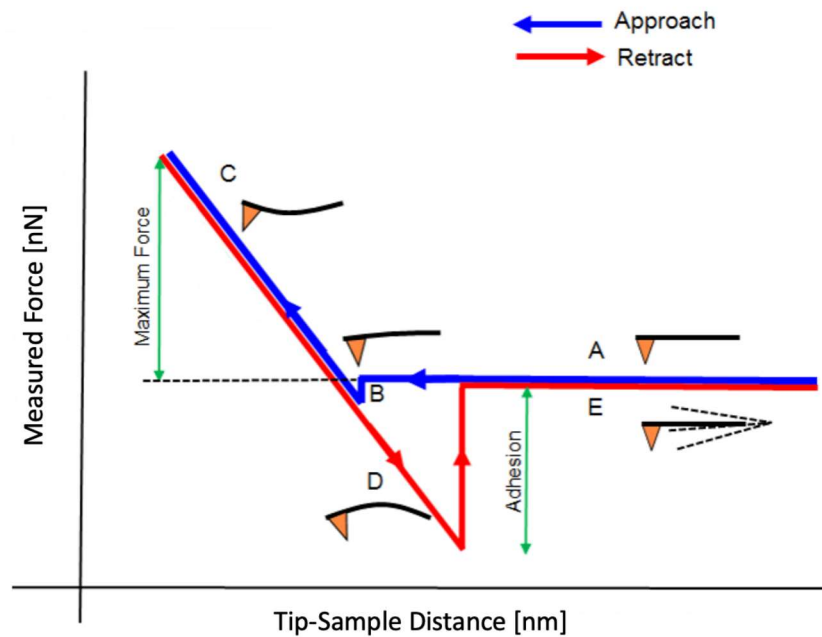


Figure 4. Indentation curve: force vs displacement. Approaching phase of the cantilever to the sample is represented in blue, retracting phase is represented in red.

Nanomechanical analysis of soft biological samples (as cells, tissues or ECM) with AFM requires special attention to the right experimental conditions, like stiffness of the cantilever, probe shape (spherical, pyramidal) and size, right choice of contact mechanical model and data analysis. Experimental details are provided in the Materials and Methods section 4.6.1. Ultimately, the Young's modulus (YM), which is the constant of proportionality between stress and strain and indicator of the elasticity/stiffness of the measured material, is extracted from the force curves.

Many diseases are accompanied by mechanical alteration of tissues and cells and thus, mechanics of disease in several organs and pathologies has been assessed by AFM (Kiio & Park, 2020), the current gold standard in the field of mechanobiology. Breast cancer has been studied at the cellular level but also using tissue sections and bulk tissue coming from biopsies (Wu *et al.*, 2018; Plodinec *et al.*, 2012; Ansardamavandi *et al.*, 2016; Lekka *et al.*, 2012). Nanomechanics of cartilage has been evaluated (Han & Grodzinsky, 2011), as well as identification of stiffness of the different dermal structures of skin (Kao *et al.*, 2016), and scarring effect on the nanomechanics of the upper dermis (Grant *et al.*, 2012). Aging effect on stiffness has also been studied in skin (Grant *et al.*, 2012; Sherratt, 2009), cartilage (Han & Grodzinsky, 2011) and aorta (Akhtar *et al.*, 2016). Stiffening has also been reported as a hallmark of cardiovascular complications, including cardiac hypertrophy (Shen *et al.*, 2018), and also reported for cirrhotic liver disease (Tian *et al.*, 2013). Additional AFM studies investigated stiffness of retina (Franze *et al.*, 2011), cornea (Last *et al.*, 2009), osteoarthritis (Hsieh *et al.*, 2008), type I diabetes (Nagy *et al.*, 2018), asthma (Zemła *et al.*, 2018) and brain (Li *et al.*, 2018; Holtzmann *et al.*, 2016; Christ *et al.*, 2010), and response to nerve injury (Wei *et al.*, 2017; Martin *et al.*, 2013). Typically, when studying stiffness of whole tissue samples, it is been shown that cancer tissues are in general stiffer than the surrounding tissues due to the increase of matrix deposition and crosslinking during cancer progression, and metastatic likelihood increases with tissue stiffness (Boyd *et al.*, 2014; Acerbi *et al.*, 2015). On the other hand, single cell measurements in general reveal that invasive cancer cells are softer than the non-invasive cell types and healthy cells (Swaminathan *et al.*, 2011). AFM allows to resolve the mechanical properties of local area in the tissue and distinguish the mechanical properties of the cells and ECM in the same tissue.

The increased interest in AFM-based cell mechanics has paralleled increased efforts by companies manufacturing AFM towards the development of specialized setups for biology research (Gavara, 2016). I here also used the new type of indenters developed by Optics11 Life. The **Chiaro nanoindenter** is, mechanically speaking, similar to an AFM, as it also relies on a cantilever with known elastic constant to measure force and indentation during an experiment. The difference lies in the probe manufacturing and sensing mechanism: whilst in AFM cantilever, laser and photodetector are separate entities that need to be assembled and aligned for each experiment, the fiber-based probes of the nanoindenter are essentially monolithic, with a cantilever glued on a glass

ferrule that also houses the optical fiber that measure the deflection. The optical fiber is pointed at the cantilever, approximately mid length. The sensing mechanism is based on a low-finesse Fabry-Perot resonator, which is formed by shining an infrared laser through the single mode fiber, onto the cantilever. The reflections that occur between the fiber end facet and the cantilever surface form an optical cavity. Its variation is tracked by measuring the phase of the Fabry-Perot resonator. By adding a high frequency wavelength modulation, and using a lock in detection tuned to the modulation frequency, it is possible to linearize the photodetector signal over an arbitrary large range of motion, which, practically, is limited by the numerical aperture of the fiber and amount of cantilever deflection. As the reading of the displacement does not occur at the contact point with the substrate, it is necessary to measure a geometrical correction factor for the deflection, akin to what is done in AFM when measuring the inverted optical lever sensitivity. This is done by moving the piezo a known amount whilst the cantilever is in contact with a surface that is approximately rigid. The ratio between the piezo movement and the measured cantilever deflection gives the geometrical correction factor.

The main difference with respect to classic AFM devices is that these indenters use an all-optical fiber interferometric readout of cantilever deflection. In this setup, the probe is manufactured by aligning and integrating together the cantilever and the optical fiber. Fabry-Perot interferometry is used to monitor cantilever displacement when performing indentation experiments. Implementation of optical interferometry results in several technical advantages with respect to classic AFM instruments (**Figure 5**):

- The cantilever has a higher bending range (up to 30 μm), which allows to test mechanically heterogeneous samples with the same probe
- The piezo has a higher movement range (100 μm), allowing to test very rough samples in which different heights in different regions of the sample are present
- While AFM typically works with a fixed maximum applied force, which corresponds to a fixed indentation only as long as the YM does not change, when using the nanoindenter the indentation range is the fixed parameter for all measurements, adjusting the maximum force if needed.

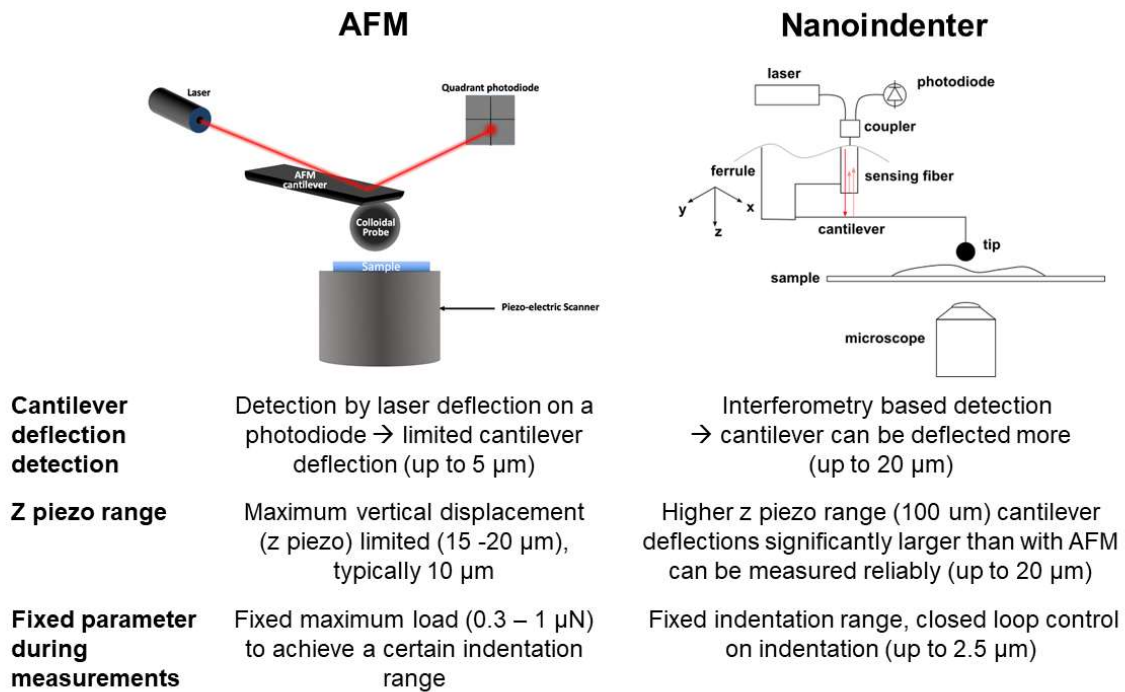


Figure 5. Indentation instruments: AFM and Chiaro nanoindenter from Optics11 Life. The main difference between both indentation instruments are the z piezo range, the detection of cantilever deflection and the fixed parameter during measurements

The Chiaro nanoindenter uses this technology, and mechanical measurements are described in more detail in the Materials and Methods section 4.6.2.

1.3.3. Brillouin imaging to assess tissue mechanics

Brillouin light scattering microscopy is a type of elastography that optically assesses the viscoelastic properties of a material. Brillouin microscopy is being increasingly used in mechanobiology to assess the mechanical properties of cells and tissues (Prevedel *et al*, 2019). It is a non-destructive method which can probe label-free samples in a non-contact mode, contrary to indentation-based techniques described in section 1.3.2.

Brillouin microscopy uses a laser as a probe to inquire the viscoelastic properties of a specimen. This information can be obtained via Brillouin scattering, an inelastic process resulting from the interaction of the incoming laser with the acoustic waves (also known as phonons) within the material. Phonons are thermally generated acoustic waves that represent collective, periodic excitations of the crystalline planes in any material at non-zero temperature. By detecting the photons coming out from the interaction with the phonons within the material it is possible to acquire a Brillouin spectrum, which provides a unique characterization of the material's mechanical properties.

Indeed, upon laser beam interaction with the sample, the following light-matter phenomena arise:

- Most of the photons from the laser do not interact with the sample: in this case, no energy exchange between light and matter happens and therefore the light is elastically scattered from the sample, i.e. with the same frequency as the illumination, resulting in **Rayleigh scattering** (**Figure 6**)
- A very small part of the photons from the laser interacts with phonons from the sample. This interaction results in an energy exchange between photons and phonons that can be quantified as a shift in frequency of the photons detected. This frequency shift is known as **Brillouin shift** (ν_B) and quantified as the central position of the two Brillouin peaks (named Stokes and anti-Stokes peaks, due to an energy increase or decrease in the detected photons).

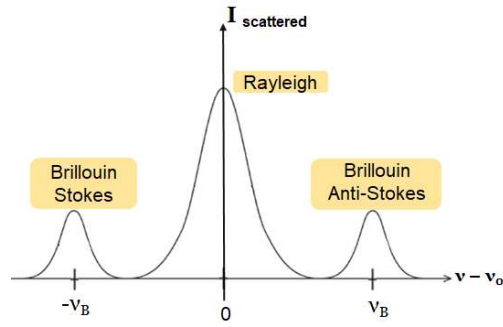


Figure 6. Brillouin Spectrum. Monochromatic laser light is inelastically scattered from phonons within the material, resulting in Brillouin stokes and anti-stokes peaks. Light scattered elastically from the sample results in the Rayleigh peak. ν_B is the Brillouin shift, ν_0 is the frequency of incident radiation

The central position of the Brillouin peaks (i.e. ν_B) is directly related to the local stiffness (**Figure 6**), while the full-width at half maximum (Γ_B) of the peaks is directly dependent on the viscosity. Phonons velocity and attenuation are governed by the viscoelastic properties of the material, and the Brillouin shift ν_B carries information on the real part of the longitudinal modulus (M') as described in the formula:

$$\nu_B = \frac{2n}{\lambda_0} \sqrt{\frac{M'}{\rho}}$$

where λ_0 is the wavelength of the laser; n is the local refractive index, and ρ is the density. Since in biological materials $n/\sqrt{\rho} \approx 1$, the Brillouin shift can be in general interpreted as directly dependent only from the local longitudinal modulus (M').

Brillouin imaging information is in general reported in terms of Longitudinal Modulus $M = M' + iM''$, where M' gives information about the elastic properties of a material (intrinsic properties of individual components in the probed region in terms of length-scale, cross-linking level, compressibility of the local microenvironment and solid-liquid volume fraction (Wu *et al*, 2019) (given by the position of Brillouin peaks) and the imaginary part iM'' which is determined by the longitudinal viscosity of the medium (Ryu *et al*, 2021).

A Brillouin microscope is composed by a confocal laser scanning microscope, which performs a point-by-point raster scanning of the sample, coupled to a spectrometer that spatially separates the frequencies of the Brillouin component and the Rayleigh one (**Figure 7**). A set of collimators and filters are used to filter the Rayleigh signal (which is not informative about the sample properties as the signal is not interacting with the sample) and reduce it to a minimum. The signal is then redirected to a spectrometer to separate the Brillouin peaks.

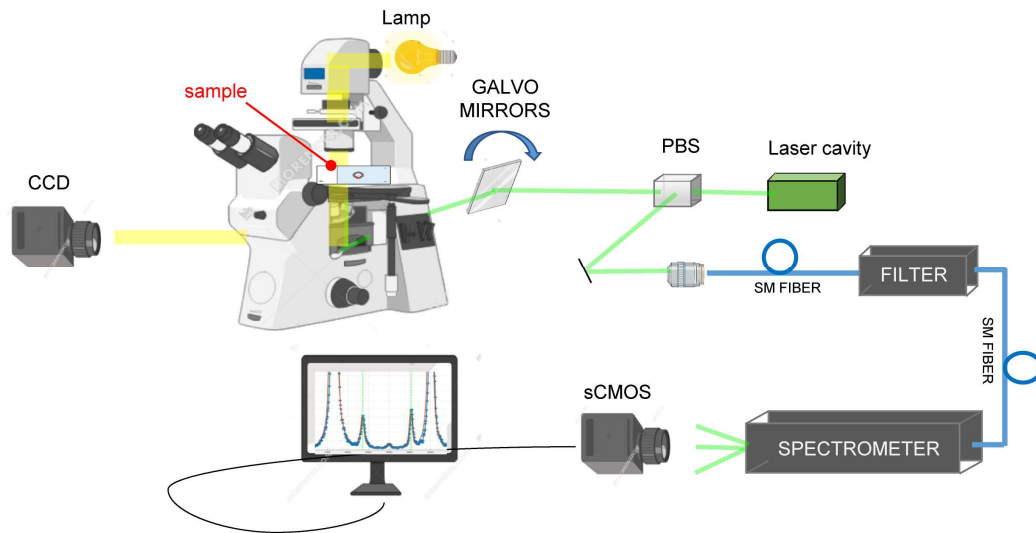


Figure 7. Brillouin microscope scheme.

Brillouin microscopy has been used to assess biomechanics of different tissues and pathological conditions (**Figure 8**). For example, it has been used to study articular cartilage and its response to proteoglycans depletion after enzymatic treatment in order to mimic osteoarthritis disease (Wu *et al*, 2019). In a different study Brillouin was used to understand the mechanics of the different stages of follicle development, by measuring ooplasm, follicles and connective tissues within intact ovaries (Chan *et al*, 2021). Rheological properties of the eye lens have been reported by Brillouin (Reiß *et al*, 2011). Detection of malignant melanoma tissues within a surrounding healthy tissue has also been performed (Trojanova-Wood *et al*, 2019), highlighting the potential of Brillouin imaging as a diagnostic tool.

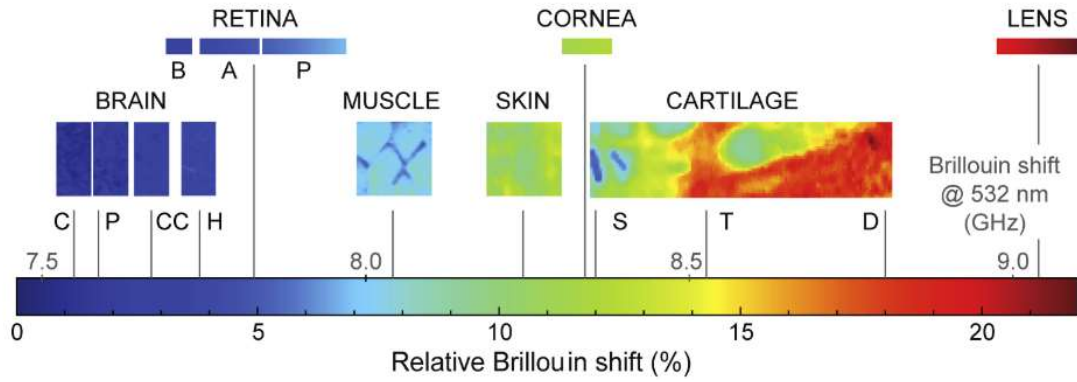


Figure 8. Range of Brillouin shift values for different tissues. Adapted from (Ryu *et al*, 2021).

Indentation-based instruments and Brillouin imaging differ in several technical aspects that are summarized in

Figure 9. Although in the field the term *stiffness* is widely used to refer to the mechanical properties measured by different techniques, it is important to highlight that the Longitudinal Modulus (M) probed by Brillouin Microscopy is a different one from the YM probed by AFM. Mechanical properties refer to the broad range of physical properties that a material can exhibit upon the application of forces, including different properties as are elasticity, viscosity, tensile strength, compressibility, etc. M probed by Brillouin microscopy is in fact a measure of *compressibility* of the material, stressing it in a confined condition: for biological materials, mostly composed by water, this modulus typically falls in GPa range. Instead, YM determined by AFM is a measure of *elasticity*, where the material is allowed to expand sideways under stress, thus keeping the volume constant: for biological systems, this modulus falls in Pa-kPa range (Prevedel *et al*, 2019). In principle, M might be related to YM in the following way:

$$M = YM \frac{1 - \nu}{(1 + \nu)(1 - 2\nu)}$$

, where ν is Poisson's ratio (Prevedel *et al*, 2019). However, this parameter bears a strong frequency and material dependency. Therefore, a universal relationship between YM and M cannot be formalized and, on the contrary, must be empirically proven for each specific tested sample. So

far, correlations between YM and M in some cell types of cells have been experimentally outlined (Scarcelli *et al*, 2015), but this information on tissues is still lacking.

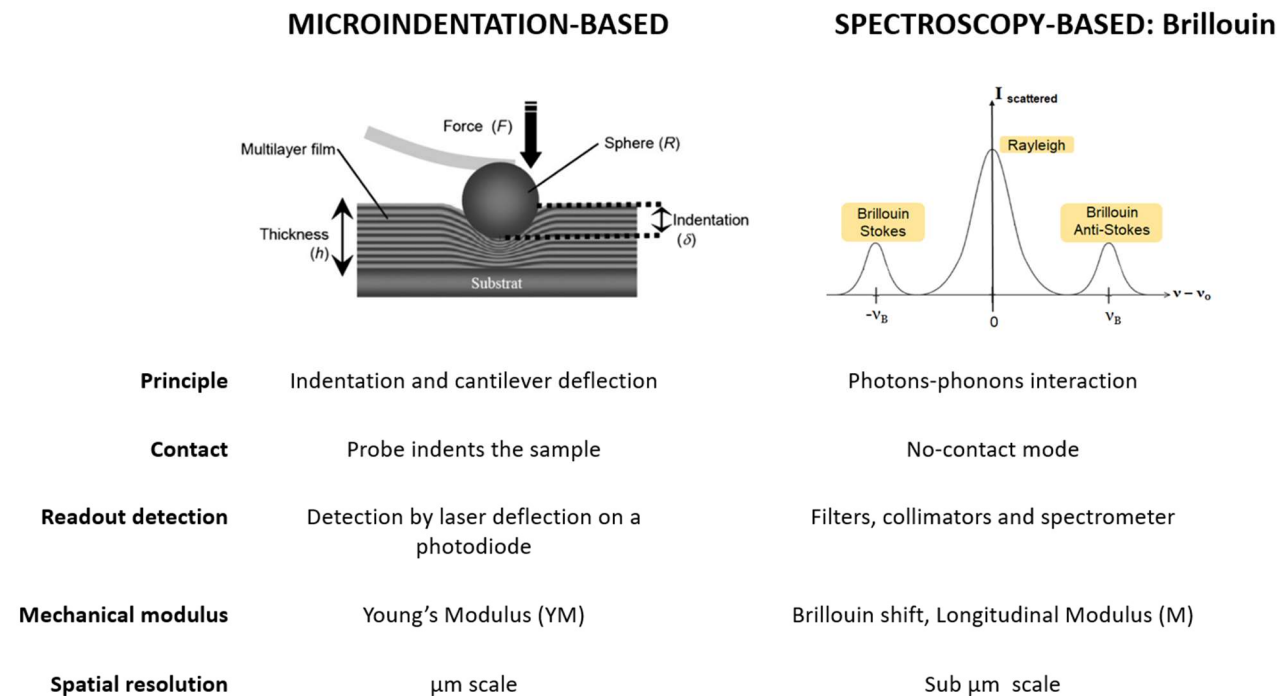


Figure 9. Comparison between microindentation-based techniques and spectroscopy-based Brillouin microscopy. Microindentation-based scheme (left) adapted from (Schneider *et al*, 2007) under fair use principle.

Experimental details, information on data collection and data analysis are provided in the Materials and Methods section 4.7.

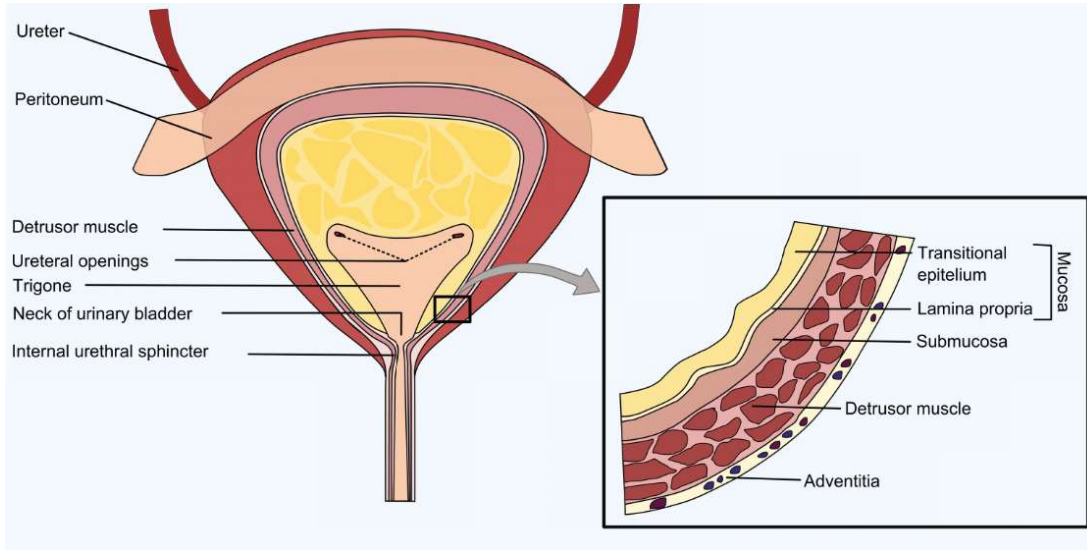
2. Introduction – Bladder

2.1. Bladder anatomy

The urinary bladder is a hollow organ located in the human pelvis that stores urine. The bladder wall can be divided into four different layers (**Figure 10**), here described from the innermost:

- **Urothelium:** it is a transitional epithelium highly specialized that lines the lower urinary tract. The urothelium has a variable number of cell layers (usually three cell layers in rodent bladder and up to ten cell layers in human bladder (Cohen, 2013)), which varies according to the degree of extension of the bladder. The urothelium consists of the basal cells, which sit on a basement membrane (composed of collagen IV and laminin) that separates it from the underlying lamina propria; the intermediate cells; and on top of the urothelium there are the umbrella cells, the most specialized cells which by expressing uroplakin plaque at their surface and establishing tight junctions between cells provide the impermeability of the bladder (Morgante & Southgate, 2022).
- **Lamina propria:** loose connective tissue separated by the overlying urothelium by the basement membrane, mainly formed by collagen I and III, elastic fibres, blood vessels, unmyelinated nervous endings and some discontinuous muscle bundles (Orabi *et al*, 2013).
- **Muscularis propria:** it consists of concentric layers of thick bundles of smooth muscle. Its contraction allows the expulsion of urine to the outside (Orabi *et al*, 2013).
- **Adventitia or serosa:** outermost layer composed of fibroadipose tissue/perivesical adipose tissue.

a)



b)

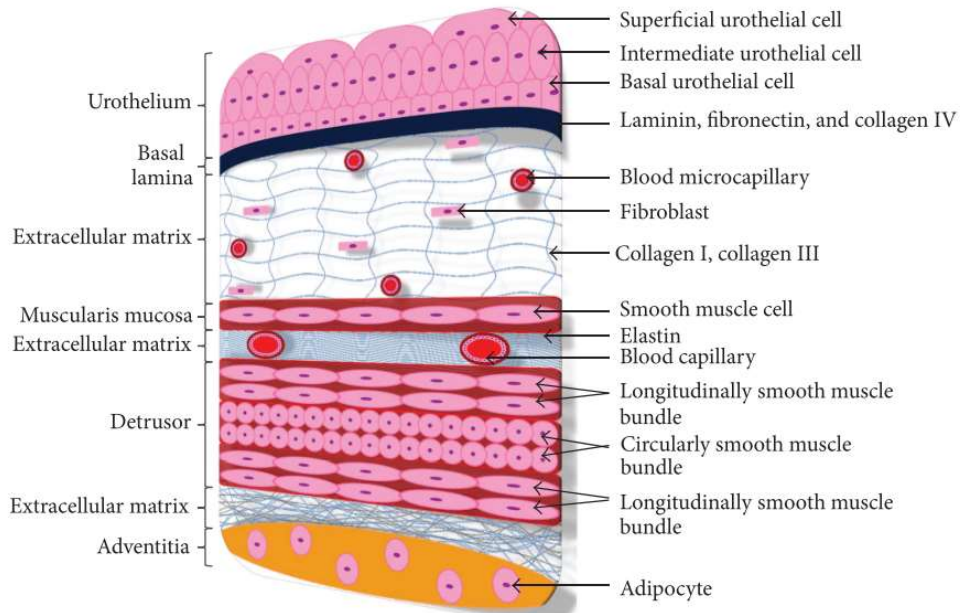


Figure 10. Bladder anatomy. a) Schematic of the anatomical regions of the bladder, reproduced from Roccabianca S & Bush TR (2016) “Understanding the mechanics of the bladder through experiments and theoretical models: Where we started and where we are heading”. *Technology* 04: 30–41; b) schematic histology of the bladder wall (Orabi *et al*, 2013).

2.2. Bladder pathologies: actinic cystitis and cancer

This thesis focuses on two pathological conditions of the bladder: actinic cystitis and bladder cancer.

Actinic cystitis is the pathological condition caused as side effect of pelvic radiotherapy, commonly used to treat prostate, colorectal, cervical and ovarian cancer (Mangano *et al*, 2018; Zwaans *et al*, 2020). Actinic cystitis is caused by accumulation of ECM proteins due to chronic inflammation, resulting in scarring and thickening of tissue and finally in organ failure, with an important impact on the quality and amount of life of the patient (Martinez-Vidal *et al*, 2021).

Onset and development of actinic cystitis include first a short acute phase, in which X-ray radiation causes cell membrane and DNA damage, as well as water radiolysis resulting in free radical formation. As a consequence, the most superficial urothelial cell layer, which contains the most specialized cells and thus, with lower turnover, is the most susceptible component to radiation. Exposure of the damaged urothelium to urine further activates inflammation mechanisms, resulting in a chronic inflammatory stage. Finally, and due to lack of oxygen supply after ischaemia of microscopical blood vessels the tissue becomes atrophic, with increased deposition of collagen (specially within the lamina propria and between muscle bundles (Fry *et al*, 2018)), increased fibroblast and myofibroblast infiltration, decreased cellular muscle relaxation, development of tissue edema and presence of massive fibrosis (Mangano *et al*, 2018). Clinical symptoms include increased urination frequency, nocturia, urinary incontinence, haematuria, pain during urination and chronic pelvic pain (Zwaans *et al*, 2022). To stop haematuria and chronic pelvic pain, patients may require radical cystectomy (bladder removal) and urinary diversion to reroute urine flow from its normal pathway (Tyson & Barocas, 2017). The main options for urinary tract reconstruction are incontinent conduit diversions, continent cutaneous diversions, and orthotopic neobladders (Tyson & Barocas, 2017), which in any case have a strong impact in the quality of life of the patients, emotional wellbeing and sexual life.

Bladder cancer is the ninth most common cancer worldwide (Ferlay *et al*, 2015) with 430.000 new patients per year (Antoni *et al*, 2017), and has the highest lifetime treatment costs per patient of all cancers (Sylvester *et al*, 2006). Disease incidence increases with age, and men are more affected than women (Sanli *et al*, 2017).

Bladder cancer originates from the urothelium, and according to the invasion of the different tissue layers the Tumor, Node, Metastasis (TNM) classification system (Sobin, 2009) divides the different bladder lesions (**Figure 11**). Within Non Muscle Invasive Bladder Cancer (NMIBC) several categories are distinguished. The most superficial lesions are non-invasive urothelial lesions, i.e., not breaking the basement membrane and therefore not reaching the lamina propria. **Carcinoma in situ** (CIS or Tis) is a very flat lesion of few μm thickness that does not invade the lamina propria, composed by poorly differentiated high cytologic grade tumor cells, and confers bad prognosis to the patient due to its propensity to progress to invasive stages. Due to its macroscopically flat morphology, CIS is difficult to detect.

pTa or papillary urothelial carcinoma, as CIS, does not invade the underlying lamina propria, with the difference that this tumor grows as a papilla towards the bladder lumen. Papillary tumours that, on the contrary, have broken the basement membrane and invaded the lamina propria are classified as **pT1**.

Muscle Invasive Bladder Cancer (MIBC) classifies as follows: **pT2** tumors have invaded the muscle layer, either superficially (pT2a) or deeply (pT2b); **pT3** tumors have invaded beyond the muscle tissue into the perivesical fat, from which it can further migrate invading the adjacent organs (stage **pT4**) as the lymph nodes, prostate, uterus, vagina, or even pelvic or abdominal walls (Sanli *et al*, 2017; Knowles & Hurst, 2015).

The most common and often the first detected symptom of bladder cancer is the presence of blood in the urine (haematuria) (Sanli *et al*, 2017), which is nevertheless associated with an advanced stage of the disease. Furthermore, as there is no active screening for bladder cancer, patients are very often diagnosed at late and advanced stages of the disease. This fact points out the need to develop methods that allow for early diagnosis of the disease. Diagnosis in patients

suspected to have bladder cancer is performed via cystoscopy (endoscopic procedure performed with a flexible scope and local anesthesia (Aaronson *et al*, 2009)). The first step in newly diagnosed bladder tumors require endoscopic resection of the tumor (transurethral resection of bladder tumor, TURBT) followed by histological analysis of the biopsy. Up to 70 % of patients at the first diagnosis are suffering from NMIBC. Most of patients with NMIBC experience relapse of the tumor because limitations in detecting small lesions and limited efficacy of intravesical adjuvant therapies, and therefore undergo multiple cycles of intervention represented by TURBT and adjuvant intravesical therapy (instillation of Mitomycin C or Bacillus Calmette–Guérin (BCG) (Sylvester *et al*, 2010). Eventually, the tumor might progress to a more aggressive state, invading also the muscle layer. In the case of MIBCs patients have to undergo radical cystectomy with or without chemotherapy (Sanli *et al*, 2017). For some specific cases, also pT1 NMIBC (tumor invading lamina propria) patients undergo radical cystectomy (Sobin, 2009).

Clinical imaging techniques can detect established fibrosis and initial tumor stages, but there is the unmet clinical need to identify even earlier disease stages and to develop a more tailored follow up of the disease, in order to identify very initial signs of any disease relapse. Understanding the link between micromechanical features and clinical phenotypes in bladder malignancies may contribute to improve prognostic classification. Moreover, this knowledge can contribute to the development of novel therapies based on the modification of the micromechanical drivers of carcinogenesis (Hajjarian *et al*, 2021).

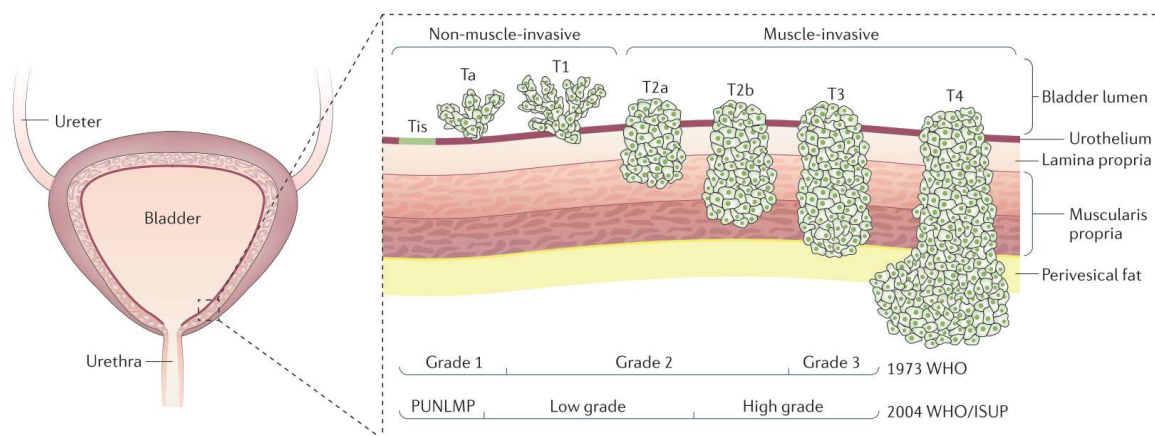


Figure 11. Types and stages of bladder cancer. Adapted from (Sanli *et al*, 2017).

2.3. Bladder – why its biomechanics?

The mechanical moduli of different human urological organs, i.e., kidney, prostate, testis and bladder have been investigated, mostly by elastography-based macroscale techniques. **Table 2** summarizes the mechanical moduli for these different urological tissues in different pathological conditions.

Regarding **kidney** mechanics, it has been established that a value of tissue stiffness higher than 4.31 kPa corresponds to a diseased kidney (**Table 2**), an information that can be used to develop early non-invasive diagnostic tools. Of interest is also the fact that a correlation has been reported between renal stiffness and degree of renal fibrosis (Cui *et al*, 2013; Nakao *et al*, 2015), with patients suffering from chronic kidney disease exhibiting a stiffer renal parenchymal than non-chronic kidney disease patients (Goya *et al*, 2015). Renal elasticity is therefore a potential predictor of chronic kidney disease (Lin *et al*, 2017). In fact, patients with later stages of chronic kidney disease had stiffer renal cortex, with stiffness increasing progressively from stage 3 to 5 of the disease.

Prostate cancer (PCa) has a higher cell and vessel density, which is discernibly stiffer than both benign and normal tissues (Fu *et al*, 2020). Given the non-invasive and cost-effective imaging technology of SWE, several studies have been published aiming to evaluate differences in stiffness between PCa and benign tissue based on YM (Yang *et al*, 2019) (**Table 2**). For all studies discussed here, it was reported that the SWE-obtained YM of prostate cancer was significantly higher than for benign prostate tissue. The stiffness of PCa in the peripheral area, where most PCa starts, gradually increases with the Gleason Score, which is the grade of the tumor: the higher the Gleason score, the stiffer the tissue is (Yang *et al*, 2019; Woo *et al*, 2014). The stiffness values corresponding to each Gleason score differ when reported by different studies. For example, the YM value to use as a threshold to discriminate benign from malignant prostate tissue has been reported to be 42 kPa (Rouvière *et al*, 2017), 35 kPa (Ma *et al*, 2012) or 31 kPa (Fu *et al*, 2020); and a value of 144 kPa has been proposed as a predictor of biochemical recurrence following radical prostatectomy (Wei *et al*, 2019).

Modulation of the tissue stiffness has also been reported in several pathologies of the **testis**. The stiffness of testicular cancer can be more than double the stiffness of normal testis, suggesting that increased stiffness could be used as a testicular malignancy marker, and detectable by ultrasound elastography (Pedersen *et al*, 2019, 2017). In testicular microlithiasis, a modest increase of tissue stiffness compared to normal testicles was measured by SWE (Pedersen *et al*, 2017), but no malignant characteristics are measured by SWE or MRI diffusion in this condition (stiffness values reported in **Table 2**) (Pedersen *et al*, 2019). Thus, benign testicular lesions can be differentiated from malignant ones both by MRI diffusion and elastography. Testis stiffness has also been investigated in the varicocele, where collagen deposition and interstitial testicular edema have been described (Abdelwahab *et al*, 2017).

Table 2. Mechanical moduli of human urological tissues				
Tissue	Technique	Modulus	Modulus value (condition)	Ref
KIDNEY				
	SWE	YM	4.31 kPa (healthy)	(Leong <i>et al</i> , 2018)
	RTE		75.1 ± 37.8 (non-CKD) 72.9 ± 37.6 (CKD stage 3a) 59.3 ± 40.3 (CKD stage 3b) 48.3 ± 33.8 (CKD stage 4) 36.6 ± 33.0 (CKD stage 5)	(Lin <i>et al</i> , 2017)
	MRE	YM	4.35 kPa (normal functioning kidneys) 4.86 kPa (cut-off value) 5.10 kPa (CKD patients)	(Han <i>et al</i> , 2020)
	MRE	YM -Cortico-medullary	3.24 kPa (functional allografts) 3.73 kPa (chronic dysfunction allografts) 3.29 kPa (no progressive decline) 4.82 kPa (graft loss/relist)	(Kennedy <i>et al</i> , 2020)
		YM -Cortical	2.43 kPa (functional allografts) 2.84 kPa (chronic dysfunction allografts) 2.48 kPa (no progressive decline) 3.67 kPa (graft loss/relist)	
	MRE	SWS	1.86 m/s (IgA nephropathy) 2.05 m/s (cut-off value) 2.34 m/s (healthy)	(Lang <i>et al</i> , 2019)
PROSTATE				
	SWE	YM	42 kPa (cut-off value healthy)	(Fu <i>et al</i> , 2020; Rouvière <i>et al</i> , 2017)
	SWE	YM	144.85 kPa (cut-off value for recurrence after radical prostatectomy)	(Wei <i>et al</i> , 2019)
	SWE	YM	31.79 ± 16.17 kPa (benign) 114.96 ± 85.25 kPa (malignant)	(Fu <i>et al</i> , 2020)
	SWE	YM	95 ± 28.5 kPa (Gleason score 6) 163 ± 63 kPa (Gleason score 7)	(Ahmad <i>et al</i> , 2013)
	SWE	YM	91.6 kPa (Gleason score 6) 102.3 kPa (Gleason score 7) 131.8 kPa (Gleason score 8)	(Wei <i>et al</i> , 2018)
	SWE	YM	32.7 ± 19.4 kPa (Gleason score 6) 55.4 ± 48.5 kPa (Gleason score 7) 57.3 ± 39.4 kPa (Gleason score 8) 88.2 ± 64.2 kPa (Gleason score 9)	(Woo <i>et al</i> , 2014)
	MRI with tomoelastography	SWS	2.8 ± 0.4 m/s (peripheral zone) 2.8 ± 0.3 m/s (transition zone) 3.1 ± 0.6 m/s (PCa)	(Asbach <i>et al</i> , 2020)

BLADDER				
	Rheology	Storage modulus	0.052-0.085 MPa (healthy)	(Barnes <i>et al</i> , 2016)
		Loss modulus	0.019-0.043 MPa (healthy)	
TESTIS				
	SWE	Velocity stiffness	0.76 m/s (normal) 0.79 m/s (testicular microlithiasis) 1.92 m/s (testicular cancer)	(Pedersen <i>et al</i> , 2017)
	SWE	Velocity stiffness	0.77 m/s (normal) 0.78 m/s (testicular microlithiasis) 1.95 m/s (testicular cancer)	(Pedersen <i>et al</i> , 2019)
	MRI	Diffusion values	$0.929 \times 10^{-3} \text{ mm}^2 \text{ s}^{-1}$ (normal) $0.978 \times 10^{-3} \text{ mm}^2 \text{ s}^{-1}$ (testicular microlithiasis) $0.743 \times 10^{-3} \text{ mm}^2 \text{ s}^{-1}$ (testicular cancer)	
	SWE	YM	4.5 kPa (cut-off value for semen parameters improvement after surgery)	(Abdelwahab <i>et al</i> , 2017)
	SWVV		1.465 m/s (cut-off normal/oligozoospermia) 1.328 m/s (cut-off normal/azoospermia)	(Yavuz <i>et al</i> , 2018)
	SWE	YM	$2.50 \pm 0.49 \text{ kPa}$ (Varicocele grade I) $2.59 \pm 0.81 \text{ kPa}$ (Varicocele grade II) $2.80 \pm 0.72 \text{ kPa}$ (Varicocele grade III)	(Jedrzejewski <i>et al</i> , 2019)
CKD: chronic kidney disease, RTE: real-time elastography (uses arbitrary units), YM: Young's modulus, SWS: shear-wave speed, SWVV: shear wave velocity values, MRI: magnetic resonance imaging diffusion values.				

Surprisingly enough **bladder mechanics** still remain partially unveiled, even though this hollow organ exerts its function by cycles of mechanical relaxation and contraction, as it has to adapt and stretch to the urine it collects and voids. Bladder cancer cells with different metastatic potential have been mechanically characterized (Liu *et al*, 2014), showing that bladder cancer cell lines with higher aggressiveness have a lower YM than lower grade cancer cells. These observations have been reported by several studies (Ramos *et al*, 2014; Canetta *et al*, 2014; Lekka *et al*, 1999, 2012; Lin *et al*, 2015), showing that cancer cells are more elastic than their benign counterparts. This increase in elasticity (indicated by a decrease in the cell's YM) means higher deformability of cancer cells, which could have implications facilitating intra and extravasation and thus, metastasis. This tendency has been observed not only on bladder cancer cells, but also in tissues as prostate (Khan *et al*, 2018) and breast (Lin *et al*, 2015; Lekka, 2016).

Although single cell mechanics are necessary to be measured, there is the need to understand bladder mechanics at a tissue-scale. Already in 1994, bladder wall elasticity was classified as a physiological biomechanical characteristic, susceptible to change with the development of different pathologies (Landau *et al*, 1994). In this study, the ratio of connective tissue to smooth muscle in patients with dysfunctional bladder was compared to the ratio of normal bladders. It was found that such ratios were increased compared to normal tissues, indicating that in the dysfunctional bladder there is a higher proportion of connective tissue compared to smooth muscle tissue. Although no mechanical tests were performed, they directly correlated these observations with a loss of elasticity in the bladder wall. Interestingly, later on published studies have suggested to use the ratio of fibrous connective tissue to smooth muscle tissue measured by SWE, as a parameter for the diagnosis of early fibrotic changes (Volikova *et al*, 2019).

Alteration of murine bladder mechanical properties after actinic cystitis development has been previously described (Zwaans *et al*, 2022). In this study, by applying loading-unloading cycles of stretching, they reported that irradiated bladder ECM were significantly less distensible than healthy bladders at the macroscale. Such macroscopical mechanical test revealed that the changes were apparent at 3 months post-irradiation and statistically significant at month 6.

Additional bladder disorders have been mechanically investigated. For example, aiming to develop non-invasive diagnostic tests for lower urinary tract disorders (LUTS), this study (Nenadic *et al*, 2016) compared three quantifiable ultrasound methods (high-frequency ultrasound, SWE and duplex doppler) to measure the biomechanics of the bladder wall in healthy individuals, in order to establish baselines and reference points for future research. Such quantitative non-invasive diagnostic tool would allow to detect bladder wall changes and decreased wall function before obvious fibrotic changes develop (Volikova *et al*, 2019). They observed that bladder wall pathology affects its structure and thickness of the bladder wall layers; and the thickness of the bladder and detrusor layer increased with age. The increase in thickness with age could be related to an increased interstitial collagen deposition or to hypertrophy of the detrusor.

About bladder cancer mechanics, the viscoelastic properties of human bladder at the macroscale have been tested by different techniques, as is by uniaxial mechanical test (Martins *et al*, 2011; Ahms *et al*, 1998), including the characterization of the different macroscopic areas of porcine bladder from the trigone to the dome (Korossis *et al*, 2009). In an additional study (Barnes *et al*, 2016) ten bladder human tumors were analyzed by dynamic mechanical analysis. Samples were collected from patients by transurethral resection procedures, and a load was applied to the tumor with increasing frequencies, up to 30 Hz, calculating both the storage and loss modulus (**Table 2**). These macroscopic measurements were previously established on porcine bladder by the same group (Barnes *et al*, 2015). This analysis quantifies the frequency-dependent viscoelastic properties on the macroscale which is rheometer, getting two different mechanical parameters for each tumor: storage modulus, ranging between 0.052-0.085 MPa; and loss modulus ranging between 0.019-0.043 MPa.

Increased stiffness by SWE has been reported for malignant bladder disease, which was associated with high content of collagen fibers (Huang *et al*, 2020). In addition, bladder tissues from patients with relapsing tumor are stiffer than those of newly diagnosed patients (Ghasemi *et al*, 2020).

Bladder wall alterations associated with a loss of bladder elasticity and dysfunction could be a consequence of inflammation, loss of urothelium and obstructive or neurogenic etiologies. These processes would lead to hypertrophy of smooth muscle cells, hyperplasia of fibroblasts and the deposition of collagen fibers between muscle bundles of detrusor (Zhu *et al*, 2019), bladder wall thickening, and consequently result in fibrosis, scarring and stiffening of the bladder, together with a progressive reduction in bladder capacity (Volikova *et al*, 2019; Uvelius *et al*, 1984).

Alteration of the mechanical properties of the bladder are associated with different diseases (Fry *et al*, 2018), as are actinic cystitis and cancer. However, what are the implications of altered tissue elasticity? In the case of the bladder, mechanics alteration first result in a dysfunction of its physiological role, dramatically affecting quality of life of patients (Martinez-Vidal *et al*, 2021; Tyson & Barocas, 2017). Second, studying bladder mechanics has a diagnostic value: by deeply characterizing mechanical fingerprints and associating them to different pathological stages, eventual novel mechanical biomarkers could be described for specific diseases. For example, in the oncological field there is an important risk of downstaging bladder cancer patients with pT1 disease

instead of pT2 when performing histopathologic analysis on tissue biopsies (Sanli *et al*, 2017). Therefore, it is of critical relevance to develop methods that can support assigning the correct disease subtype and staging tools using routine clinical samples. Due to its biological relevance tissue elasticity could potentially help and/or be used in combination with routine analysis in order to improve accuracy of diagnosis and bladder cancer staging. In addition, there are additional factors that highlight the relevance of studying bladder mechanics: stiff tissue might increase interstitial pressure in the tumor, which contributes to tumor progression, activates durotaxis sensing pathways which guide cell migration following stiffness gradients, impedes drug delivery and blood vessels function. Altered blood vessels compliance, as well as impaired vessels function due to increase solid stress that can compress blood and lymphatic vessels (Nia *et al*, 2020), result in blood flow impairment, and consequently altered oxygen delivery, immune cells and drug delivery.

The biological consequences of altered tissue mechanics has a vast effect on organ homeostasis and function. I here have reviewed different studies that investigate bladder mechanics in different pathological conditions using different techniques and mechanical tests. While these studies on clinical specimens are very informative, they show macroscale measurements. Nevertheless, the bladder is a multilayer organ, in which each different layer structure performs different functions within the organ, and it is therefore crucial to understand the contribution to the different anatomical components to mechanical alteration in disease. This means, it is needed to understand tissue mechanics at the microscale, spatially resolving the different bladder components (cells, ECM, muscle bundles...) and their contribution to altered tissue mechanics. On the other hand, the discussed studies here represent mostly a snapshot of the clinical situation, which although being very informative, does not fully describe the evolution of the mechanical properties with onset, establishment and progression of the disease. Understanding the progression of such mechanical alteration is crucial, as well to understand whether elasticity alteration could be used as a prognostic marker or indicator of tissue priming for disease development, eventually setting the path for early diagnostic/prognostic tools. Furthermore, there is the need to develop artificial bladders for bladder transplantation for patients that underwent radical cystectomy due to actinic cystitis or bladder tumor. To do so, it is required a deep understanding of the mechanical properties of the physiological bladder, in order to mimic them closely and produce functional artificial bladders that will notably improve quality of life of patients.

3. Aim of the research project

The bladder is a multilayer organ which strongly relies on its mechanical properties to perform its physiological function. My PhD project aims to mechanically characterize the healthy bladder spatially resolving its different tissue layers at the microscale, as well as in the pathological conditions of bladder cancer and actinic cystitis. For this purpose, I here aimed to first establish a sample preparation protocol that allows for a standardized network-wide measurements of tissue mechanics, both by microindentation-based instruments and spectroscopy based imaging. Such sample preparation protocol allows also for correlation of tissue mechanics with the gold standard diagnosis by pathologist assessment. This thesis can be then divided into two main chapters. The first chapter is dedicated to the characterization of bladder tissues by two microindenter instruments. This includes characterization of the micromechanics of the bladder wall, considering its different anatomical tissue layers and the evolution of tissue mechanics with aging of the animal among its adult life. In order to model the pathological condition of actinic cystitis, I here characterized bladder elasticity of X-ray irradiated animals and followed the kinetics of the fibrotic process on the stiffness of the tissue. This thesis also investigated a second pathological condition, bladder cancer in an orthotopic murine model, to understand the onset and evolution of the disease. Last, and as a proof of concept, I here characterized the tissue mechanics of clinical specimens from a bladder cancer patient that underwent radical cystectomy.

Aiming to bring the study of tissue mechanics closer to a more clinical setup and increase the translation potential of these experiments, the second chapter of this thesis exploited the non-contact mode technique Brillouin imaging to characterize bladder tissues. In this chapter I studied murine bladder tissues in health and in the pathological condition of actinic cystitis by Brillouin imaging, a spectroscopy based technique. I here provided a comparison of the gold standard technique on biomechanics, AFM, and emerging techniques that might have the potential to be used in the clinics, as Brillouin imaging.

I established mechanical fingerprints of bladder in health and disease and evaluated potential associations between the mechanical properties of tissues, the stage of the tumor and remodeling of extracellular matrix and compared to the gold standard diagnosis by pathologist evaluation.

4. Materials and Methods

4.1. Ultrasound image analysis

Fischer female rats were handled according to the ethical protocol #1114. In order to induce a physiological stretching stress of the bladder, ultrasound (US) imaging was performed prior sacrificing the animals in order to infer the instillation volume that corresponds to a physiologically stretched bladder (**Figure 12**). US imaging was performed on a Vevo3100 LAZR-X Imaging Station equipped with a MX250D transducer (FUJIFILM VisualSonics, Amsterdam, the Netherlands). US signal was collected acquiring axial sections of the rat bladder using the following settings: frequency: 21 MHz; gain: 15dB; step size: 200 μ m. B-mode 3D ultrasound images of the rat bladder were acquired and analysed with VevoLab 3.2.5 software.

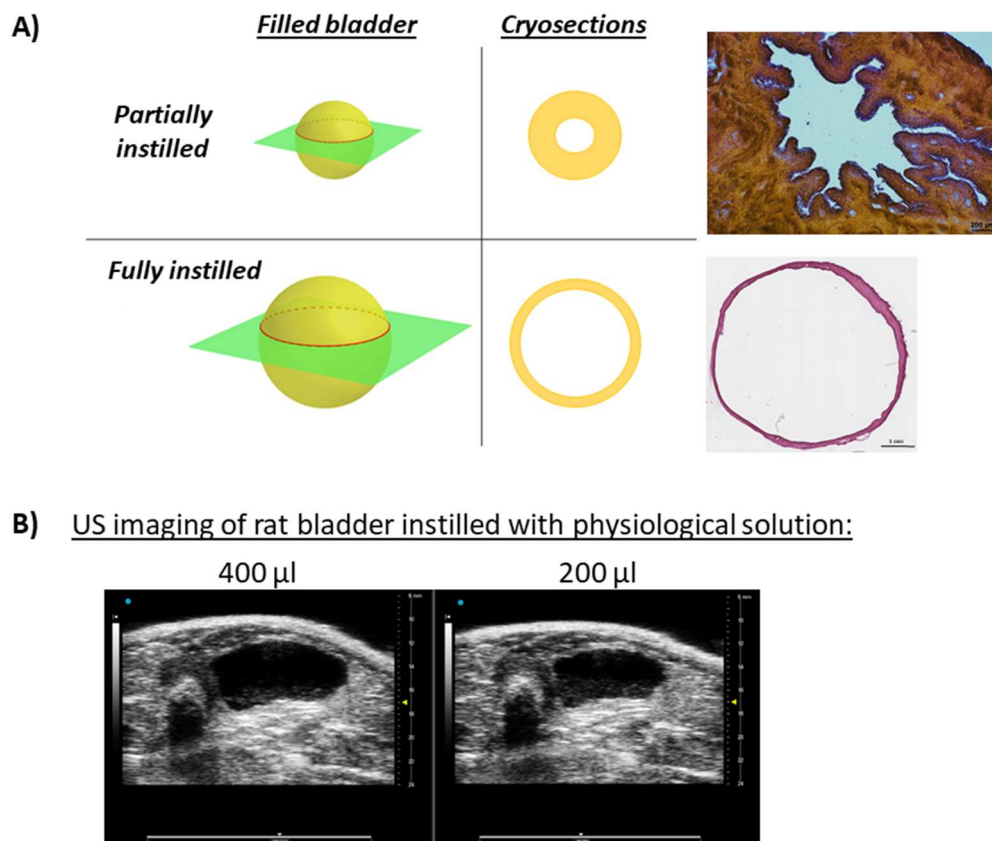


Figure 12. Ultrasound imaging (US) for physiological volume determination. a) Scheme of partially and fully instilled bladders (left), image of hematoxylin-eosin stained cryosections (right). b) US imaging of rat bladders instilled with different PBS volumes

4.2. Rat model of actinic cystitis

Two months old, 150-175 grams female Fisher rats (Charles River, Germany) were housed in the animal facility at IRCCS San Raffaele Hospital under standard conditions (temperature: $22^{\circ}\text{C} \pm 2$; humidity: $50 \pm 10\%$; light/dark cycle: 12-h light and 12-h dark). After a 1-week period of acclimatization, the rats were x-ray irradiated. Animals were anesthetized with isoflurane 2-4% 0.3-0.8 L, and the bladder filled with 450 μl of sterile saline solution through PE50 catheter (Brown & Avian, 2011). The bladder was irradiated with a single show of 20 Gy. The radiation dose was delivered using a dedicated small animal micro-irradiator (X-RAD225Cx SmART, PXI North Branford, CT, USA) with micro-cone beam computed tomography (CBCT) guidance (Spinelli *et al*, 2020). The anesthetized rats were positioned prone on the animal stage and CBCT images were acquired using the following settings: tube voltage = 40 kVp, current = 5 mA, voxel size = 0.2 mm^3 . The bladder was contoured on the CT scan and three equal-sized dose beams were set at 130° , 180° and 230° angles respectively, using a collimator of $10 \times 10 \text{ mm}^2$. Dose distribution was calculated by means of a Monte Carlo algorithm (Hoof *et al*, 2013) and the mean dose to the bladder was adjusted to the prescribed dose of 20 Gy. Irradiation settings were: tube voltage = 225 kVp, current = 13 mA. Delivery time ranged approximately between 2 and 5 min/field and the entire procedure (CT imaging and radiotherapy) was performed within 20–25 min/animal. Rats were then sacrificed 2, 4 and 6 months after radiotherapy, (3 rats per condition) and bladders were prepared for histology and mechanical testing.

4.3. Rat model of bladder carcinogenesis (BBN model)

Two months old female Fisher rats (Charles River, Germany) were housed in the animal facility at IRCCS San Raffaele Hospital under standard conditions (temperature: $22^{\circ}\text{C} \pm 2$; humidity: $50 \pm 10\%$; light/dark cycle: 12-h light and 12-h dark). After a 1-week period of acclimatization, the rats were evenly divided in two groups: one group (tumor) that was watered with 0.05% N-(4-hydroxybutyl)nitrosamine (BBN; Sigma Aldrich) and the second group (control) watered with normal water. Rats were then sacrificed 2, 4 and 6 months after treatment initiation, (3 rats per condition) and bladders were prepared for histology and mechanical testing.

All procedures and studies involving animals were performed under protocols approved by the IRCCS Ospedale San Raffaele Animal Care and Use Committee, and in accordance with national and international standard guidelines.

4.4. Human specimens

Paired specimens of non-neoplastic tissue and urothelial carcinoma of the bladder were obtained from one patient (male, 62 years, with MIBC-pT2 G3) through the Unit of Pathology at the IRCCS Ospedale San Raffaele (Milan, Italy). A formal written consent was obtained by the local Institutional Review Board (Ethic Committee IRCCS Ospedale San Raffaele; amended version of URBBAN protocol approved on November 2020). Data collection and all experimental protocols were approved by the Ethic Committee IRCCS Ospedale San Raffaele, in accordance with the relevant guidelines and regulations outlined in the Declaration of Helsinki. All methods were carried out in accordance with the approved guidelines. All patients signed written informed consent agreeing to supply their own anonymous information for this and future studies.

4.5. Sample preparation for mechanical analysis

For the rat specimens, bladder ultrasound imaging was performed in order to characterize the instillation volume that causes a physiological stretching of the bladder. Animals were then euthanized by CO₂ and through bladder catheterization (22 G cannula, BD, Italy) the cryoprotectant OCT (Bio-Optica, IT) was instilled into the bladder (volume previously defined by US imaging, ranging from 200-400 µl depending on size and stretch ability to each bladder) (**Figure 13**). The urethra was closed and the bladder was explanted. In order to preserve specimen integrity, bladders were snap frozen in tissue embedding medium (OCT Compound for Cryostat Sectioning) at -80 °C (isopentane and dry ice) (Tuttle *et al*, 2022). Human specimens were frozen in the same way.

For the mechanical analysis 50 µm thick tissue sections were prepared using a microtome cryostat, and the fresh-frozen sections were thawed at room temperature on polarized superfrost glass slides in order to immobilize them for mechanical measurements. OCT was removed with phosphate buffer solution (PBS) wash prior mechanical testing. Paired 10 µm thick frozen sections

were thawed, formalin fixed and hematoxylin-eosin stained for comprehensive histological analyses.

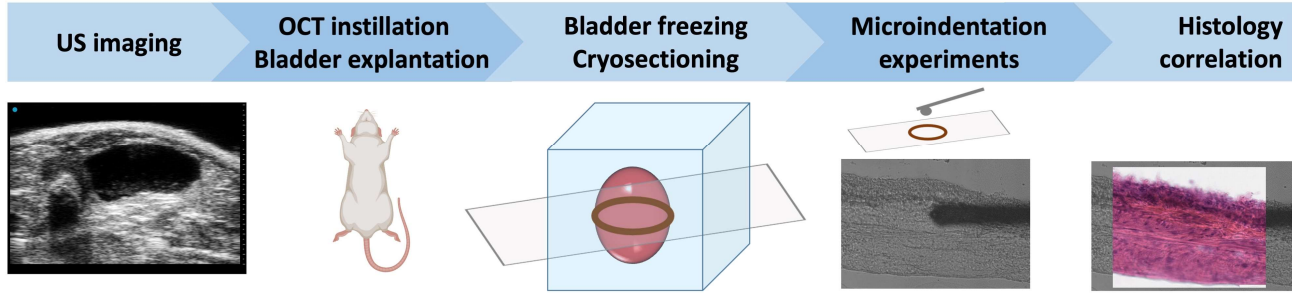


Figure 13. Methodological approach for bladder stiffness characterization. Sample preparation protocol and pipeline of experiments. First, ultrasound (US) imaging is performed in order to determine the physiological OCT cryoprotectant bladder instillation volume. Animals are then sacrificed, the cryoprotectant is instilled into the bladder through a catheter and the bladder is then explanted and frozen. Cryosections are prepared and microindentation experiments are performed on the tissue slides both by AFM and nanoindenter. Afterwards, histology analysis was performed to confirm the location of the bladder anatomical layers.

4.6. Indentation techniques

The YM of bladder tissue specimens was characterized using the Chiaro nano-indenter (Optics11), and the Bioscope Catalyst AFM (Bruker).

4.6.1. AFM-based indentation measurements

YM values of the different layers of the bladder tissue were determined by fitting the Hertz model (Kontomaris, 2018; Hertz, 1881) to sets of force versus indentation curves (simply force curves, FCs) acquired by AFM on 50 μm thick tissue sections, as described elsewhere (Schillers *et al.*, 2017; Nebuloni *et al.*, 2016; Cappella & Kappl, 2005):

$$F = \frac{4}{3} \left(\frac{E}{1 - \nu^2} \left(R^{\frac{1}{2}} \delta^{\frac{3}{2}} \right) \right)$$

, which is accurate as long as the indentation δ is small compared to the radius R . In Eq. (1), ν is the Poisson's coefficient, which is typically assumed to be equal to 0.5 for incompressible materials, and E is the Young's modulus.

Custom monolithic borosilicate glass probes consisting of spherical glass beads (SPI Supplies), with radii R in the range of 5–10 μm , were attached to tipless cantilevers (Nanosensor, TL-FM) with nominal spring constant $k = 3\text{-}5 \text{ N/m}$ (Varinelli *et al*, 2022). Probes were fabricated and calibrated, in terms of tip radius, according to an established custom protocol (Indrieri *et al*, 2011). Variations in the contact radius were due to the technical availability of the single probes during the measurements and to internal variations of the glass beads (within the same batch) used for fabrication of the colloidal probes. The spring constant of the cantilever was measured using the thermal noise calibration method (Hutter & Bechhoefer, 1993; Jaschke, 1995) and corrected for the contribution of the added mass of the sphere (Laurent *et al*, 2013; Chighizola *et al*, 2021). The deflection sensitivity was calibrated in situ and non-invasively before every experiment by using the previously characterized spring constant as a reference, according to the SNAP procedure (Schillers *et al*, 2017).

All mechanical measurements have been performed with tissue samples immersed in PBS solution. Sets of FCs (force volumes, or FVs) were collected in selected regions of interest identified exploiting the accurate alignment of optical and AFM images obtained using the Miro software module integrated in the AFM software. The optical access and the design of the tissue slices allowed to move the probe directly over the different layers of the bladder (urothelium, lamina propria, muscle layer) and to localize the regions of interest to be analyzed for local mechanical properties.

Each FV typically consisted of an array of 144-225 FCs, spatially separated by 5-10 μm , each FC containing 8192 points, with ramp length $L = 6\text{-}10 \mu\text{m}$, maximum load $F_{\text{max}} = 200\text{-}1500 \text{ nN}$, and ramp frequency $f = 1 \text{ Hz}$. The maximum load was adjusted in order to achieve a typical maximum indentation in the range was around 2-5 μm . Typical approaching speed of the probe during indentation was 12-20 $\mu\text{m/s}$.

Each tissue layer was characterized by collecting at least 15 independent FVs in different macroscopically separated regions of interest on three different tissue slices for each rat (i.e. for each different bladder organ). Tissue slides from the middle region of the bladder were selected in order to normalize for the bladder wall thickness (bladder cross section closer to the ends of the

bladder have thicker muscle layer). Furthermore, in order to avoid bias due to sampling a particular area of the bladder, we randomly chose at least four locations within each investigated tissue section to sample the three tissue layers, taking as reference the four cardinal points of the tissue section. In total, each layer has been characterized by more than 2000 FCs per single organ. Data analysis was performed as described before elsewhere (Puricelli *et al*, 2015b).

After the mechanical test, tissue sections were fixed on 4 % paraformaldehyde (PFA) and hematoxylin-eosin staining was performed on the same slice in order to provide a retrospective confirmation of the anatomical location of each single region of interest measured during the nanoindentation experiment (**Figure 13**).

4.6.2. Nanoindenter measurements

Mechanical maps on murine bladders were collected using a Chiaro nanoindenter (Optics11 B.V.) in at least three well separated areas in each collected slice. Dimensions wise, a pixel size of 10 μm was chosen with an overall map dimension of 100 μm in the tangential direction (through the different layers), and whatever length was necessary to cover the whole thickness of the bladder wall, from urothelium to muscle (typically a few 100s of μm).

Mechanical characterization of human bladder specimens was performed with the same Chiaro nanoindenter. Maps of up to 1 mm by 1mm (pixel size of 10 μm) were collected in the three different tissue layers from two different tissue pieces per bladder. Three to five tissue slides per tissue piece were measured. The Hertz model (Eq. 1) was fit to the force curves.

The tissues were probed using cantilevers with ~ 0.5 N/m spring constant and ~ 9 μm radius. All measurements were performed in Indentation control mode (that is, in a closed loop so the indentation rate is constant throughout the loading phase), with 5 $\mu\text{m/s}$ indentation rate and a target indentation of 5 μm ; as for the case of AFM, this choice was also done to comply both with the parabolic indenter approximation of Hertzian theory and to avoid bottom effect given by the finite thickness of the sample (Dimitriadis *et al*, 2002; Garcia & Garcia, 2018).

To establish the optimum indentation depth, YM's obtained at different indentation ranges were compared, and the surface roughness was analyzed by means of optical profilometry (Veeco WYKO NT9100 and OCT, (**Figure 14**)). The latter techniques showed a scale-dependent roughness, with arithmetic roughness values of around 2-300 nm when areas of $\sim 10 \mu\text{m}$ radii were analyzed (that is, the scale of the contact of the indenter sphere). To ensure conformal tissue/indenter contact, we performed Hertzian fit after excluding the first portion of contact. We considered a fit to be valid when R^2 was ≥ 0.90 .

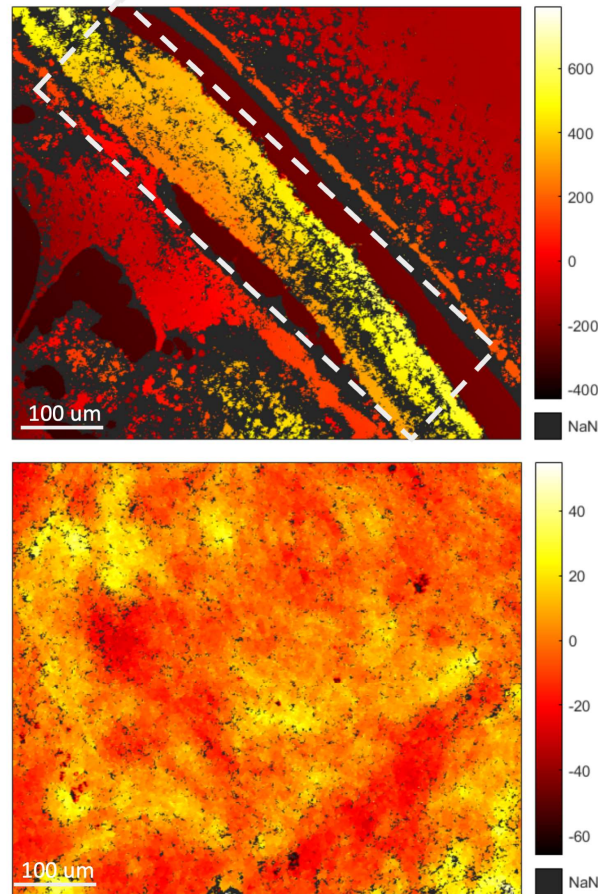


Figure 14. Surface roughness image of bladder tissue cryosections. In order to ensure conformal contact between probe and sample, it is important to assess the surface roughness of the tissue under study. To quantify this, we characterized the topography of both rat (top) and human (bottom) samples using a non-contact approach. The images represent $620 \times 480 \mu\text{m}$ scans of the surface of frozen tissue samples. These were obtained with an optical scanning profiler, using white light illumination (Veeco Wyko NT9100). In the rat image, it is possible to see the arched bladder wall (brighter area highlighted by white dashed line) surrounded by the OCT. Heatmap represents elevation, in nm. In both cases, we found that the surface roughness was in the order of hundreds of nm ($R_a \sim 200\text{-}400 \text{ nm}$) when analyzing small areas, approximately equal to the contact area during indentation, and in the order of microns in regions separated by hundreds of μm .

I also compared the fitting results for different indentation depth ranges (1-3 μm , 3-5 μm): I observed that at different indentation depth the YM remained mostly the same, with a slight increase in the number of rejected fits with increasing depth of indentation (**Figure 15**), hinting at a mild non-linear behavior at larger strains. I chose to limit the analysis to shallow indentations (0.2-1.2 μm) to maintain more consistent results and more easily compare the results to the AFM dataset; this choice also assured that the maximum indentation was significantly larger than the typical roughness value.

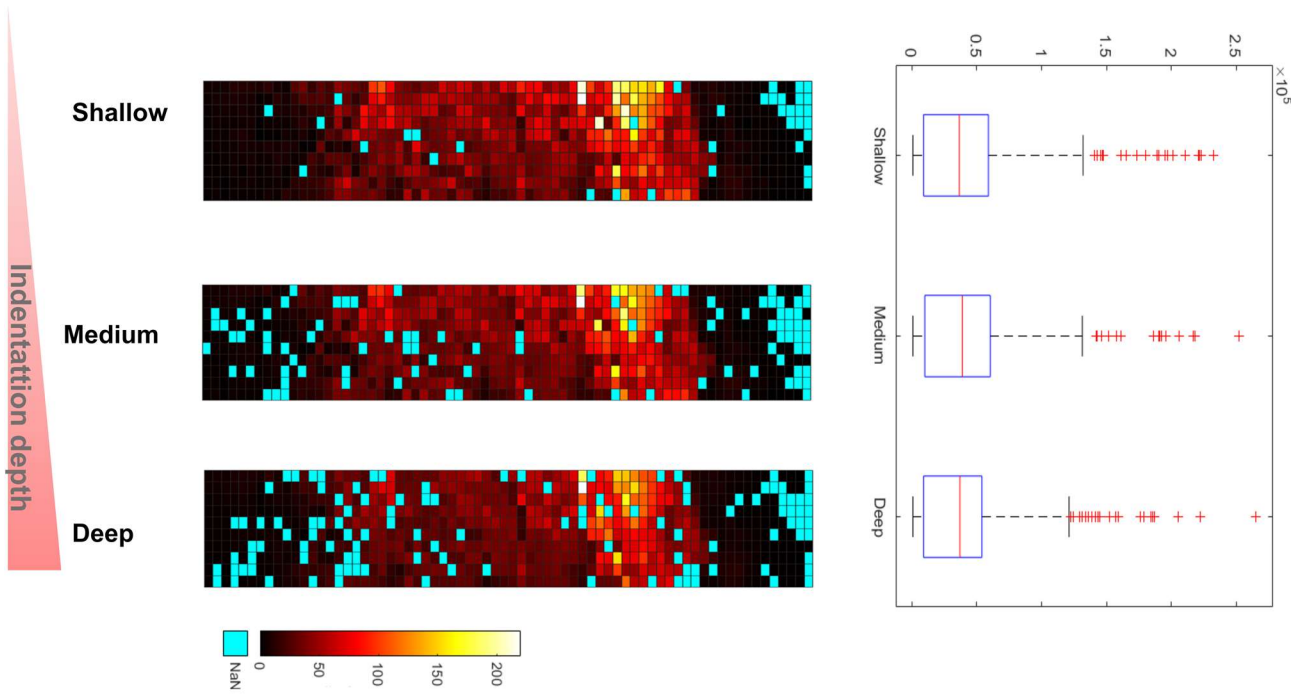


Figure 15. YM's at different indentation depths obtained using the nanoindenter. YM's was analyzed at shallow (1.5 μm), medium (2.5 μm) and deep (5 μm) indentation depths. With increasing indentation depth, the number of non-valid pixels (blue) increased due to bottom effect, while YM values remain equivalent.

4.7. Brillouin microscopy

The Longitudinal Modulus of intact cells and tissues can be quantified by obtaining the point-by-point spectrum of the light inelastically scattered by longitudinal phonons, i.e. the Brillouin spectrum: here, it is possible to measure the Brillouin frequency shift with respect to the incoming radiation, directly related to the Longitudinal Modulus, and the Full Width at Half Maximum (FWHM), directly related to sample's viscosity. The Brillouin shift ν_B measured by Brillouin microscopy is directly dependent on the longitudinal modulus M ; the extrapolation of M , however, is not so straightforward since we should know samples' index of refraction n and density ρ with sub-micrometric precision, but these values cannot be easily accessed from literature in such inhomogeneous samples with the adequate resolution. Therefore, in this study we chose not to extrapolate M from ν_B and just refer to ν_B values.

We here used a custom-built Confocal Brillouin Microscope which consisted of an inverted microscope (Olympus IX-73) coupled to a single VIPA-based spectrometer through single-mode optical fibers. The 3D mechanical properties of the sample are recovered in confocal laser scanning mode thanks to a pair of galvanometric mirrors (THORLABS) and a piezo stage (MadCity Labs). The laser source (a continuous-wave single mode laser at 532 nm wavelength, VERDI) passes through a polarizing beam splitter, the galvo mirrors and then is focused on the sample plane via a 60x objective (Olympus, NA = 1.45) to have high resolution Brillouin maps of biological samples. The retrieved Brillouin and Rayleigh signals, scattered from a specific point of the sample, are then collimated on a single-mode fiber through a 20x objective: The core of the optical fiber (diameter = 1.5 μm) acts as a pinhole and allows for confocal sectioning of the sample: thus, the spatial resolution of Brillouin maps is comparable to confocal ones (~ 400 nm on xy plane, ~ 800 nm on z). To partially suppress the background signal, *i.e.* the Rayleigh component, a glass prism is used as a filter (Lepert *et al*, 2016).

In this way, it is possible to correlate Brillouin maps with morphological ones by using on the same microscope: *i)* a laser scanning system based on galvanometric mirrors, for point-by-point Brillouin spectrum imaging; *ii)* a lamp and a camera for widefield transmission images in Differential Interference Contrast (DIC) mode. The setup is controlled in MATLAB via a custom-built GUI. During data acquisitions, the stage longitudinal step size on the sample was 800 nm, the acquisition time 100/150 ms and the optical power delivered to the specimen was 25 mW.

We acquired Stokes and Anti-Stokes Brillouin signals and fitted them with a sum of Lorentzian functions after pixel-to-GHz conversion (obtained after distilled water calibration of the microscope): the maps of Brillouin shifts reported in section 5.2 are the results of the fit. All data analysis has been performed using custom-made programs in MATLAB.

For bladder tissues acquisitions, we thawed the samples (treated as described in section 2.3) and removed OCT cryoprotectant with several washes in PBS; then we added some drops of PBS to keep the tissues fresh and hydrated during the acquisition. The presence of buffer throughout the acquisition was confirmed by its Brillouin spectrum, similar to water. We first choose the bladder portion to investigate through the DIC imaging module via a large field of view (i.e., a 10x objective), then we switched to a high magnification, small field of view (60x) objective, used also for Brillouin acquisition.

We acquired at least 4 sections per slice, at least 2 slices per rat, and at least 2 rats per condition. We then fitted the data and collected all the Brillouin shifts in histograms.

4.8. Histological analysis pairing

Histological analysis pairing. Bladder cryosections of 10 μm thick were prepared, OCT was washed away with PBS and tissues slides were fixed on 4 % PFA. Then Hematoxylin Eosin (HE) staining was performed as follows; slides were washed twice on MilliQ water and cell nuclei were stained with Hematoxylin for 50 seconds, next washed for 5 minutes in MilliQ water and incubated on Eosin for 15 seconds. After washing, tissue slides were dehydrated on an increasing gradient of ethanol and then incubated on xylene as a clearing agent. Samples were then mounted with Eukit. A comprehensive histopathological analysis from HE slides was performed by our experienced uro-pathologist (Dr Roberta Lucianò) blindly with respect to the mechanical data. In addition, same tissue slices previously used for mechanical measurements (50 μm thick) were fixed and HE stained in order to confirm the tissue layers (20 seconds Hematoxylin and 15 seconds Eosin).

4.9. Collagen quantification

Collagen quantification from HE stained tissues was performed by quantifying collagen birefringence from images acquired with polarized light in dark field microscope (Zeiss AxioImager M2M). All images were captured using 10X objective (APOCHROMAT 10X - NA 0.45) and analyzed with ImageJ software. Images were first transformed into 8 bit images, threshold was manually adjusted in order to remove background noise and collect all positive pixels from the tissue. The percentage of area fraction above the established threshold was quantified.

4.10. Statistical methods

The median YM value per tissue layer and rat was calculated. Since both AFM and nanoindenter instruments provide comparable YM values and the force curves are conceptually measured in the same way, reported results here represent data in duplicate collected both by AFM and nanoindenter, and pulled median values as obtained by both instruments per rat and tissue layer.

In order to analyze the effect of X-ray irradiation and BBN treatment in each tissue layer, we calculated the median YM fold changes with respect to the healthy rats. To do so, we first averaged each rat's AFM and nanoindenter median YM value for each tissue layer at a specific time point. This gives 3 median values (one per rat), at each of the studied conditions. Since we were interested in the (mechanical) changes as a consequence of a diseased condition, we paired treated/control animals. As every rat measured was an end-point, we assumed that any diseased condition could be originated from any of the healthy rats. This means, the possible fold-changes per conditions are the combinations of 3 control and 3 treated rats per time point;

(C=control, T=treated) Rat1T/Rat1C, Rat2T/Rat1C, Rat3T/Rat1C,
Rat1T/Rat2C, Rat2T/Rat2C, Rat3T/Rat2C,
Rat1T/Rat3C, Rat3T/Rat3C, Rat3T/Rat3C.

This gives 9 number per treatment and time point. If we subtract 1 (no fold change from control rats) from each, we can then test the resulting distribution with a 2-way t-test to verify the hypothesis that it has a non-zero mean.

To study kinetics of treatment 2-way Anova with Tukey's multiple comparison test was performed, by comparing the mean of the median YM values of each tissue layer of each single rat at the different time points. I checked for normality of the YM distributions by performing quantile-quantile (QQ) plots per rat and tissue layer for both instruments. For those YM distributions that were not normally distributed, a non-parametric statistical test was performed (Mann Whitney test).

5. Results

5.1. Chapter 1. Micromechanical fingerprints of bladder in health and disease investigated by microindentation techniques

5.1.1. *Establishment of a standardized protocol for network-wide mechanical characterization of tissues*

Although several research papers show that AFM can be applied to investigate mechanics of clinical samples for diagnostic purposes, this technique is still not widely used in clinical practice. One of the obstacles to overcome is the relativeness of the mechanical measurements, as different research groups report values of tissue elasticity that vary substantially (Wu *et al*, 2018). Such lack of reproducibility indicates that differences in data collection and analysis are not consistent within groups. Therefore, protocols that allow for reliable evaluation of YM of biological samples are required. Standardization of mechanical measurements of tissue samples is one of the primary goals of the Phys2BioMed consortium, Marie Curie ITN network that studies biomechanics in health and disease in order to develop advanced physical tools for innovative early diagnosis (www.phys2biomed.eu). The aim is to determine how to investigate the mechanical properties of tissue samples by AFM in a well-defined, consistent and standardized way, which allows to characterize the mechanical properties of tissues in a reproducible way within and across labs. In order to determine the mechanical properties of tissue samples in a reproducible and standardized way, several steps are required: (1) tissue sample preparation, (2) experimental conditions for AFM measurements definition, (3) AFM calibration, (4) mechanical measurements, and (5) data analysis, including choice of suitable modelling of the indentation.

It has been previously established that the the main source of variability when comparing YM by different AFMs and operators are uncertainties in the determination of the deflection sensitivity and subsequently cantilever's spring constant (Schillers *et al*, 2017). Aiming to overcome this difficulty, the SNAP procedure (Standardized Nanomechanical Atomic Force Microscopy) for Measuring Soft Biological Samples emerged. Basically, SNAP relies on vibrometry in order to characterize the spring constants and calculate the correct deflection sensitivity of the cantilevers, highly improving the reproducibility of elasticity measurements.

Therefore I here established the following sample preparation protocol to be used by Phys2BioMed consortium in order to standardize AFM-based mechanical measurements of soft biological samples. To do so, murine bladder tissues were chosen as biological material. The decision to choose bladder as a reference material was based on the following facts: (1) the bladder is a complex tissue, composed of different tissue layers and components, therefore it is a good candidate to standardize mechanical measurements on complex biological samples; (2) the bladder undergoes high mechanical stress, as in order to perform its physiological function it is exposed to stretching cycles, thus its mechanical properties are crucial for its function; (3) studying bladder mechanics is clinically relevant, as tissue elasticity could eventually be used for diagnosis/prognosis purposes for bladder pathologies as bladder cancer and actinic cystitis. In addition, there is the unmet clinical need to reconstruct the bladder closely recapitulating its mechanical properties. There are clinical cases in which the bladder is removed from the patients and they need to receive a functional artificial bladder, i.e. able to store urine, and perform contraction and voiding of the urine volume, purpose for which tissue mechanical properties are crucial.

The tissue sample preparation for AFM-mechanical investigation includes a procedure performed at San Raffaele Hospital (**Figure 16a**), which includes animal sacrifice, organ extraction and cryosection preparation. A total of two rats were used. Five tissue sections from each rat were distributed among the participating labs, frozen in 5 kg of dry ice, and received within 24-48 hours.

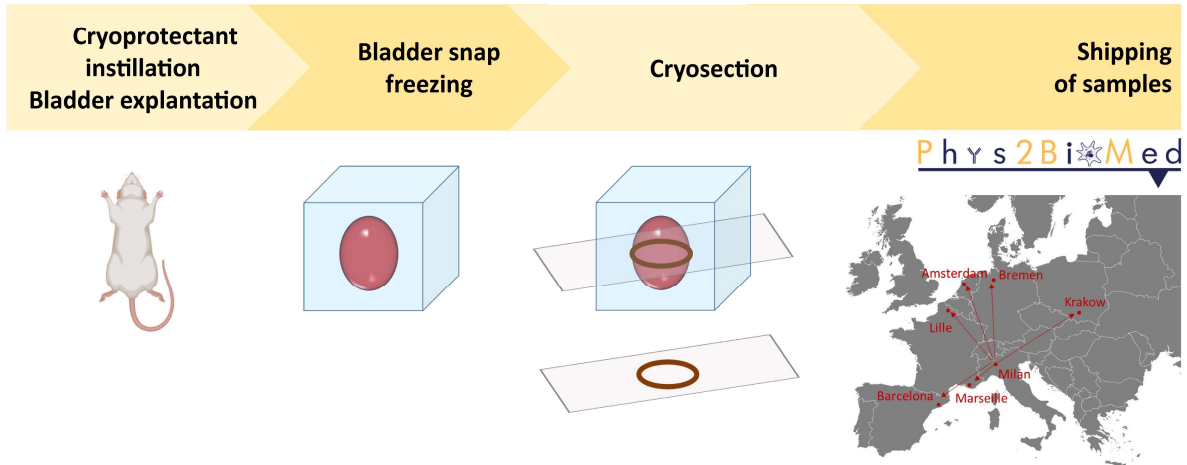
Samples were stored frozen. Each participating lab has to perform a local sample pre-handling, which includes thawing the tissue and washing away the cryoprotectant OCT (**Figure 16b**). Samples were distributed among the participating labs including a circle drawn with a hydrophobic pen surrounding the tissue section that allows hydrating the tissue with a PBS drop, gently added to the tissue in order to perform AFM in liquid and avoid dehydration of the sample. Samples were checked regularly during measurements and when needed, additional PBS was added in case of evaporation.

Visualizing the tissue sections by phase contrast microscopy during nanoindentation allows for positioning the AFM tip directly over the different layers of the bladder (urothelium, lamina propria, muscle layer), i.e. the area to be analyzed for local mechanical properties. The central region of the bladder tissue was chosen for mechanical testing (**Figure 16c**), which roughly corresponds to the lamina propria/muscle tissue layer of the bladder. Each region was characterized by 3 sets of force volumes, which contained 12 by 12 force curves, separated by 10 μm .

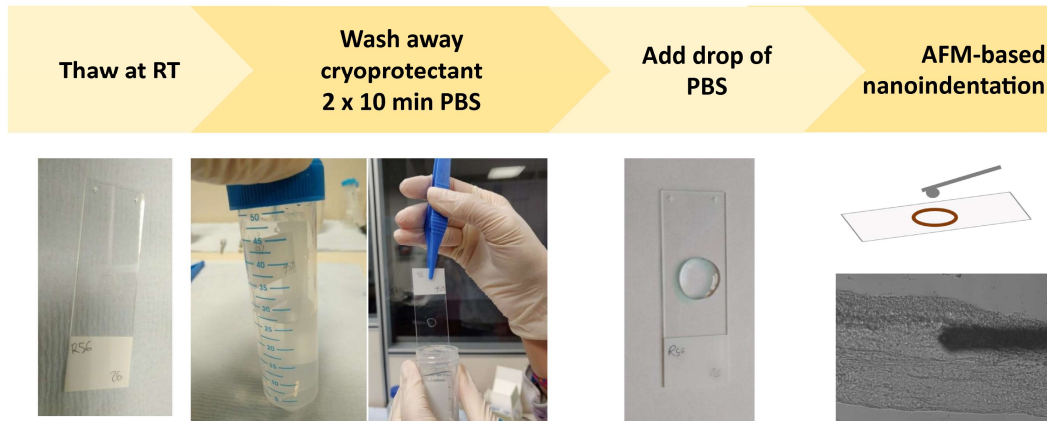
Centralized data analysis was done by University of Bremen.

The results of the successful standardization will be reported elsewhere (ongoing work).

a) Sample preparation pipeline at San Raffaele Hospital



b) Sample handling prior to AFM experiments by participating labs



c) Data collection

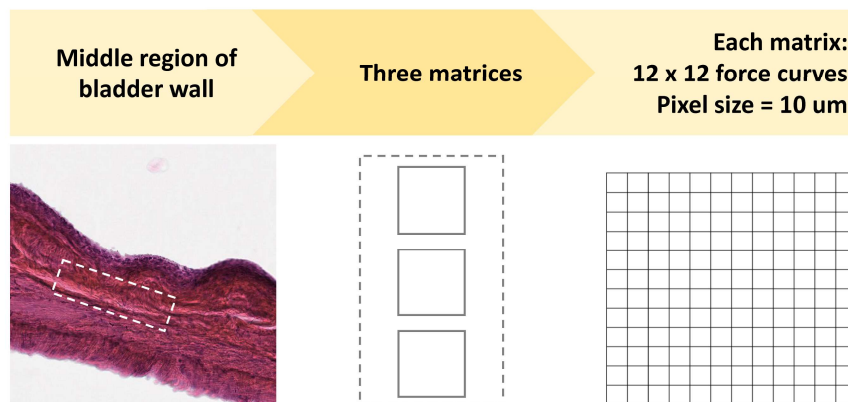


Figure 16. Standardized AFM-based measurements of murine bladder tissues. a) Sample preparation pipeline performed at San Raffaele Hospital. B) Sample handling of participating labs prior AFM experiments. C) Data collection by AFM. Histology of a healthy rat bladder. Left: scheme of region to be measured by AFM. 3 sets of force curves are taken on that middle zone.

Once the standardized protocol was established, I here used an AFM and a nanoindenter to investigate bladder tissues. Identification of mechanical markers for diseases must rely on simplified protocols and instrumentation to be performed in the clinics, therefore my strategy was to start with a widely used technique in mechanobiology, that is the AFM as reference, and then move towards a more handy and potentially easily transferable to the clinics indentation device for soft matter that is a nanoindenter.

I characterized the static elastic properties of the three tissue layers composing the healthy bladder wall spatially resolved at the micro-scale level, to identify modifications associated with the onset and progression of pathological conditions of actinic cystitis and bladder cancer and compare such mechanical fingerprints to the gold standard of diagnosis, i.e., histological examination by experienced pathologist.

5.1.2. The healthy bladder wall exhibits regional differences in tissue stiffness

Murine bladder elasticity was measured by two microindentation instruments: AFM and nanoindenter. Bladder wall emerged to be mechanically inhomogeneous, with local YM covering values ranging from few kPa to hundreds of kPa (**Figure 17a, b**). To identify the origin of this mechanical inhomogeneity, we investigated the existence of an association between the YM distribution and the different anatomical layers of the bladder wall. When performing AFM-based indentation focalized on the single tissue layers (**Figure 17a**) it was observed that the urothelium had a median YM value of 16 kPa, the lamina propria of 63 kPa and the muscle of 72 kPa (4.20, 4.80 and 4.86 respectively in $\text{Log}_{10}(\text{YM}/\text{Pa})$). In spatially resolved micromechanical maps acquired using the nanoindenter, we observed that the healthy bladder wall is characterized by a tissue stiffness gradient (**Figure 17b**): the urothelium exhibits the lowest YM (10 kPa), which gradually increases when reaching the second bladder tissue layer, the lamina propria (100 kPa), and transiently decreases when reaching the outer muscle tissue layer (70 kPa) (**Figure 17b**). Both AFM and nanoindenter instruments provided comparable YM values for the different bladder tissue layers, both in physiology and pathology (**Figure 18**). Therefore, the following results derive from data collected in duplicate using both AFM and nanoindenter.

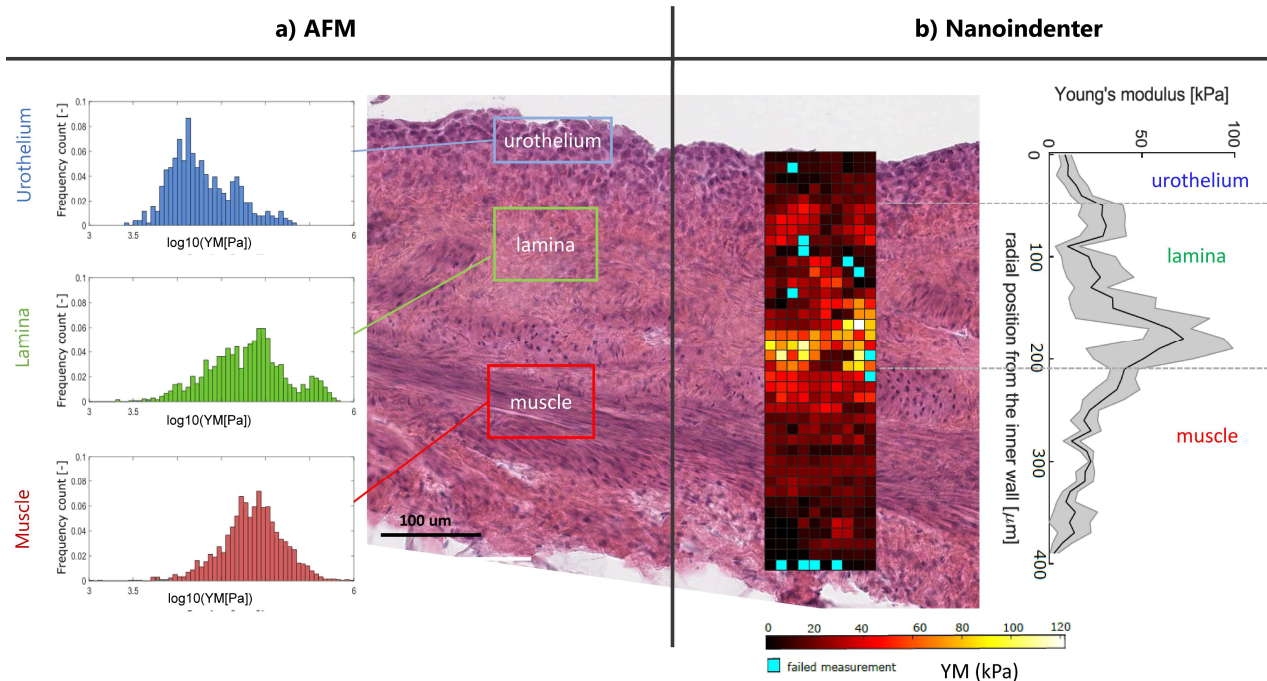


Figure 17. Healthy bladder wall exhibits regional differences in tissue elasticity. a) YM by AFM represented in logarithm in base 10 (\log_{10}) in Pa for the different bladder tissue layers. b) YM values obtained with the nanoindenter. Graph on the right represents the mean of each horizontal line of YM pixel values from the map \pm standard deviation of the mean in gray shade. The mechanical heterogeneity of the bladder correlates with its anatomical distribution: there is a gradient of YMs, being the urothelium the softest layer, with increasing stiffness when reaching the lamina propria, and then decreasing over the muscle layers. The association of stiffness gradients with the anatomical bladder tissue layers is shown by overlay of the mechanical map with hematoxylin-eosin staining. Blue pixels indicate rejected measurements.

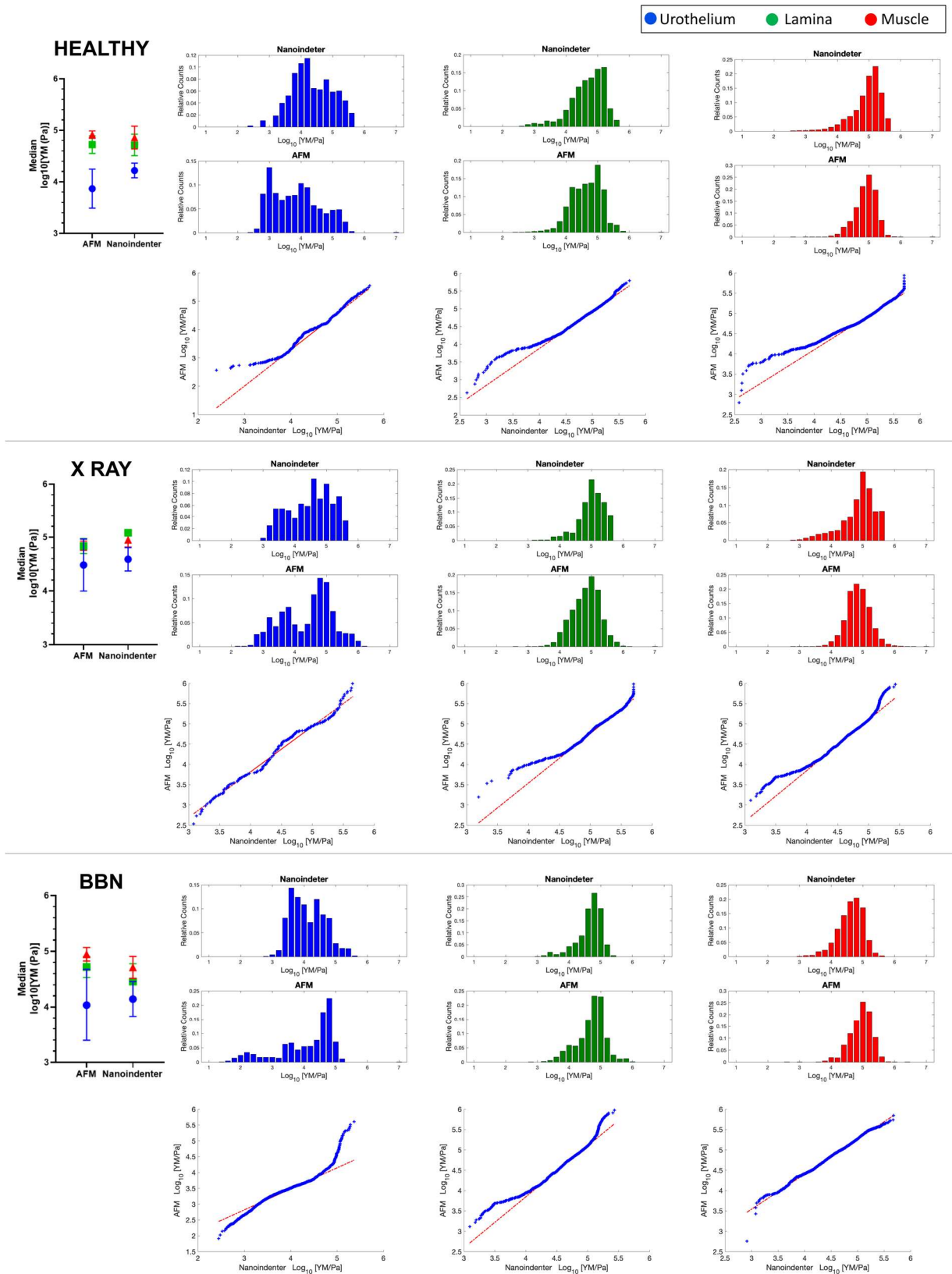


Figure 18 . Representation of YM data extracted by the two instruments (AFM and nanoindenter) of each single tissue layer, at month 2, extracted from healthy, X-ray irradiated and BBN rats, shown as: mean of the median values, distribution of single YM values, and quantile-quantile (QQ) plots comparing the two distribution.

5.1.3. The healthy bladder exhibits temporal evolution in tissue elasticity (stiffening) among aging of the adult animal

In order to provide an accurate comparison of the bladder mechanics during disease progression in the rat model versus healthy animals, we here characterized the evolution of healthy bladder YM throughout aging process of the animals during their adult life (i.e., from 4 months old, which equals 2 months post treatment, to 8 months old, that corresponds to 6 months post treatment). Aging of the animals among their adult life results in an overall stiffening of the bladder tissue (**Figure 19a**). Of interest, focusing on each tissue layer such a tendency was confirmed. Indeed, the urothelium exhibited a very wide distribution of values, which shifted towards higher values with aging: at Month 2 we can appreciate that the urothelium exhibited a bimodal distribution, which moved towards higher values at Month 6, and the stiffer population got enriched. It could be observed that the highest peak of the urothelium distributions overlapped with the peak of the lamina propria, indicating that the boundaries between the different tissue layers are divided by stiffness transitions, rather than drastic and well separated tissue boundaries.

Similarly, the lamina propria followed the same tendency: at Month 2 the mean of the median values is $4.72 \pm 0.2 \text{ Log}_{10}(\text{YM}/\text{Pa})$, up to $5.18 \pm 0.25 \text{ Log}_{10}(\text{YM}/\text{Pa})$ at Month 6 (**Figure 19b**). Likewise, YM increased with aging also for the muscle tissue, and at Month 6 it exhibited a bimodal distribution. Such increase of stiffness does not correlate with an increase of collagen within the bladder tissue (**Figure 19c**).

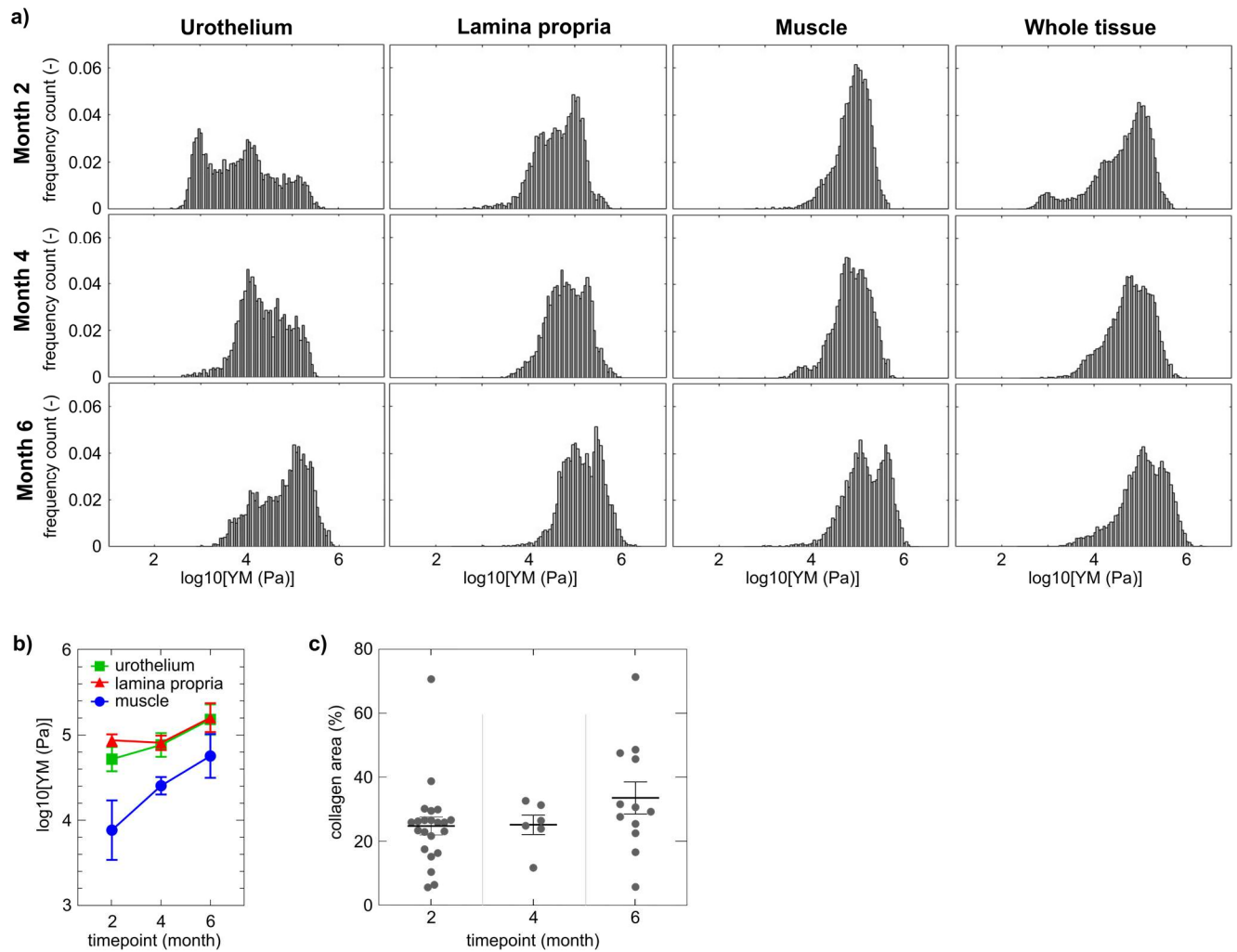


Figure 19. Micromechanical map of healthy bladder wall and aging effect on stiffness. a) Evolution of the stiffness of the different bladder tissue layers (urothelium, lamina propria and muscle) with aging of the adult animal (AFM and nanoindenter data pulled together). The distribution of YM values for the whole tissue (i.e. all layers together) is also shown. N = 3 rats per time point, each tissue layer of each single rat is characterized by over 3000 force curve measurements. Data shown are logarithm in base 10 of YM's (in Pa). b) Mean of the median values of each rat \pm SEM. Non parametric Mann Whitney test showed no statistical significant differences when comparing the different tissue layers at the studied time points. c) Quantification of the bladder area that expresses collagen from control rats at different time points; each symbol represents the measurement in a tissue slice, with multiple slices measured for each bladder, in three animals.

5.1.4. Microscale mechanics in the actinic cystitis model and during disease progression

X-ray irradiated animals developing actinic cystitis were used as model to characterize the mechanical fingerprints of fibrotic bladder tissue (**Figure 20a**). X-ray irradiation resulted in an increase of frequency in micturition and a decrease of the urine volume per each micturition (**Figure 20b,c,d,e**).

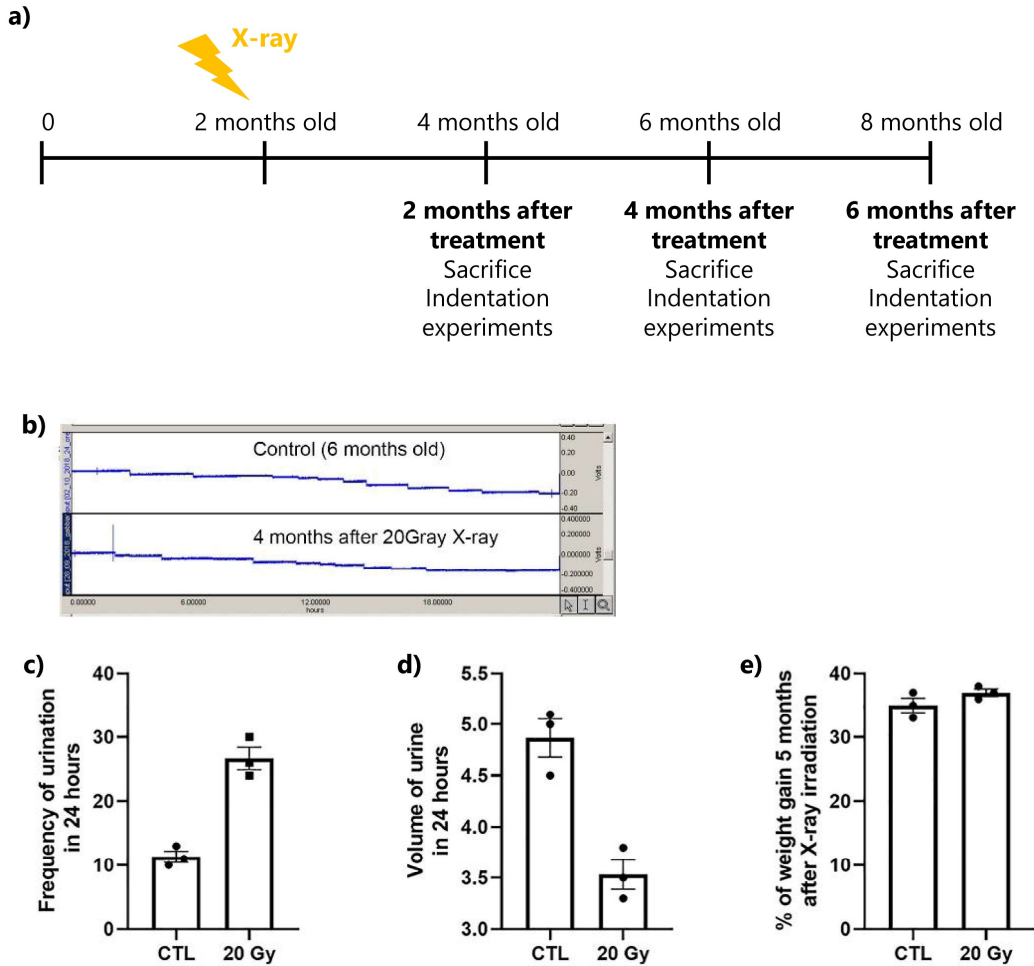


Figure 20. Murine model of actinic cystitis (X ray radiation). a) Schematic representation of the experiment: X-ray radiotherapy is used to induce actinic cystitis on the bladder. Rats are sacrificed at different time points and tissue elasticity is assessed. b) Micturition in X-ray irradiated rats: Frequency and urine volume were monitored for 24 hours using metabolic cages connected with AC/DC strain gage amplifier (model CP122, GRASS Instrument Division, Astro-Med Inc., West Warwick US); one representative animal each condition is shown. Frequency of urination (c), urine volume (d) and percentage of weight gain (e) are shown for 3 animals each condition.

Such biological effect was accompanied by elasticity alterations: irradiation induced actinic cystitis as a consequence of bladder fibrosis and a more dense ECM deposition, which on the one hand resulted in an increase of bladder wall stiffness, but on the other the elasticity gradient within the bladder wall was maintained (urothelium was characterized by lowest YM, which increased over lamina propria and further decreased when reaching the outer muscle layer) (**Figure 21**).

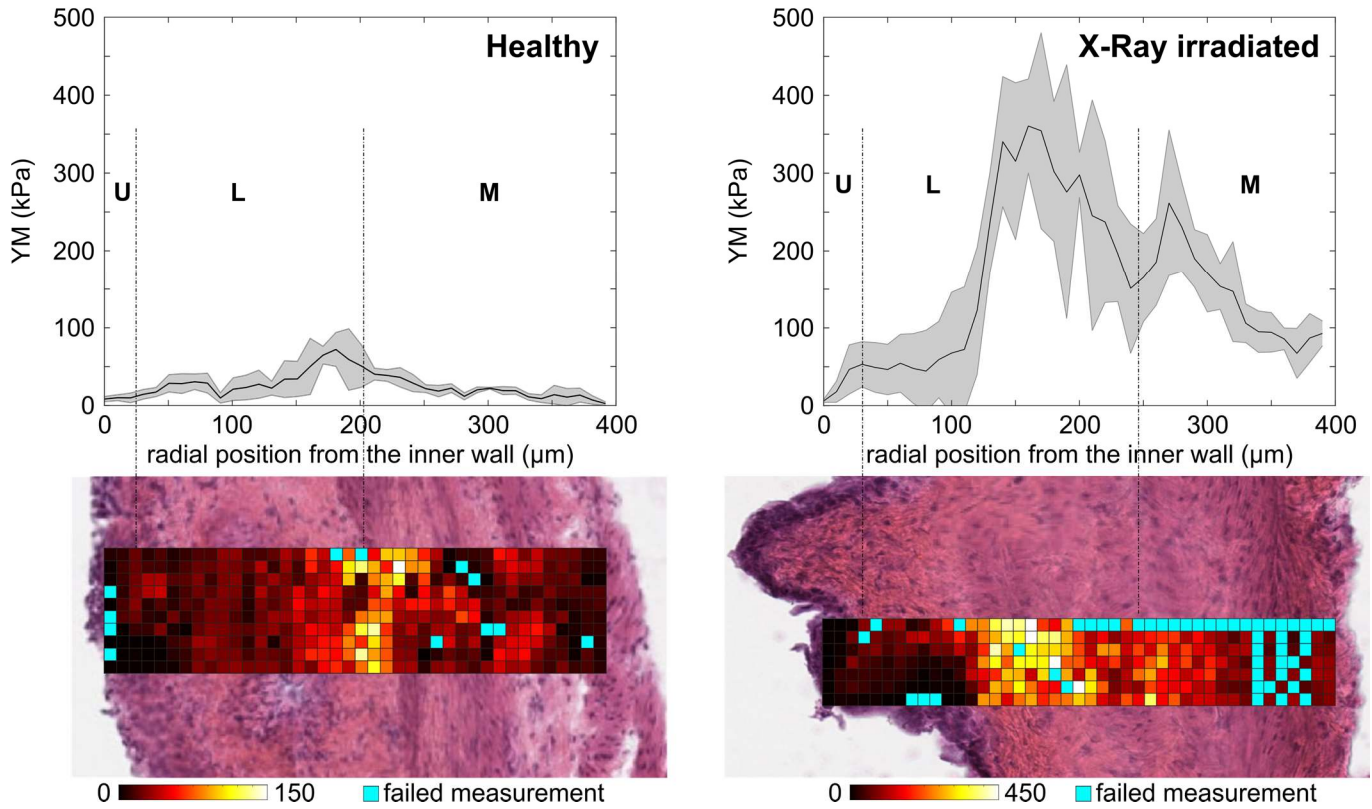


Figure 21. Representative bladder wall stiffness gradient collected with the nanoindenter at month 4. Bottom micromechanical maps obtained with nanoindenter and overlap with HE staining. Graph on the top represent the mean of each horizontal line of YM pixel values from the map \pm standard deviation of the mean in gray shade. X-ray caused a stiffening of the whole bladder wall compared to non-treated healthy animals. Mechanical spatial differences within the fibrotic bladder are maintained and associated to the different tissue layers (U: urothelium, L: lamina propria, M: muscle).

To characterize the kinetics of YM after irradiation, bladder elasticity of irradiated animals at different time points after treatment was analyzed and compared to those of healthy animals of the same age. Two months after treatment, the urothelium was the tissue component which mostly responded to irradiation, as it is evidenced both when comparing the histogram distribution of the data (**Figure 22a**), as well as the fold change of the mean respect to controls (**Figure 22b**). The lamina propria showed a slightly narrower distribution as compared with controls of the same age (**Figure 22a**), accompanied by increased collagen deposition respect to control animals (**Figure 22d**). The muscle does not show differences at this time point.

Four months after the irradiation treatment the urothelium exhibited a large spread of moduli comparable to the control of the same age (**Figure 22a**). In contrast, both lamina propria and muscle layers appeared to be particularly responsive to the fibrotic process: indeed, both appeared stiffer and more narrowly distributed than their healthy counterparts (**Figure 22a**). Similarly, higher mean values were observed compared to the previous time point (**Figure 22c**). When comparing mean of the median values of the distributions to healthy counterparts, the lamina propria and muscle were stiffer (**Figure 22b**), stiffening that associates with an increased collagen deposition on the fibrotic bladders (**Figure 22d**).

When comparing the YM profile from Month 4 to Month 6, the distributions did not shift significantly towards higher YM values (**Figure 22a**), suggesting that the damage remains stable over time and does not further cause stiffening at the later time point (**Figure 22c**). Indeed, due to the bladder physiological aging that results in stiffening, differences on irradiated and healthy animals were less drastic in older animals, as the treatment effect was likely masked by the aging of the animals and stiffening was only reported for the urothelium (**Figure 22b**). Collagen quantification in the tissue from irradiated animals showed an increase in collagen deposition compared to non-treated animals at Month 2 and Month 4, but not at Month 6 (**Figure 22d**). Nevertheless, older treated animals exhibit a less broad distribution, suggesting that the decrease in stiffness heterogeneity is caused by the replacement by collagen of tissue components due to a fibrotic response.

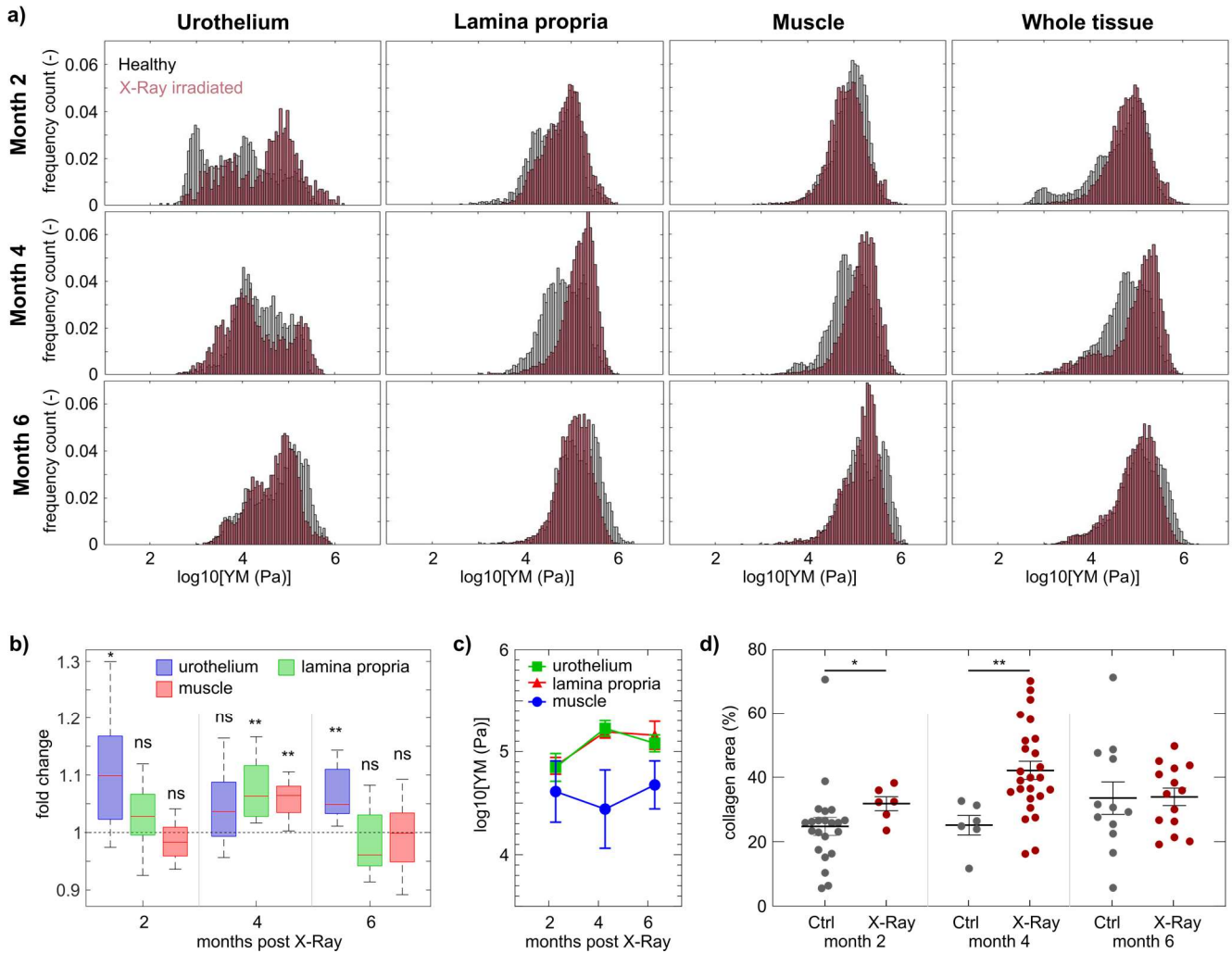


Figure 22. Micromechanics of murine bladder in a model of actinic cystitis (X ray radiation).

a) Kinetics of YM from X-ray radiated bladders at different time points (red) and comparison to healthy animals of the same age (grey) measured both with nanoindenter and AFM. N = 3 rats per time point and condition, each tissue layer of each single rat was characterized by over 3000 force curve measurements. Data shown are logarithm in base 10 of YM's (in Pa). b) Fold of change of mean of the median log₁₀ YM values of tissue layers of treated rats respect to age-matched control rats. T-test showed statistically significant stiffening with respect to the control animals (mean ± standard deviation with propagated error are shown. ns=not significant, *=p-value<0.05, **=p-value<0.005). c) Mean of the median log₁₀ YM values of tissue layers of each rat ± SEM. 2-way Anova showed no statistical significant differences in kinetics of fibrosis development. d) Quantification of the bladder area that expressed collagen from control rats and X ray-irradiated animals at different time points; each symbol represents the measurement in a tissue slice, with multiple slices measured for each bladder, in three animals.

Interestingly, I observed that the micromechanical profile of one of the irradiated animals did not show any effect in terms of stiffening, and it was comparable to those of the control healthy animals of same age (4 months after treatment) (**Figure 23a**). After following histological analysis and fibrosis evaluation, we confirmed that this specific animal had not developed bladder fibrosis (**Figure 23b**), therefore highlighting the potential of microindentation to detect fibrosis caused by irradiation, and showing that stiffening is not detected by microindentation in the absence of histological fibrotic ECM deposition.

Effect by X-ray

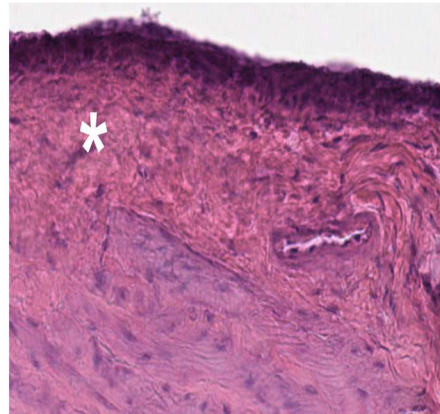


Figure 23. Animal not responding to X-ray treatment. a) The micromechanical profile (blue) was comparable to those of control healthy tissues of the same age (4 months after irradiation) (grey). b) The histological analysis showed denser deposition of ECM (*) in an X-ray responding animal (left) accompanied by increasing of stiffness. Histology on the bladder with no stiffening (right) revealed absence of fibrotic damage (4 months after irradiation).

5.1.5. Bladder cancer tissue elasticity

5.1.5.1. Lessons learned from the BBN murine model: microscale mechanics in the orthotopic bladder cancer model and during disease progression

In order to study the effect of tumor development and progression on bladder mechanics, the evolution of bladder elasticity was studied on an orthotopic rat model, in which rats were watered with water containing the bladder specific carcinogen nitrosamine (BBN) (**Figure 24a**). This model allows to monitor for all stages of bladder cancer establishment and progression, mimicking the pathological processes that happen in humans.

After 2 months of BBN treatment, bladder tissues presented low grade dysplasia, which means there are epithelial cells with abnormal organization (**Figure 24b**). The presence of abnormal cells was limited to the urothelium, which increased its thickness and cellularity, without invading the lamina propria below. Furthermore, the BBN activates inflammation pathways in the bladder. At this stage, dysplastic bladder tissues were characterized by elasticity alteration of the urothelium (**Figure 25a**), which correlated with broadening of the cell layer and presence of abnormal cells (**Figure 24b**). The lamina propria and muscle layers exhibited YM profiles equivalent to those of control animals of the same age, and the overall tissue did not differ significantly from healthy bladder tissue.

After 4 months of BBN treatment, the bladder tissues exhibited non-invasive tumors localized in the urothelium (pTa), and there were few points of focal invasion in which few groups of cells invaded superficially the lamina propria below (pT1) (**Figure 24c**). These bladder tissues showed a softening in the urothelium compared to controls (**Figure 25a**) of 0.81 fold change (**Figure 25b**), as well as in the lamina propria which exhibited a very broad stiffness distribution (0.78 fold change). It could be appreciated that the elasticity distribution of the muscle slightly started to shift towards lower YM values in comparison with the healthy muscle, with a fold change of 0.87 respect to control muscle tissue, even though cancer cells did not invade this tissue layer yet. YM distribution of the whole tissue was characterized by a bimodal profile: one lower peak which corresponded to the presence of tumor cells in the urothelium and in the lamina propria, and a stiffer peak that corresponded to the muscle tissue layer without the presence of tumor cells, which partially overlapped with the healthy tissue (**Figure 25a**).

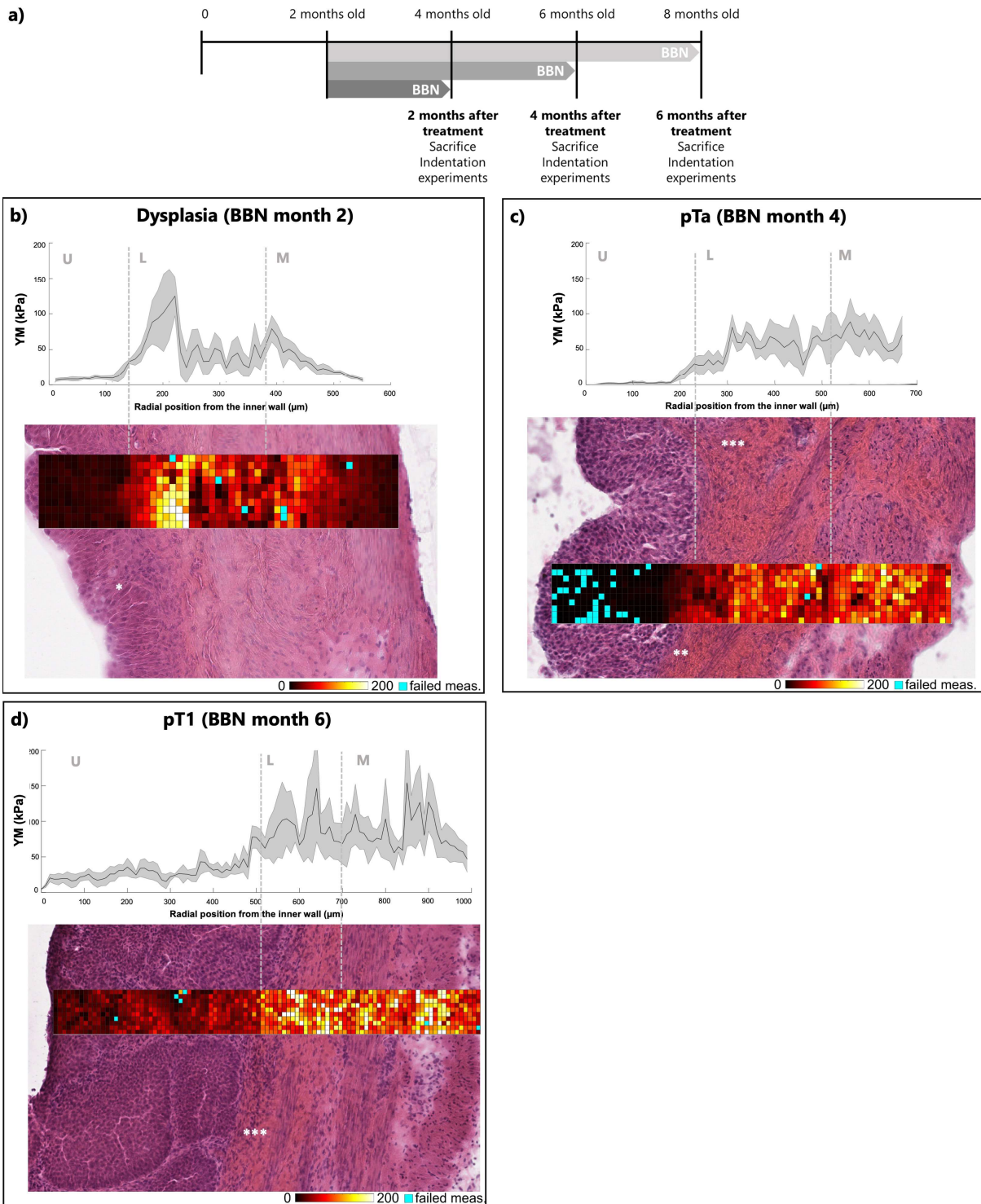


Figure 24. Murine model of bladder cancer (BBN). a) Animal model establishment. Representative bladder wall stiffness gradients collected with nanoindenter at b) 2 months of BBN treatment, where urothelium dysplasia is marked by *; c) 4 months of BBN treatment, where Ta tumor limited to the urothelium without invading the lamina propria is marked by **. T1 tumors in which urothelial tumor cells break the basal membrane and invade the lamina propria below at 4 and d) 6 months BBN treatment are marked by ***. U: urothelium, L: lamina propria, M: muscle.

After 6 months of BBN treatment tumor cells were present in the lamina propria (pT1) (**Figure 24d**). Also, at this time point the treated bladders were characterized by elasticity distributions shifter towards softer values for urothelium and lamina propria (**Figure 25a**). The muscle tissue exhibited a bimodal distribution with one peak shifted towards lower values and a second peak that overlapped with those of healthy bladder (**Figure 25a**). Likely due to the physiological aging of the animals leading to increase in tissue elasticity, fold change respect to controls were less dramatic, being the lamina 0.93 softer and muscle 0.90 softer (**Figure 25b**). I hypothesized that the main contributor to this bladder softening was the presence of tumor cells within the tissue, which are widely known to be softer than their healthy counterparts. Nevertheless, softening of the different layers was detected prior to tumor cell invasion (for lamina and muscle at month 4, and for muscle at month 6). Overall, the neoplastic microenvironment was softer than those of healthy animals, even when such softening effect was combined with the physiological aging of these animals.

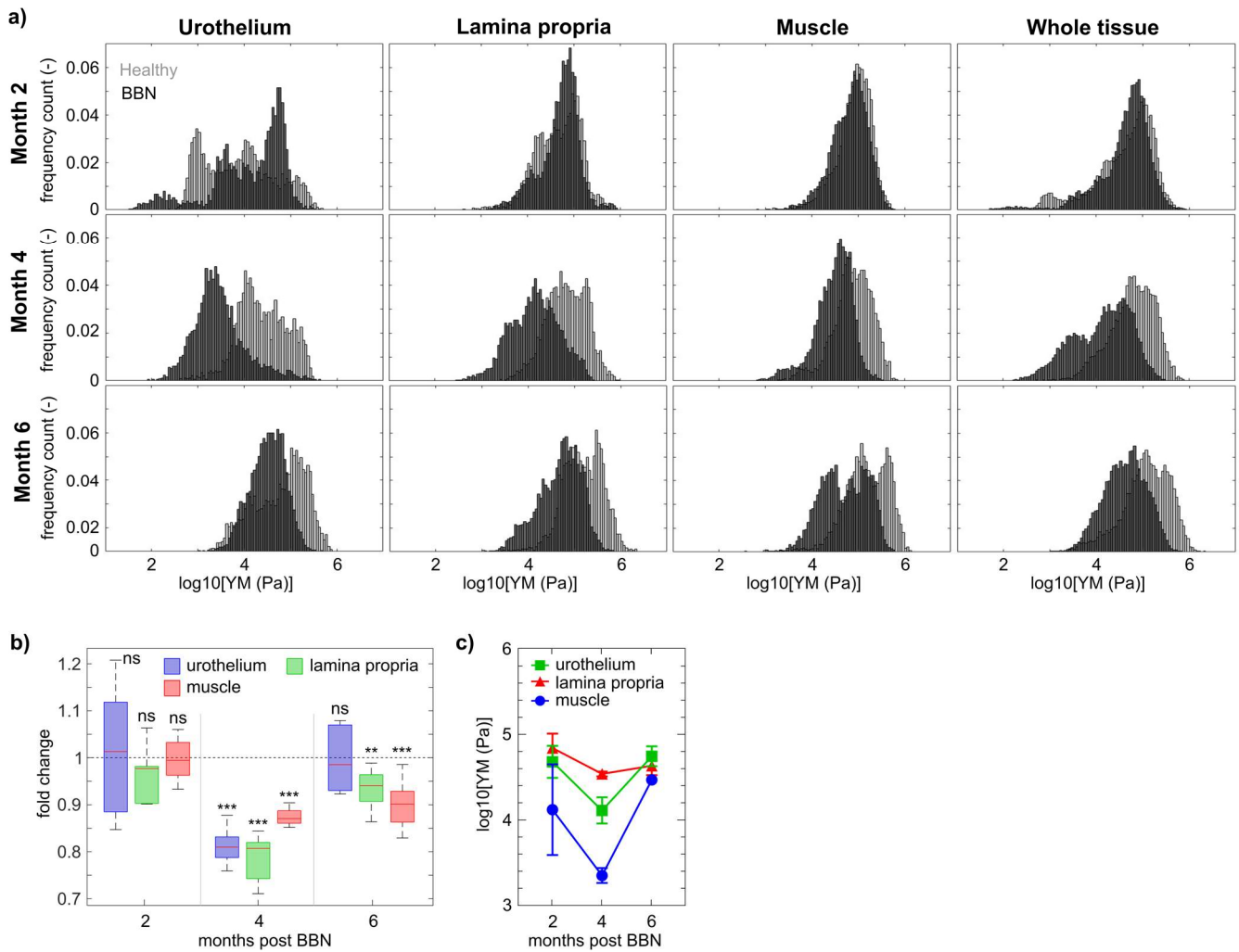


Figure 25. Micromechanics of BBN model. a) YM's from BBN treated bladders (black) at 2 months, 4 months and 6 months of BBN treatment; and comparison to healthy animals of the same age (grey) measured both with nanoindenter and AFM. $N = 3$ rats per time point and condition, each tissue layer of each single rat is characterized by over 3000 force curve measurements. Data shown are logarithm in base 10 of YM's (in Pa). b) Fold of change of mean of the median \log_{10} YM values of treated rats \pm standard deviation (with propagated error) respect to control rats. T-test showed statistically significant softening with respect to the control animals (mean \pm standard deviation with propagated error are shown. ns=not significant, *=p-value<0.05, **=p-value<0.005, ***=p-value<0.0005). c) Mean of the median values of each rat. 2-way Anova showed that statistically significant differences in the BBN model were observed in the urothelium from month 2 to month 4, and from month 4 to month 6; and for the lamina propria from month 4 to month 6.

5.1.5.2. *A preliminary mechanical fingerprint of high-grade human urothelial carcinoma*

Once studied bladder tumor mechanics on murine model that allows for closer follow up of earlier stage tumors, I characterized the micromechanical profile of a high-grade MIBC from a patient that underwent radical cystectomy. In this context, I investigated paired surgical samples including the muscle tissue infiltrated by neoplastic cells and the non-invaded muscle tissue (**Figure 26a**). This strategy allows to characterize neoplastic vs non-neoplastic tissue, but avoiding variability between donors. Normal muscle tissue was characterized by a YM that follows approximately a Gaussian distribution after logarithmic transformation, with median value of 3.52 $\text{Log}_{10}(\text{YM}/\text{Pa})$ (33 kPa in linear scale), while neoplastic infiltration of tumor cells on the muscle tissue resulted in an increase of the mechanical heterogeneity and an overall softening of the tissue (median value of 3.28 $\text{Log}_{10}(\text{YM}/\text{Pa})$, 2 kPa in linear scale) (**Figure 26b**).

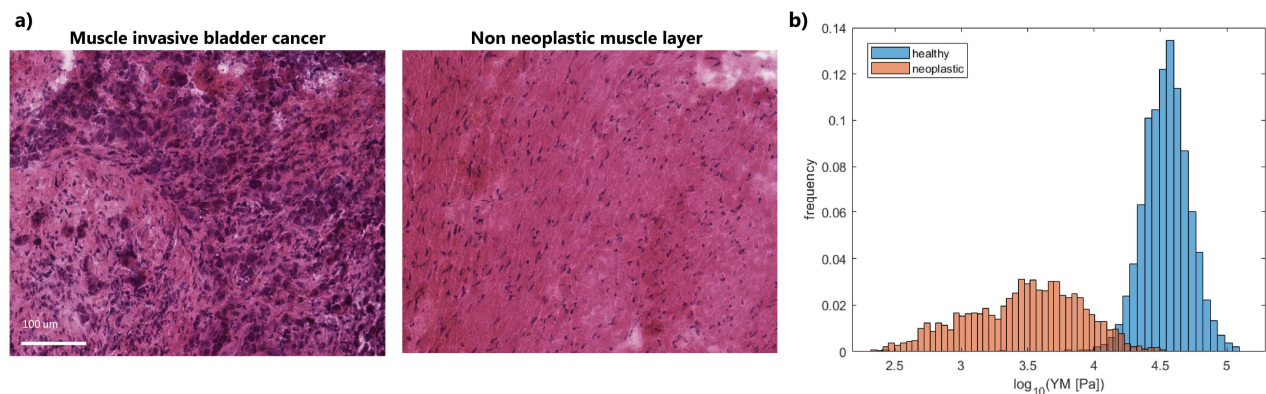


Figure 26. Micromechanics of bladder cancer patients. a) Hematoxylin-eosin staining of muscle invasive bladder cancer and paired non-neoplastic muscle tissue from a patient with high-grade urothelial carcinoma. b) Mechanical profile of neoplastic (orange) and non-neoplastic (blue) muscle tissue from the same patient ($n = 1$). Data collected with the nanoindenter. Data are shown as logarithm in base 10 of YM's (in Pa).

5.2. Chapter 2. Towards a more clinical set-up – micromechanical fingerprints of bladder in health and disease by Brillouin imaging. Indentation vs spectroscopy based techniques

AFM-based indentation is the gold standard technique widely used in mechanobiology to investigate mechanical properties of biological systems. Brillouin microscopy is a non-contact imaging technique, whose biological applications are emerging on the mechanobiology field to assess biomechanics of different tissues and pathological conditions. After deeply characterizing healthy, fibrotic and bladder cancer tissues by microindentation, this present chapter addresses the validation of such observations on healthy and fibrotic tissues by Brillouin imaging. This would allow not only to validate the here previously reported results, but also to decipher whether this non-contact technique has the potential to be translated into the clinics, as the interaction with the tested sample is only by means of light, which means that it could eventually be used in more various sample types and not necessarily fresh tissue samples to investigate tissue mechanics.

Here, by exploiting a custom-built Brillouin Microscope, I provided data on Brillouin shift on bladder tissues in healthy and fibrotic conditions, in order to establish associations between mechanical properties of bladder and the fibrotic damage induced by irradiation. I also investigated the physiological effect of aging on bladder mechanical properties. Finally, I compared the acquired Brillouin maps to microindentation-based mechanical measurements performed on the same sample and find correlations and anti-correlations between the two techniques, shedding light on YM and Brillouin shift relation in tissues.

5.2.1. Brillouin imaging of the healthy bladder wall

Murine bladder mechanical properties were evaluated by Brillouin microscopy. From **Brillouin shift (v_B) maps**, biomechanical features of bladder walls of healthy rats were recovered in a label-free and contact-less fashion while tissues were kept fresh and hydrated. Bladder walls were evaluated in different regions per slice, whose location under the microscope was achieved by optical transmission microscopy in differential interference contrast (DIC) mode, and Brillouin maps covering the whole width of the bladder wall were collected with a sub-micrometric spatial resolution, a resolution much more accurate than the macroscopical ones available with other techniques (**Figure 27a**).

I found out that the inner tissue layer - the urothelium - exhibited the lowest Brillouin shift values (ranging from 7.5 to 8.3 GHz, that are typical values of Brillouin shift for cells (Scarcelli *et al*, 2015)). When moving towards the middle layer of the bladder wall - the lamina propria - a sharp increase in Brillouin shift occurred: this region of the bladder was highly heterogeneous in v_B , reaching its maximum at values as high as 10 GHz. Overall, healthy bladder lamina propria's Brillouin shift was highly heterogeneous and had values distributed from 7.5 to 10.5 GHz (**Figure 27a**), a range that is much higher than the urothelium one and that is consistent with other ECM v_B values previously reported (Ryu *et al*, 2021). The muscle layer of the bladder was characterized by a Brillouin shift that ranged from 9 to 9.2 GHz; finally, the shift decreased in the perivesical fat layer of the bladder.

An important difference between DIC and Brillouin shift images was clearly visible from these data (**Figure 27a**): DIC showed very little contrast and poor sensitivity to sample morphology, while Brillouin imaging allowed for optimal differentiation of anatomically different parts of the specimen, confirming its use as a cutting-edge imaging technique for biological systems. Indeed, raw Brillouin spectra of different parts of the specimen highlighted the sensitivity of the technique to their various biophysical components with high signal-to-noise ratio (yellow and red dots in (**Figure 27b**)); moreover, PBS buffer Brillouin spectrum (blue spot in (**Figure 27b**)) presence confirmed that the tissue was kept hydrated during the whole acquisition.

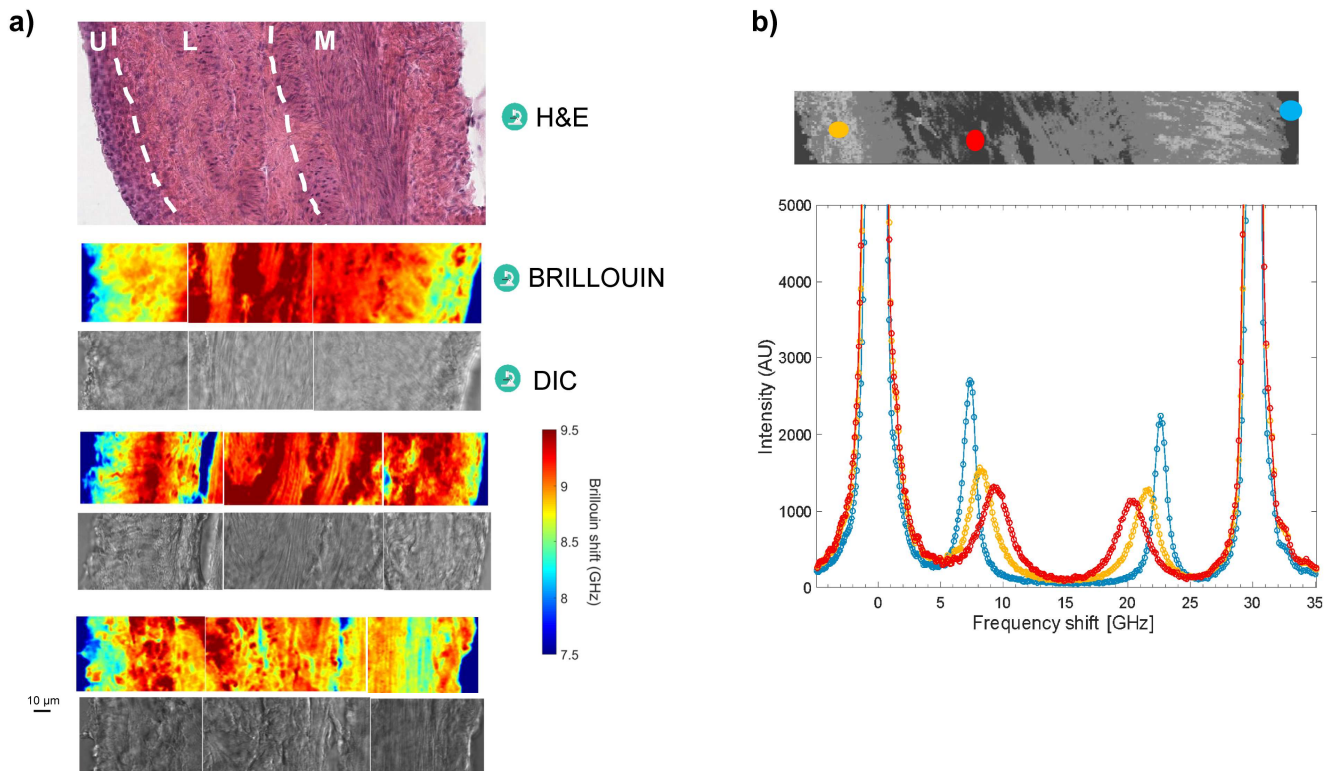


Figure 27. Brillouin imaging of the healthy bladder wall. a) HE staining of the healthy bladder wall (top), the different anatomical tissue layers are indicated by U: urothelium, L: lamina propria, M: muscle. DIC images and corresponding Brillouin maps of the whole width of the healthy bladder wall, from urothelium (left) to muscle (right). Scale bar = 20 μm. c) Raw Brillouin data spectra of different parts of an image shown in panel b, shown here in grayscale. The blue spot is located in the vicinity of the sample, and in blue it is shown the raw spectra of PBS buffer, similar to water ($v_B = 7.51 \pm 0.03$ GHz). The yellow spot located in the urothelium and in yellow the corresponding raw spectra of urothelium ($v_B = 8.25 \pm 0.04$ GHz). The red dot is located in the lamina propria, and in red its corresponding raw spectra of the stiffest part of lamina propria layer ($v_B = 9.72 \pm 0.02$ GHz).

In order to account for possible aging effects on bladder mechanical properties, healthy bladder tissues belonging to rats of different ages (namely 2, 4 or 6 months) were characterized by Brillouin imaging (**Figure 28**). I observed that physiological aging among the adult life of the animals resulted in a slight shift of ν_B towards higher values from Month 2 to Month 4 and Month 6. Histograms recapitulating mechanical properties of Month 4 and Month 6 were quite similar and differences between these two time points were minor (**Figure 28b**).

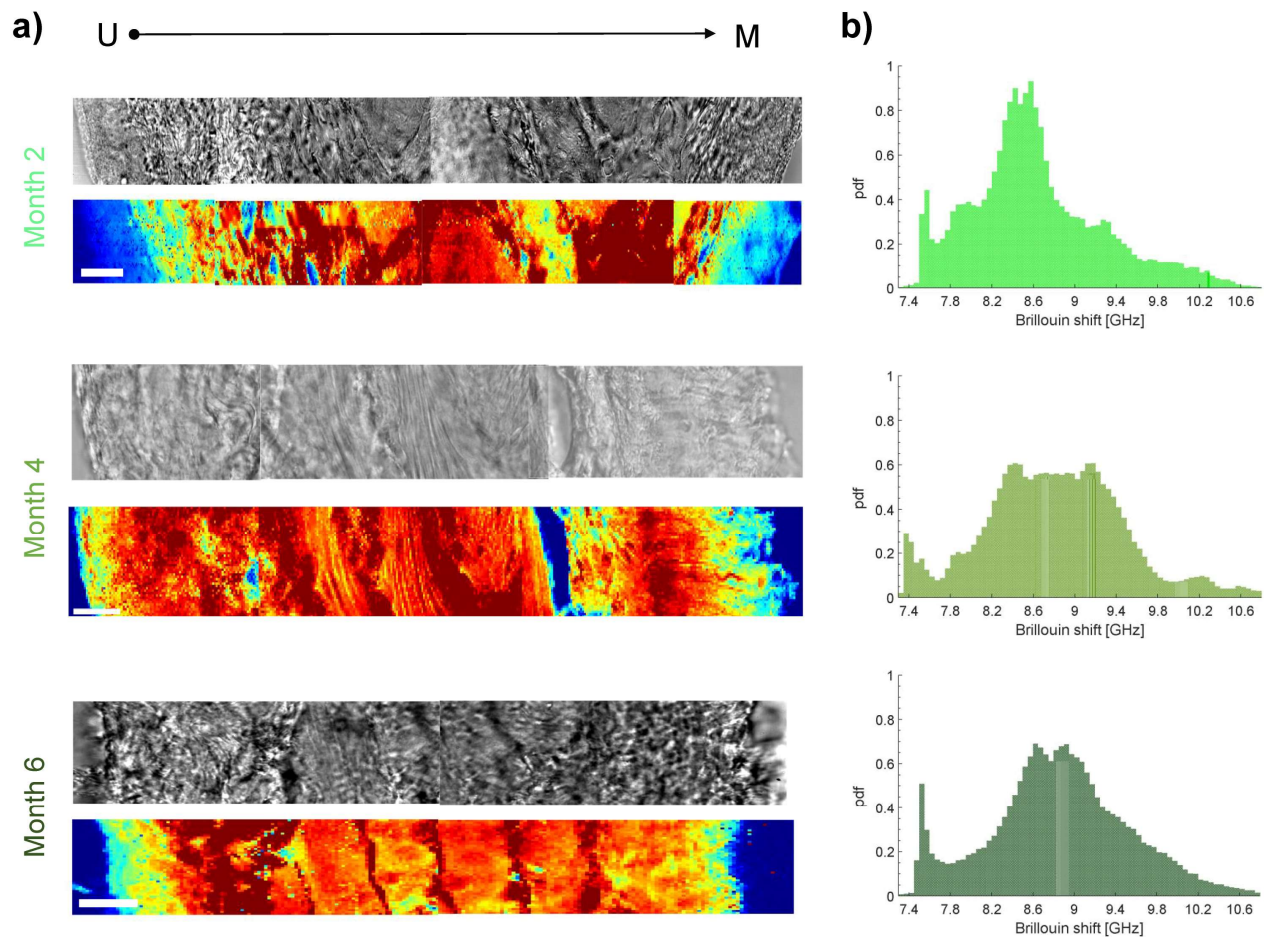


Figure 28. Brillouin imaging of healthy bladder wall at different ages of the adult rat life. a) Representative healthy bladder Brillouin shift maps at Month 2, 4 and 6, from urothelium (left) to muscle (right). b) Histogram representation of evolution of bladder mechanics with physiological aging of the adult rat.

5.2.2. X-ray irradiation causing actinic cystitis resulted in a decrease of tissue Brillouin shift and lowered the Brillouin shift heterogeneity respect to healthy animals

Mechanical properties of irradiated bladders that developed fibrosis were here characterized by Brillouin imaging (**Figure 29**). Fibrotic remodeling of the bladder resulted in an overall decrease of v_B of the bladder wall in comparison to healthy animals of the same age, while the gradient from urothelium to lamina propria and muscle was maintained (**Figure 29a**), in particular, the longer the time since irradiation, the lower the Brillouin shift (**Figure 29b**). Moreover, Brillouin shift distributions of fibrotic animals were less broad than the wild-type ones, and tended to be bi- or single-modal. At Month 6, this peak collapsed towards 8.3 GHz, a peak common to all conditions (**Figure 29b**).

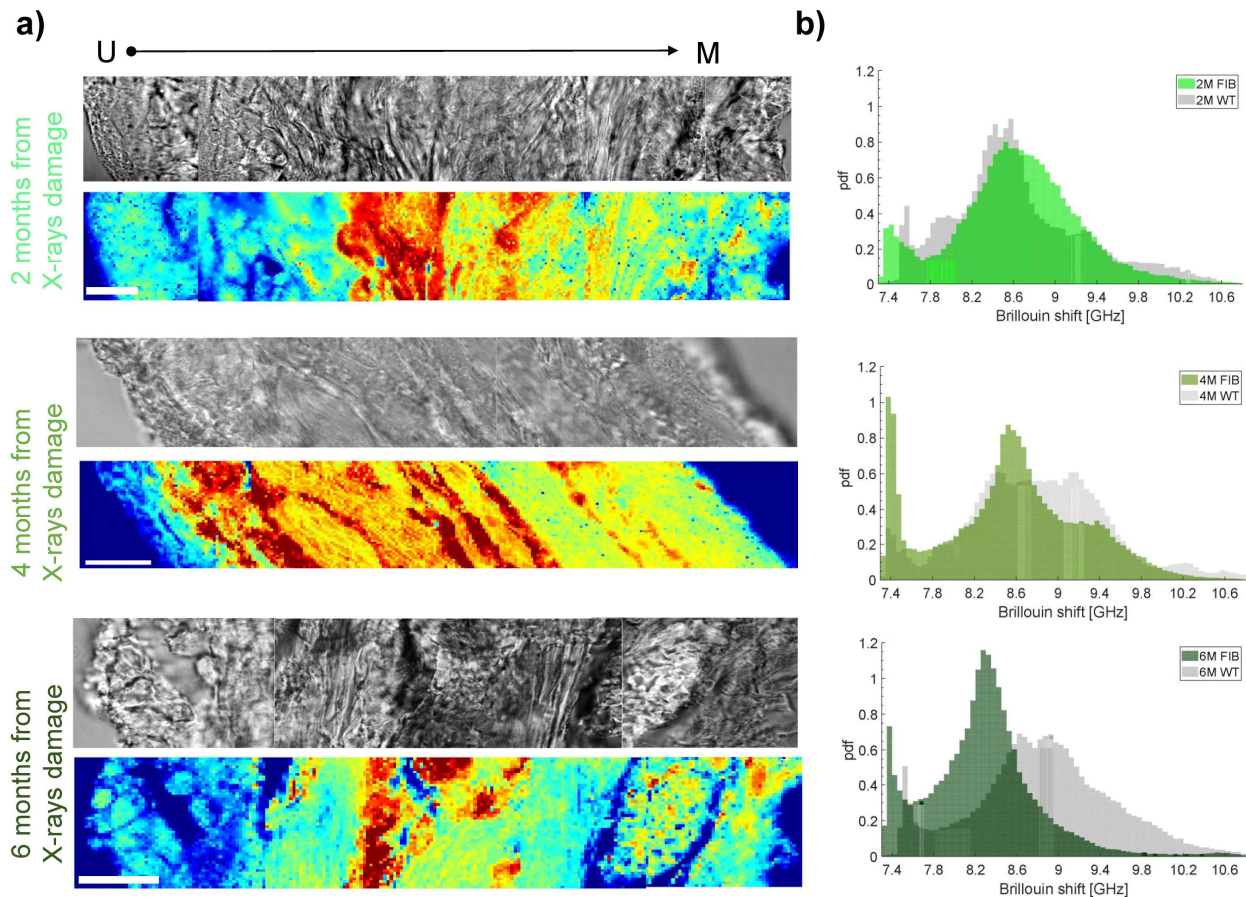


Figure 29. Micromechanics of murine bladder in a model of actinic cystitis (X ray radiation). a) Representative Brillouin maps of fibrotic bladder at Month 2, 4 and 6, from urothelium (left) to muscle (right). b) Kinetics of bladder tissue elasticity from X-ray irradiated rats at different time points (green histograms) and comparison to healthy animals of the same age (grey histograms) by Brillouin imaging.

6. Discussion

This study details the mechanics of the three tissue layers of bladder at microscale level, thus unveiling the heterogeneity in terms of elasticity of the three tissue layers, tissue stiffening for actinic cystitis and softening of all three layers during the onset and progression of bladder cancer. By providing mechanics characterization at the microscale level, here we provide novel information regarding changes in the neoplastic environment according to the way of invasion of bladder cancer that is by single cells or small cluster of cells.

To the best of my knowledge, in this study I performed the first spatial and temporal micro-mechanical mapping of the whole bladder wall, with micron-level spatial resolution, both in health condition, actinic cystitis and bladder cancer. The indentation methodology here used was first AFM, the gold standard in mechanobiology to investigate cell mechanics. Nevertheless, the investigation of the mechanical properties of tissues needs to deal with bigger sampling regions, which means increased testing scale, surface roughness and mechanical heterogeneity of the sample. This requires first, increased Z piezo range, and second, closed indentation loop to measure all mechanical heterogeneities (to probe very soft and very stiff regions within a big sampling area). On the other hand, nanoindentation-based mechanics investigation has been previously reported to suffer from replication issues, which has been overcome at the cell scale (Schillers *et al*, 2017), but not yet at the tissue scale. Thus, aiming to overcome the technical challenges of testing such complex samples and increase the robustness and reproducibility of our results, as well as its eventual translation to the clinics, I here combined two indentation-based instruments: AFM and a nanoindenter, which overcomes such technicalities and allowed for validation of our own data.

I demonstrated that the bladder wall is a highly mechanical heterogeneous tissue, characterized by a gradient of stiffness from urothelium to lamina propria and muscle layer. I also showed an effect of aging on tissue mechanics, which is known to alter murine bladder histology (Al-hayyali, 2020). Understanding tissue mechanics and the distribution corresponding to different anatomical tissue layers - as it was previously reported for organs as the cornea (Last *et al*, 2012) or the skin (Kao *et al*, 2016) - is also of relevance for the bladder, as its physiological function

comprehends high elastic tension and mechanical stress, and it may be crucial for bladder reconstruction purposes.

Fibrosis results from the pathological accumulation of ECM proteins due to chronic inflammation, resulting in scarring and thickening of tissue and, finally, in organ failure (Mangano *et al*, 2018). We used X-ray irradiation to establish an animal model of actinic cystitis, in order to characterize the mechanical fingerprints of fibrotic bladder tissue. By using the histogram representation of the YM I identified stiffening of the urothelium 2 months after irradiation, suggesting that the main effect of irradiation was on the cells, which it is well known to induce cell apoptosis (Zhao, 2019), and apoptotic cells have been previously reported to be stiffer (Islam *et al*). At the second studied time point, i.e., 4 months, stiffening of the lamina propria and muscle occurred, in agreement with a previous study (Zwaans *et al*, 2022). The YM in 6-months irradiated animal did not change compared to the 4-months treated animal, while the mechanics of bladder in control animal increased from 4 to 6 months of age, masking the effect of the treatment.

The investigation of tissue elasticity by microindentation was also able to detect the absence of bladder fibrosis on an irradiated animal that did not develop actinic cystitis. This information supports the diagnostic potential of quantifying tissue elasticity at the microscale, which could be used to have more detailed information about the reactive stroma characteristic of fibrotic processes, which is usually investigated by histological techniques.

I also observed an increase in tissue compliance in the presence of bladder tumor, both in the rat model and in humans, similar to what has been reported for liver cancer tissues (Tian *et al*, 2013). In principle this observation may seem controversial and opposite to the general tendency of solid tumors (i.e., breast (Plodinec *et al*, 2012) and lung (Friedl *et al*, 2012) cancer, dominated by collective cell invasion (Ilina *et al*, 2018)), where stiffening usually takes place. Tissue stiffening is also observed when studying urological organs as the prostate or the testis by non-invasive macroscale techniques (Martinez-Vidal *et al*, 2021). Nevertheless, by providing spatially resolved micro-mechanical maps, we here were able to measure the contribution to tissue elasticity both from cells and ECM. In the MIBC tumor we found an increase in the heterogeneity of the elasticity of the tissue when the tissue is invaded by neoplastic cells, as previously reported for breast cancer (Plodinec *et al*, 2012). In addition, it has been previously established that tumor cells are softer than

their benign counterparts, and that softening of cancer cells increases with increased malignancy (Lekka *et al*, 1999).

On the other hand, ECM stiffening is increasingly recognized as a major mechanical signal, which alters cell behaviour and in part confers cancer cell hallmark capabilities including sustained growth, invasion, and metastasis (Li *et al*, 2019). Such increase in ECM stiffness is mainly associated to increased collagen deposition (Oudin & Weaver, 2016; Ertler & Weaver, 2009) especially at the invasive front of tumors, which furthermore often corresponds to the stiffest region of the tumoral tissue (Acerbi *et al*, 2015). One example of tumoral fibrotic stroma is the case of breast cancer, in which breast tumors are characterized by increased collagen deposition together with increased linearization and thickening of collagen fibers (Provenzano *et al*, 2006, 2008). Those tumors characterized by fibrotic stroma deposition are known to be stiffer, as breast and pancreas (Whatcott *et al*, 2015). In addition, it has been reported for NMIBC patients an association with COL1A1 and COL1A2 (Brooks *et al*, 2016). Therefore, it would be eventually interesting to study decellularized bladder tissues to investigate the contribution of ECM to the whole organ stiffness, and study eventual associations with the increase in collagen expression reported in non-muscle invasive bladder cancer patients with poor prognosis (Brooks *et al*, 2016).

Furthermore, in bladder tumors, cancer cells migrate as single cells or small nests (Friedl *et al*, 2012), contrary to tumors in which stiffening is reported, e.g., breast, prostate and lung cancer (Friedl *et al*, 2012). Single cell invasion, can be divided into mesenchymal and amoeboid migration (Friedl *et al*, 2012). Few studies have shown that muscle invasive bladder cancer promotes enhanced contractility of cells using amoeboid migration, which contrary to mesenchymal migration, takes place when surrounding matrix is relatively soft (Krakhmal *et al*, 2015). By investigating elasticity profiles of bladder tumor in the rat model, we detected softening in those tissue layers under the tumor when the tumor did not invade yet. These results indicate that the tissue layers undergo mechanical remodelling being primed before it is invaded by the tumor cells, thus highlighting the clinical potential of measuring tissue elasticity by microindentation for early bladder cancer prognosis. This observation goes in line with a previous study, which reports that mechanical remodelling of tissue surrounding neoplastic cells precedes invasion in head and neck squamous cell carcinoma spheroids (Chen *et al*, 2019). Further tests on clinical specimens are needed to validate the information here obtained by investigating tissue mechanics using a preclinical model.

A limitation of this study is that bladder specimens were snap frozen prior to mechanical measurements. Even though there was no chemical treatment performed and samples were considered fresh/frozen, it cannot be excluded that the freezing/unfreezing procedure might include some artifact on the specimens, raising the possibility of selection biases. Aiming to reduce this effect we used a cryoprotectant (OCT) that protects the sample from ice crystal formation and used a snap freezing protocol. Furthermore, we here performed a comparative study between different conditions, therefore the samples were always subjected to identical protocol. Previous studies have shown little impact on the mechanical properties on freezing tissue (Delgadillo *et al*, 2010). However, working with frozen tissues has several advantages, and different AFM studies used fresh-frozen clinical specimens (Kao *et al*, 2016; Babu & Radmacher, 2019; Usukura *et al*, 2017; Grant *et al*, 2012; Graham *et al*, 2010). Furthermore, frozen tissue allows to prepare semi-thin sections, which allows histological analysis and correlation with histological examination.

Another limitation of this work has to do with the mechanical modeling: when estimating the elastic properties, we neglected viscous effects. We assumed the values we report can be considered characteristic of a low frequency material response, where viscous effects play a negligible role. Nevertheless, the YM only gives a partial insight into the mechanical response of the material. For example, a recent work (Tsvirkun *et al*, 2022) highlighted how different amounts of collagen affect both tissue stiffness and viscosity in cellular aggregates. Future studies should focus on the characterization of layer-specific viscoelastic effects.

The second part of this thesis focused on using Brillouin imaging to mechanically investigate bladder tissues in health and in the pathological condition of actinic cystitis. In order to characterize bladder mechanical properties by this spectroscopy based technique, I here used the same sample preparation protocol used to investigate bladder mechanical properties via microindentation techniques. In this way, I provided a robust experimental setup for comparing the results from the two different techniques, avoiding detecting different artifacts introduced by different sample preparation protocols that could eventually affect mechanical properties measured by the different techniques. In addition, I here analyzed adjacent tissue slices from the same bladder organ by the two different techniques, therefore investigating mechanical properties of the same region of the same organ.

The healthy bladder wall was characterized by a gradient of Brillouin shift, which revealed high mechanical heterogeneity of this tissue on its cross section, from the urothelium to the lamina propria and muscle layer. Such broad differences in mechanical properties between adjacent layers of bladder can be ascribed to their diverse biochemical scenario: cells are a mostly composed by water, while the lamina propria is an interlaced mesh of water, proteoglycans and fibrous proteins (as collagens, elastins...); and the outer layer of the bladder is formed by muscle bundles and fibers. A direct correlation between Brillouin microscopy and microindentation-based measurements on the intrinsic bladder wall mechanical properties was observed (**Figure 30a**): urothelium exhibited both the lowest YM and Brillouin shift, these parameters increased over the lamina propria and transiently decreased over the muscle layer, although their absolute values were completely different and non-comparable.

While we observed the same trend of tissue mechanical properties by microindentation and Brillouin when checking intrinsic variations within the bladder wall, opposite trends were observed when comparing healthy and fibrotic bladders (**Figure 30b**): while YM measured by microindentation increased after X-ray radiation-driven fibrosis, Brillouin imaging showed the opposite correlation, i.e. fibrotic tissues had lower Brillouin shift than non-treated animals, being this value lower the longer the time since X-ray irradiation. Alteration of murine bladder mechanical properties after actinic cystitis development has been previously described. In this study (Zwaans *et al*, 2022), by applying loading-unloading cycles of stretching, they reported that irradiated bladder ECMs were significantly less distensible than healthy ones at the macroscale. Such macroscopical mechanical test revealed that the changes were apparent at 3 months post-irradiation and statistically significant at month 6.

Brillouin microscopy

Microindentation-based

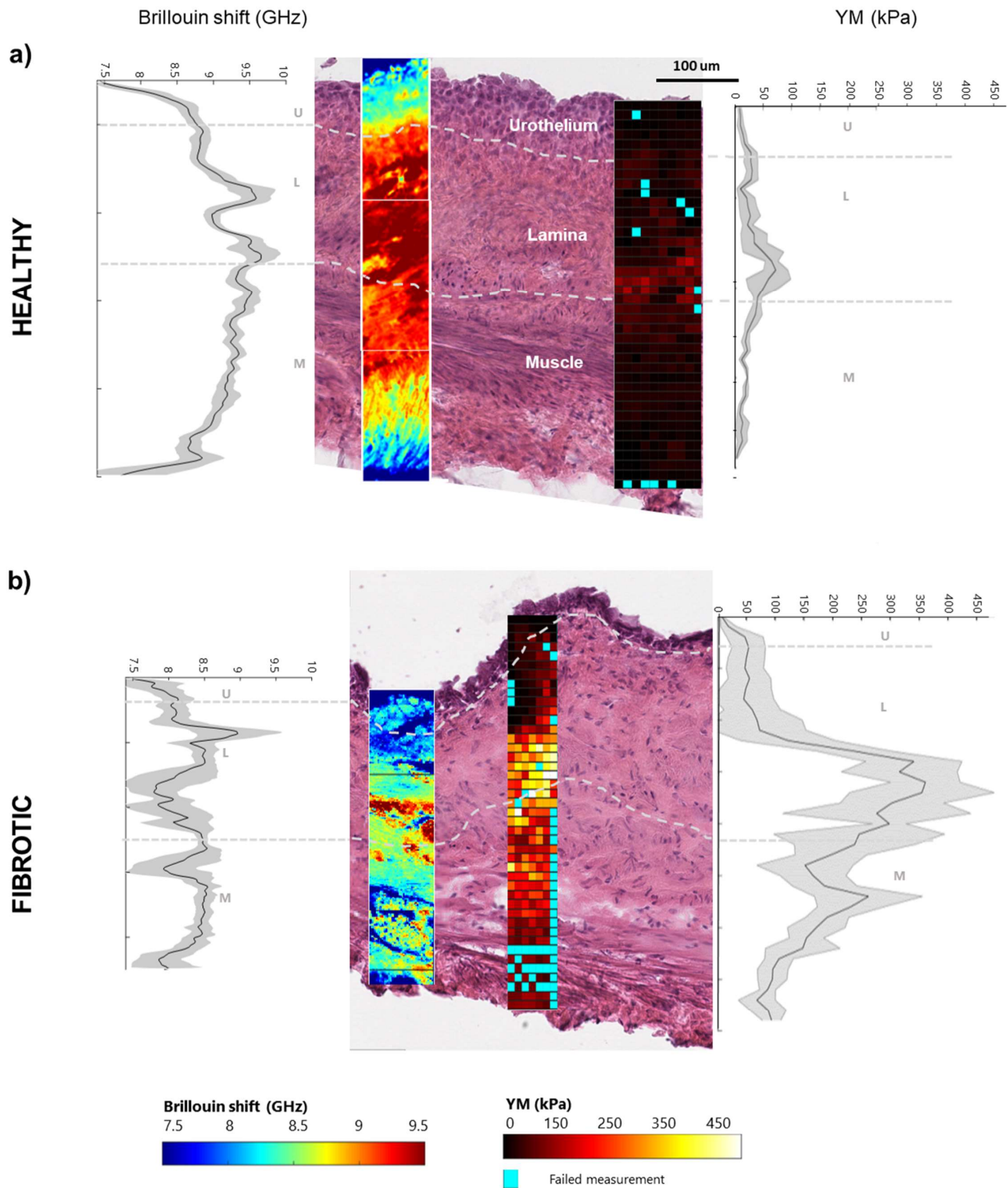


Figure 30. Comparison of Brillouin and YM maps of bladder in a) health and b) fibrosis. Graphs on the left of Brillouin map and right of nanoindenter maps represent the mean of each horizontal line of YM pixel values from the map \pm standard deviation of the mean in gray shade.

A possible explanation to this apparent incongruence in our data lies in the differences between Brillouin Microscopy and microindentation techniques such as AFM. In fact, although both these techniques are sometimes interchanged in sensing a common property named “stiffness”, they differ in many significant aspects, specifically:

(i) They measure different elastic moduli: the AFM-based microindentation is a sample volume preserving measurement, that is the sample is deformed at constant volume, which implies a lower resistance to the applied external force. On the contrary, Brillouin light scattering is related to the Longitudinal Modulus, where the system's volume (or density) is changed when applying the stress. The Young modulus lies in the kPa range, while the Longitudinal Modulus in the GPa range, six orders of magnitude apart. AFM provides information about material elasticity, while Brillouin microscopy informs about material's compressibility.

(ii) The two techniques work at very different frequencies (AFM works in Hz/kHz regime, Brillouin in the GHz regime). This is a critical point in the evaluation of mechanical properties of a material, since the response to a mechanical stimulus depends on the frequency at which it is applied (Wu *et al*, 2018). This phenomenon is known as viscoelasticity, for which the mechanical response of a material can be described as a combination of two ideal behaviors, those of an elastic solid and of a viscous liquid: depending on the frequency, one may dominate over the other. Broadly speaking, both Young's Modulus and Longitudinal Modulus depend on the probing frequency: their values increase almost stepwise when the frequency of the probe ν_0 becomes comparable to the inverse of the relaxation time τ_{relax} present in the sample. Without entering in the details (the interested readers can refer to standard textbook on the matter (Berne & Bruce, 2000)) it is sufficient to mention that in condensed matter such times are in the ps-ns time scale, depending on the aggregation state (liquid, glasses, ...) of the probed region. While to a good extent the Young's Modulus measured in AFM-based microindentation experiments is almost frequency independent, the Longitudinal Modulus (proportional to the square of the Brillouin shift) is often strongly frequency dependent. Therefore, a change in the Brillouin shift is seen -in a given tissue/compartiment- when $\nu_0 * \tau_{relax} \approx 1$, which can happen either if one changes the measurement's frequency ν_0 , or, more importantly, if the relaxation time τ_{relax} changes (Mattana *et al*, 2017). Consequently, we speculate that the biophysical modifications caused by fibrosis (e.g., increased collagen deposition and crosslinking) have a broad impact on tissues' relaxation time, passing from a condition where $\nu_0 * \tau_{relax} > 1$ in

healthy samples towards another in which $\nu_0^* \tau_{relax} < 1$ in fibrotic samples, thus leading to a lowering in ν_B .

(iii) The spatial resolution of the Brillouin maps here shown is much higher than the microindentation-based Young's Modulus maps. The Brillouin microscope here used exploited a high-numerical aperture objective and its three-dimensional resolution is $\approx 1 \mu\text{m}^3$. Instead, AFM indentation, involving a deformation of a large area of approximately $8 \mu\text{m}$ provided mechanical maps with a pixel size of $10 \mu\text{m}$.

Different attempts have been made to correlate Brillouin with microindentation measurements in biomechanics in cells (Scarcelli *et al*, 2015). However, to our knowledge, this is the first time that such a correlation was achieved also in tissues. This was possible due to the use of a sample preparation protocol that allows both for spectroscopy based mechanical investigation, as well as by microindentation techniques. Because of the different moduli probed, and of viscoelasticity, the comparison cannot give universal results, rather a material dependent outcome.

This study highlights the intrinsic mechanical heterogeneity of the different bladder layers. By providing high resolution micromechanical maps, which account for the three anatomical layers of bladder, I report an alteration of the mechanical properties of the bladder tissue in the pathological conditions of actinic cystitis (decreased elasticity and increased compressibility) and tumor (increased elasticity). Such mechanical fingerprints could eventually pave the way for future clinical diagnostic and prognostic tools, likewise laying out eventual hints for bladder reconstruction purposes. Furthermore, another potential clinical application of this study could be the investigation of response to therapy, by first testing whether an efficient therapy is able to restore the mechanical properties of the pathological tissue to its physiological state, and once developing this database of mechanical information, test mechanics as a parameter of response to therapy. In addition, taking together Brillouin and indentation-based results, I here highlight the complex viscoelastic properties of bladder tissue and the need of characterizing such complex tissues spatially resolving its different components at the microscale. Furthermore, consistent with the literature, I reported an alteration of tissue viscoelastic properties in presence of actinic cystitis, a pathological condition well known to dramatically affect bladder function and patient's life quality. By providing a direct comparison

between the gold standard technique in nanomechanics (microindentation-based measurements) and the emerging and non-contact Brillouin microscopy imaging technique, I here aimed to improve the translatability of such mechanical tests to the clinics as a potential diagnostic and prognostic tool complementary to the gold standard histopathological investigation.

7. References

- Aaronson DS, Walsh TJ, Smith JF, Davies BJ, Hsieh MH & Konety BR (2009) Meta-analysis: Does lidocaine gel before flexible cystoscopy provide pain relief? *BJU Int* 104: 506–510
- Abdelwahab K, Eliwa AM, Seleem MM, El Galaly H, Ragab A, Desoky EA, Naguib M, Ali MM, Saber S & Kamel H (2017) Role of Preoperative Testicular Shear Wave Elastography in Predicting Improvement of Semen Parameters After Varicocelelectomy for Male Patients With Primary Infertility. *Urology* 107: 103–106
- Acerbi I, Cassereau L, Dean I, Shi Q, Au A, Park C, Chen YY, Liphardt J, Hwang ES & Weaver VM (2015) Human breast cancer invasion and aggression correlates with ECM stiffening and immune cell infiltration. *Integr Biol (United Kingdom)* 7: 1120–1134
- Ahmad S, Cao R, Varghese T, Bidaut L & Nabi G (2013) Transrectal quantitative shear wave elastography in the detection and characterisation of prostate cancer. *Surg Endosc* 27: 3280–3287
- Ahms SED, Hota HJP, Dahiya R, Lue TF, Ho EAT & Francisco S (1998) Composition and biomechanical properties of the bladder acellular matrix graft : comparative analysis in rat , pig and human. 411–419
- Akhtar R, Graham HK, Derby B, Sherratt MJ, Trafford AW, Chadwick RS & Gavara N (2016) Frequency-modulated atomic force microscopy localises viscoelastic remodelling in the ageing sheep aorta. *J Mech Behav Biomed Mater* 64: 10–17
- Al-hayyali FQM (2020) Effect of age on histological changes of urogenital tract in albino rats. *Al Anbar J Vet Sci* 13: 109–121
- Alcaraz J, Buscemi L, Grabulosa M, Trepas X, Fabry B, Farré R & Navajas D (2003) Microrheology of human lung epithelial cells measured by atomic force microscopy. *Biophys J* 84: 2071–2079
- Alfano M, Nebuloni M, Allevi R, Zerbi P, Longhi E, Lucianò R, Locatelli I, Pecoraro A, Indrieri M, Speziali C, *et al* (2016) Linearized texture of three-dimensional extracellular matrix is mandatory for bladder cancer cell invasion. *Sci Rep* 6: 1–12
- Alibert C, Goud B & Manneville JB (2017) Are cancer cells really softer than normal cells? *Biol Cell* 109: 167–189
- Ansardamavandi A, Tafazzoli-Shadpour M, Omidvar R & Jahanzad I (2016) Quantification of effects of cancer on elastic properties of breast tissue by Atomic Force Microscopy. *J Mech*

Behav Biomed Mater 60: 234–242

- Antoni S, Ferlay J, Soerjomataram I, Znaor A, Jemal A & Bray F (2017) Bladder Cancer Incidence and Mortality: A Global Overview and Recent Trends. *Eur Urol* 71: 96–108
- Apte RS, Chen DS & Ferrara N (2019) VEGF in Signaling and Disease: Beyond Discovery and Development. *Cell* 176: 1248–1264
- Asbach P, Ro SR, Aldoj N, Snellings J, Reiter R, Lenk J, Köhlitz T, Haas M, Guo J, Hamm B, *et al* (2020) In Vivo Quantification of Water Diffusion, Stiffness, and Tissue Fluidity in Benign Prostatic Hyperplasia and Prostate Cancer. *Invest Radiol* 55: 524–530
- Babu PKV & Radmacher M (2019) Mechanics of brain tissues studied by atomic force microscopy: A perspective. *Front Neurosci* 13 doi:10.3389/fnins.2019.00600 [PREPRINT]
- Barak MM & Black MA (2018) A novel use of 3D printing model demonstrates the effects of deteriorated trabecular bone structure on bone stiffness and strength. *J Mech Behav Biomed Mater* 78: 455–464
- Barcus CE, O’Leary KA, Brockman JL, Rugowski DE, Liu Y, Garcia N, Yu M, Keely PJ, Eliceiri KW & Schuler LA (2017) Elevated collagen-I augments tumor progressive signals, intravasation and metastasis of prolactin-induced estrogen receptor alpha positive mammary tumor cells. *Breast Cancer Res* 19: 1–13
- Barnes SC, Lawless BM, Shepherd DET, Espino DM, Bicknell GR & Bryan RT (2016) Viscoelastic properties of human bladder tumours. *J Mech Behav Biomed Mater* 61: 250–257
- Barnes SC, Shepherd DET, Espino DM & Bryan RT (2015) Frequency dependent viscoelastic properties of porcine bladder. *J Mech Behav Biomed Mater* 42: 168–176
- Berne, Bruce J. and RP (2000) Dynamic light scattering: with applications to chemistry, biology, and physics.
- Boyd NF, Li Q, Melnichouk O, Huszti E, Martin LJ, Gunasekara A, Mawdsley G, Yaffe MJ & Minkin S (2014) Evidence That Breast Tissue Stiffness Is Associated with Risk of Breast Cancer. 9: 1–8
- Brooks M, Mo Q, Krasnow R, Ho PL, Lee YC, Xiao J, Kurtova A, Lerner S, Godoy G, Jian W, *et al* (2016) Positive association of collagen type I with non-muscle invasive bladder cancer progression. *Oncotarget* 7: 82609–82619
- Brown C & Avian DA (2011) clinical techniques Urethral catheterization of the female rat. *Nat Publ Gr* 40

- Canetta E, Riches A, Borger E, Herrington S, Dholakia K & Adya AK (2014) Discrimination of bladder cancer cells from normal urothelial cells with high specificity and sensitivity: Combined application of atomic force microscopy and modulated Raman spectroscopy. *Acta Biomater* 10: 2043–2055
- Cappella B & Kappl M (2005) Force measurements with the atomic force microscope : Technique , interpretation and applications. 59: 1–152
- Chan CJ, Bevilacqua C & Prevedel R (2021) Mechanical mapping of mammalian follicle development using Brillouin microscopy. *Commun Biol* 4: 1–10
- Chen YQ, Kuo JC, Wei MT, Chen YC, Yang MH & Chiou A (2019) Early stage mechanical remodeling of collagen surrounding head and neck squamous cell carcinoma spheroids correlates strongly with their invasion capability. *Acta Biomater* 84: 280–292
- Chighizola M, Puricelli L, Bellon L & Podestà A (2021) Large colloidal probes for atomic force microscopy: Fabrication and calibration issues. *J Mol Recognit* 34: 1–14
- Cho NH, Shim HS, Rha SY, Kang SH, Hong SH, Choi YD, Hong SJ & Cho SH (2003) Increased Expression of Matrix Metalloproteinase 9 Correlates with Poor Prognostic Variables in Renal Cell Carcinoma. *Eur Urol* 44: 560–566
- Christ AF, Franze K, Gautier H, Moshayedi P, Fawcett J, Franklin RJM, Karadottir RT & Guck J (2010) Mechanical difference between white and gray matter in the rat cerebellum measured by scanning force microscopy. *J Biomech* 43: 2986–2992
- Cohen SM (2013) Systems Toxicologic Pathology in Haschek and Rousseaux’s Handbook of Toxicologic Pathology (Third Edition)
- Conklin MW, Gangnon RE, Sprague BL, Germert L Van, Hampton M, Eliceiri KW, Bredfeldt JS, Liu Y, Newcomb PA, Friedl A, *et al* (2018) Collagen alignment as a predictor of recurrence after ductal carcinoma in situ. *Cancer Epidemiol Biomarkers* 27: 138–145
- Crichton ML, Donose BC, Chen X, Raphael AP, Huang H & Kendall MAF (2011) The viscoelastic, hyperelastic and scale dependent behaviour of freshly excised individual skin layers. *Biomaterials* 32: 4670–4681
- Cross SE, Jin Y, Rao J & Gimzewski JK (2007) Nanomechanical analysis of cells from cancer patients.
- Cui G, Yang Z, Zhang W, Li B, Sun F, Xu C & Wang K (2013) Evaluation of acoustic radiation force impulse imaging for the clinicopathological typing of renal fibrosis. *Exp Ther Med* 7:

- Cui X, Wang G, Shen W, Huang Z, He H & Cui L (2018) Lysyl oxidase-like 2 is highly expressed in colorectal cancer cells and promotes the development of colorectal cancer. *Oncol Rep* 40: 932–942
- Darnell M, Gu L & Mooney D (2018) RNA-seq reveals diverse effects of substrate stiffness on mesenchymal stem cells. *Biomaterials* 181: 182–188
- DeLeon-Pennell KY, Barker TH & Lindsey ML (2020) Fibroblasts: The arbiters of extracellular matrix remodeling. *Matrix Biol* 91–92: 1–7
- Dimitriadis EK, Horkay F, Maresca J, Kachar B & Chadwick RS (2002) Determination of elastic moduli of thin layers of soft material using the atomic force microscope. *Biophys J* 82: 2798–2810
- DuChez BJ, Doyle AD, Dimitriadis EK & Yamada KM (2019) Durotaxis by Human Cancer Cells. *Biophys J* 116: 670–683
- Eble JA & Niland S (2019) The extracellular matrix in tumor progression and metastasis. *Clin Exp Metastasis* 36: 171–198
- Egeblad M & Werb Z (2002) New functions for the matrix metalloproteinases in cancer progression. *Nat Rev Cancer* 2: 161–174
- Emon B, Bauer J, Jain Y, Jung B & Saif T (2018) Biophysics of Tumor Microenvironment and Cancer Metastasis - A Mini Review. *Comput Struct Biotechnol J* 16: 279–287
- Erler, Janine T., Weaver VM (2009) Three-dimensional context regulation of metastasis. *Clin Exp Metastasis* 26: 35–49
- Esbona K, Yi Y, Saha S, Yu M, Van Doorn RR, Conklin MW, Graham DS, Wisinski KB, Ponik SM, Eliceiri KW, *et al* (2018) The Presence of Cyclooxygenase 2, Tumor-Associated Macrophages, and Collagen Alignment as Prognostic Markers for Invasive Breast Carcinoma Patients. *Am J Pathol* 188: 559–573
- Etich J, Koch M, Wagener R, Zaucke F, Fabri M & Brachvogel B (2019) Gene expression profiling of the extracellular matrix signature in macrophages of different activation status: Relevance for skin wound healing. *Int J Mol Sci* 20: 1–21
- Farajzadeh Valilou S, Keshavarz-Fathi M, Silvestris N, Argentiero A & Rezaei N (2018) The role of inflammatory cytokines and tumor associated macrophages (TAMs) in microenvironment of pancreatic cancer. *Cytokine Growth Factor Rev* 39: 46–61

- Faria EC, Ma N, Gazi E, Gardner P, Brown M, Clarke NW & Snook RD (2008) Measurement of elastic properties of prostate cancer cells using AFM. *Analyst* 133: 1498–1500
- Ferlay J, Soerjomataram I, Dikshit R, Eser S, Mathers C, Rebelo M, Parkin DM, Forman D & Bray F (2015) Cancer incidence and mortality worldwide: Sources, methods and major patterns in GLOBOCAN 2012. *Int J Cancer* 136: E359–E386
- Fields GB (2019) The rebirth of matrix metalloproteinase inhibitors: Moving beyond the dogma. *Cells* 8: 20–23
- Frantz C, Stewart KM & Weaver VM (2010) The extracellular matrix at a glance. *J Cell Sci* 123: 4195–4200
- Franze K, Francke M, Günter K, Christ AF, Kö rber N, Reichenbach A & Guck J (2011) Spatial mapping of the mechanical properties of the living retina using scanning force microscopy. *Soft Matter* 7: 3147–3154
- Friedl P, Locker J, Sahai E & Segall JE (2012) Classifying collective cancer cell invasion. *Nat Cell Biol* 14: 777–783
- Friedrich-Rust M, Ong MF, Herrmann E, Dries V, Samaras P, Zeuzem S & Sarrazin C (2007) Real-time elastography for noninvasive assessment of liver fibrosis in chronic viral hepatitis. *Am J Roentgenol* 188: 758–764
- Fry CH, Kitney DG, Paniker J, Drake MJ, Kanai A & Andersson KE (2018) Fibrosis and the bladder, implications for function ICI-RS 2017. *Neurourol Urodyn* 37: S7–S12
- Fu S, Tang Y, Tan S, Zhao Y & Cui L (2020) Diagnostic Value of Transrectal Shear Wave Elastography for Prostate Cancer Detection in Peripheral Zone: Comparison with MRI. *J Endourol*: 1–25
- Garcia PD & Garcia R (2018) Determination of the Elastic Moduli of a Single Cell Cultured on a Rigid Support by Force Microscopy. *Biophys J* 114: 2923–2932
- Gavara N (2016) A beginner’s guide to atomic force microscopy probing for cell mechanics. *Microsc Res Tech* 80: 75–84
- Ghasemi H, Mousavibahar SH, Hashemnia M, Karimi J, Khodadadi I, Mirzaei F & Tavilani H (2020) Tissue stiffness contributes to YAP activation in bladder cancer patients undergoing transurethral resection. *1473*: 48–61
- Glentis A, Oertle P, Mariani P, Chikina A, El Marjou F, Attieh Y, Zaccarini F, Lae M, Loew D, Dingli F, *et al* (2017) Cancer-associated fibroblasts induce metalloprotease-independent

- cancer cell invasion of the basement membrane. *Nat Commun* 8: 1–13
- Gonzalez-Avila G, Sommer B, Mendoza-Posada DA, Ramos C, Garcia-Hernandez AA & Falfan-Valencia R (2019) Matrix metalloproteinases participation in the metastatic process and their diagnostic and therapeutic applications in cancer. *Crit Rev Oncol Hematol* 137: 57–83
- Goulet CR, Champagne A, Bernard G, Vandal D, Chabaud S, Pouliot F & Bolduc S (2019) Cancer-associated fibroblasts induce epithelial-mesenchymal transition of bladder cancer cells through paracrine IL-6 signalling. *BMC Cancer* 19: 1–13
- Goya C, Kilinc F, Hamidi C, Yavuz A, Yildirim Y, Cetincakmak MG & Hattapoglu S (2015) Acoustic radiation force impulse imaging for evaluation of renal parenchyma elasticity in diabetic nephropathy. *Am J Roentgenol* 204: 324–329
- Graham HK, Hodson NW, Hoyland JA, Millward-Sadler SJ, Garrod D, Scothern A, Griffiths CEM, Watson REB, Cox TR, Erler JT, *et al* (2010) Tissue section AFM: In situ ultrastructural imaging of native biomolecules. *Matrix Biol* 29: 254–260
- Grant CA, Twigg PC & Tobin DJ (2012) Static and dynamic nanomechanical properties of human skin tissue using atomic force microscopy: Effect of scarring in the upper dermis. *Acta Biomater* 8: 4123–4129
- Grant D. Stewart, Kelly Gray, Caroline J. Pennington, Dylan R. Edwards, Antony C.P. Riddick, James A. Ross FKH (2008) Analysis of hypoxia-associated gene expression in prostate cancer: lysyl oxidase and glucose transporter-1 expression correlate with Gleason score. *Oncol Rep* 20: 861–867
- Guimarães CF, Gasperini L, Marques AP & Reis RL (2020) The stiffness of living tissues and its implications for tissue engineering. *Nat Rev Mater*
- Hadden M, Mittal A, Samra J, Zreiqat H, Sahni S & Ramaswamy Y (2020) Mechanically stressed cancer microenvironment: Role in pancreatic cancer progression. *Biochim Biophys Acta - Rev Cancer* 1874: 188418
- Haeger A, Alexander S, Alexander S, Alexander S, Vullings M, Kaiser FMP, Veelken C, Flucke U, Koehl GE, Hirschberg M, *et al* (2020) Collective cancer invasion forms an integrin-dependent radioresistant niche. *J Exp Med* 217
- Haeger A, Krause M, Wolf K & Friedl P (2014) Cell jamming: Collective invasion of mesenchymal tumor cells imposed by tissue confinement. *Biochim Biophys Acta - Gen Subj* 1840: 2386–2395

- Hajjarian Z, Brachtel EF, Tshikudi DM & Nadkarni SK (2021) Mapping mechanical properties of the tumor microenvironment by laser speckle rheological microscopy. *Cancer Res* 81: 4874–4885
- Han JH, Ahn JH & Kim JS (2020) Magnetic resonance elastography for evaluation of renal parenchyma in chronic kidney disease: a pilot study. *Radiol Medica* 125: 1209–1215
- Herszényi L, Hritz I, Lakatos G, Varga MZ & Tulassay Z (2012) The Behavior of matrix metalloproteinases and their inhibitors in colorectal cancer. *Int J Mol Sci* 13: 13240–13263
- Hertz H (1881), Über die Berührung fester elastischer Körper, *Journal für die reine und angewandte Mathematik* 92, 156-171 (1881). *J für die reine und Angew Math* 171: 156–171
- Hines MJB and WC (2011) Why don't we get more cancer? A proposed role of the microenvironment in restraining cancer progression. *Nat Med* 17: 320–329
- Hinz B (2015) The extracellular matrix and transforming growth factor- β 1: Tale of a strained relationship. *Matrix Biol* 47: 54–65
- Holtzmann K, Gautier HOB, Christ AF, Guck J, Káradóttir RT & Franze K (2016) Brain tissue stiffness is a sensitive marker for acidosis. *J Neurosci Methods* 271: 50–54
- Hong Zhao YZRLYLZMZHYZ (2019) Effects of different doses of X-ray irradiation on cell apoptosis, cell cycle, DNA damage repair and glycolysis in HeLa cells. *Oncol Lett* 17: 42–54
- Hood JL, San Roman S & Wickline SA (2011) Exosomes released by melanoma cells prepare sentinel lymph nodes for tumor metastasis. *Cancer Res* 71: 3792–3801
- Hoof SJ Van, Granton P V & Verhaegen F (2013) Development and validation of a treatment planning system for small animal radiotherapy : SmART-Plan. *Radiother Oncol* 109: 361–366
- Høye AM & Erler JT (2016) Structural ECM components in the premetastatic and metastatic niche. *Am J Physiol - Cell Physiol* 310: C955–C967
- Hsieh CH, Lin YH, Lin S, Tsai-Wu JJ, Herbert Wu CH & Jiang CC (2008) Surface ultrastructure and mechanical property of human chondrocyte revealed by atomic force microscopy. *Osteoarthr Cartil* 16: 480–488
- <https://www.phys2biomed.eu/index.php> Phys2BioMed consortium. Biomechanics in health and disease: advanced physical tools for innovative early diagnosis.
- Huang D, Huang Y, Xiao Y, Yang X, Lin H, Feng G, Zhu X & Zhang X (2019) Viscoelasticity in natural tissues and engineered scaffolds for tissue reconstruction. *Acta Biomater* 97: 74–92
- Hutter, J. & Bechhoefer J (1993) Calibration of atomic-force microscope tips. *Rev Sci Instrum* 64:

1868–1873

- Iliina O, Campanello L, Gritsenko PG, Vullings M, Wang C, Bult P, Losert W & Friedl P (2018) Intravital microscopy of collective invasion plasticity in breast cancer. *DMM Dis Model Mech* 11
- Indrieri M, Podestà A, Bongiorno G, Marchesi D & Milani P (2011) Adhesive-free colloidal probes for nanoscale force measurements: Production and characterization. *Rev Sci Instrum* 82
- Islam M, Mezencev R, Mcfarland B, Brink H, Campbell B, Tasadduq B, Waller EK, Lam W, Alexeev A & Sulchek T Microfluidic cell sorting by stiffness to examine heterogenic responses of cancer cells to chemotherapy.
- Jabłońska-Trypuć A, Matejczyk M & Rosochacki S (2016) Matrix metalloproteinases (MMPs), the main extracellular matrix (ECM) enzymes in collagen degradation, as a target for anticancer drugs. *J Enzyme Inhib Med Chem* 31: 177–183
- Janmey PA & Miller RT (2011) Mechanisms of mechanical signaling in development and disease. *J Cell Sci* 124: 9–18
- Jaschke H-JB and M (1995) Calculation of thermal noise in atomic force microscopy. *Nanotechnology* 6
- Jedrzejewski G, Osemlak P, Wiczorek AP & Nachulewicz P (2019) Prognostic values of shear wave elastography in adolescent boys with varicocele. *J Pediatr Urol* 15: 223.e1-223.e5
- Johnston KA & Lopez KM (2018) Lysyl oxidase in cancer inhibition and metastasis. *Cancer Lett* 417: 174–181
- Kagan HM (2000) Intra- and extracellular enzymes of collagen biosynthesis as biological and chemical targets in the control of fibrosis. *Acta Trop* 77: 147–152
- Kaler SG, Gallo LK, Proud VK, Percy AK, Mark Y, Segal NA, Goldstein DS, Holmes CS & Gahl WA (1994) Occipital horn syndrome and a mild Menkes phenotype associated with splice site mutations at the MNK locus. *Nat Genet* 8: 195–202
- Kalluri R (2016) The biology and function of fibroblasts in cancer. *Nat Rev Cancer* 16: 582–598
- Kao AP, Connelly JT & Barber AH (2016) 3D nanomechanical evaluations of dermal structures in skin. *J Mech Behav Biomed Mater* 57: 14–23
- Kelley LC, Chi Q, Cáceres R, Hastie E, Schindler AJ, Jiang Y, Matus DQ, Plastino J & Sherwood DR (2019) Adaptive F-Actin Polymerization and Localized ATP Production Drive Basement Membrane Invasion in the Absence of MMPs. *Dev Cell* 48: 313-328.e8

- Kessenbrock K, Plaks V & Werb Z (2010) Matrix Metalloproteinases: Regulators of the Tumor Microenvironment. *Cell* 141: 52–67
- Khan ZS, Santos JM & Hussain F (2018) Aggressive prostate cancer cell nuclei have reduced stiffness. *Biomicrofluidics* 12: 1–19
- Kiio TM & Park S (2020) Nano-scientific application of atomic force microscopy in pathology: From molecules to tissues. *Int J Med Sci* 17: 844–858
- Knowles MA & Hurst CD (2015) Molecular biology of bladder cancer: New insights into pathogenesis and clinical diversity. *Nat Rev Cancer* 15: 25–41
- Kollmannsberger P & Fabry B (2007) High-force magnetic tweezers with force feedback for biological applications. *Rev Sci Instrum* 78: 1–7
- Kontomaris S-V (2018) The Hertz Model in AFM Nanoindentation Experiments: Applications in Biological Samples and Biomaterials. *Micro Nanosyst* 10: 11–22
- Korossis S, Bolland F, Southgate J, Ingham E & Fisher J (2009) Regional biomechanical and histological characterisation of the passive porcine urinary bladder: Implications for augmentation and tissue engineering strategies. *Biomaterials* 30: 266–275
- Krakhmal N V., Zavyalova M V., Denisov E V., Vtorushin S V. & Perelmuter VM (2015) Cancer invasion: Patterns and mechanisms. *Acta Naturae* 7: 17–28
- Kwon JK, Kim DK, Lee JY, Kim JW & Cho KS (2019) Relationship between Lower Urinary Tract Symptoms and Prostatic Urethral Stiffness Using Strain Elastography: Initial Experiences. *J Clin Med* 8: 1929
- L.H. Sobin MKG and CW (2009) TNM classification of malignant tumors
- Laghezza Masci V, Taddei AR, Gambellini G, Giorgi F & Fausto AM (2016) Microvesicles shed from fibroblasts act as metalloproteinase carriers in a 3-D collagen matrix. *J Circ Biomarkers* 5: 1–11
- Lambert V, Wielockx B, Munaut C, Galopin C, Jost M, Itoh T, Werb Z, Baker A, Libert C, Krell H-W, *et al* (2003) MMP-2 and MMP-9 synergize in promoting choroidal neovascularization. *FASEB J* 17: 2290–2292
- Landau EH, Jayanthi VR, Churchill BM, Shapiro E, Gilmour RF, Khoury AE, Macarak EJ, McLorie GA, Steckler RE & Kogan BA (1994) Loss of elasticity in dysfunctional bladders: Urodynamic and histochemical correlation. *J Urol* 152: 702–705
- Lang ST, Guo J, Bruns A, Dürr M, Braun J, Hamm B, Sack I & Marticorena Garcia SR (2019)

- Multiparametric Quantitative MRI for the Detection of IgA Nephropathy Using Tomoelastography, DWI, and BOLD Imaging. *Invest Radiol* 54: 669–674
- Last JA, Liliensiek SJ, Nealey PF & Murphy CJ (2009) Determining the mechanical properties of human corneal basement membranes with atomic force microscopy. *J Struct Biol* 167: 19–24
- Last JA, Thomasy SM, Croasdale CR, Russell P & Murphy CJ (2012) Compliance profile of the human cornea as measured by atomic force microscopy. *Micron* 43: 1293–1298
- Laurent J, Steinberger A & Bellon L (2013) Functionalized AFM probes for force spectroscopy: Eigenmode shapes and stiffness calibration through thermal noise measurements. *Nanotechnology* 24
- Lekka M (2016) Discrimination Between Normal and Cancerous Cells Using AFM. *Bionanoscience* 6: 65–80
- Lekka M, Gil D, Pogoda K, Dulińska-Litewka J, Jach R, Gostek J, Klymenko O, Prauzner-Behcicki S, Stachura Z, Wiltowska-Zuber J, *et al* (2012a) Cancer cell detection in tissue sections using AFM. *Arch Biochem Biophys* 518: 151–156
- Lekka M, Laidler P, Gil D, Lekki J, Stachura Z & Hryniewicz AZ (1999) Elasticity of normal and cancerous human bladder cells studied by scanning force microscopy. *Eur Biophys J* 28: 312–316
- Lekka M, Pogoda K, Gostek J, Klymenko O, Prauzner-Behcicki S, Wiltowska-Zuber J, Jaczewska J, Lekki J & Stachura Z (2012b) Cancer cell recognition - Mechanical phenotype. *Micron* 43: 1259–1266
- Leong SS, Wong JHD, Shah MNM, Vijayanathan A, Jalalonmuhali M & Kwan Hoong NG (2018) Shear wave elastography in the evaluation of renal parenchymal stiffness in patients with chronic kidney disease. *Br J Radiol* 91
- Lepert G, Gouveia RM, Cannon CJ & Paterson C (2016) Assessing corneal biomechanics with Brillouin spectro-microscopy. *Faraday Discuss* 187: 415–428
- Levental KR, Yu H, Kass L, Lakins JN, Egeblad M, Erler JT, Fong SFT, Csiszar K, Giaccia A, Weninger W, *et al* (2009) Matrix Crosslinking Forces Tumor Progression by Enhancing Integrin Signaling. *Cell* 139: 891–906
- Li J, Zormpas-Petridis K, Boulton JKR, Reeves EL, Heindl A, Vinci M, Lopes F, Cummings C, Springer CJ, Chesler L, *et al* (2019) Investigating the contribution of collagen to the tumor biomechanical phenotype with noninvasive magnetic resonance elastography. *Cancer Res* 79:

- Li T, Wu C, Gao L, Qin F, Wei Q & Yuan J (2018) Lysyl oxidase family members in urological tumorigenesis and fibrosis. *Oncotarget* 9: 20156–20164
- Lim HY, Lim SY, Tan CK, Thiam CH, Goh CC, Carbajo D, Chew SHS, See P, Chakarov S, Wang XN, *et al* (2018) Hyaluronan Receptor LYVE-1-Expressing Macrophages Maintain Arterial Tone through Hyaluronan-Mediated Regulation of Smooth Muscle Cell Collagen. *Immunity* 49: 326-341.e7
- Lin Han, Alan J. Grodzinsky² and CO (2011) Nanomechanics of the Cartilage Extracellular Matrix. *Annu Rev Mater Res* 41: 133–168
- Lin HH, Lin HK, Lin IH, Chiou YW, Chen HW, Liu CY, Harn HIC, Chiu WT, Wang YK, Shen MR, *et al* (2015) Mechanical phenotype of cancer cells: Cell softening and loss of stiffness sensing. *Oncotarget* 6: 20946–20958
- Lin HYH, Lee YL, Lin K Der, Chiu YW, Shin SJ, Hwang SJ, Chen HC & Hung CC (2017) Association of Renal Elasticity and Renal Function Progression in Patients with Chronic Kidney Disease Evaluated by Real-Time Ultrasound Elastography. *Sci Rep* 7: 1–8
- Linder S, Wiesner C & Himmel M (2011) Degrading devices: Invadosomes in proteolytic cell invasion. *Annu Rev Cell Dev Biol* 27: 185–211
- Littlepage LE, Sternlicht MD, Rougier N, Phillips J, Yu Y, Williams K, Brenot A, Gordon JI & Werb Z (2010) Matrix Metalloproteinases Contribute Distinct Roles in Neuroendocrine Prostate Carcinogenesis, Metastasis, and Angiogenesis Progression. *Cancer Res* 70: 2224–2234
- Liu H, Tan Q, Geddie WR, Jewett MAS, Phillips N, Ke D, Simmons CA & Sun Y (2014) Biophysical Characterization of Bladder Cancer Cells with Different Metastatic Potential. *Cell Biochem Biophys* 68: 241–246
- Liu T, Zhou L, Li D, Andl T & Zhang Y (2019) Cancer-associated fibroblasts build and secure the tumor microenvironment. *Front Cell Dev Biol* 7: 1–14
- Liu Y, Wang G, Liang Z, Mei Z, Wu T, Cui A, Liu C & Cui L (2018) Lysyl oxidase: A colorectal cancer biomarker of lung and hepatic metastasis. *Thorac Cancer* 9: 785–793
- Lu P, Weaver VM & Werb Z (2012) The extracellular matrix: A dynamic niche in cancer progression. *J Cell Biol* 196: 395–406
- Lu X & Kang Y (2007) Organotropism of breast cancer metastasis. *J Mammary Gland Biol*

Neoplasia 12: 153–162

- Ma J, Gharaee-Kermani M, Kunju L, Hollingsworth JM, Adler J, Arruda EM & MacOska JA (2012) Prostatic fibrosis is associated with lower urinary tract symptoms. *J Urol* 188: 1375–1381
- Mancini ML & Sonis ST (2014) Mechanisms of cellular fibrosis associated with cancer regimen-related toxicities. *Front Pharmacol* 5 MAR: 1–9
- Mangano MS, De Gobbi A, Ciaccia M, Lamon C, Beniamin F & Maccatrozzo L (2018) Actinic cystitis: causes, treatment and experience of a single centre in the last five years. *Urologia* 85: 25–28
- Marta Alonso-Nocelo, Theresa M. Raimondo, Kyle H. Vining, Rafael Lopez-Lopez, Maria de la Fuente DJM (2017) Matrix Stiffness and Tumor-Associated Macrophages Modulate Epithelial to Mesenchymal Transition of Human Adenocarcinoma Cells. *Biofabrication* 176: 139–148
- Martin M, Benzina O, Szabo V, Végh AG, Lucas O, Cloitre T, Scamps F & Gergely C (2013) Morphology and Nanomechanics of Sensory Neurons Growth Cones following Peripheral Nerve Injury. *PLoS One* 8
- Martinez-Vidal L, Murdica V, Venegoni C, Pederzoli F, Bandini M, Necchi A, Salonia A & Alfano M (2021) Causal contributors to tissue stiffness and clinical relevance in urology. *Commun Biol* 4: 1–16
- Martins PALS, Lopes A, Filho S, Mascarenhas T, Jorge RMN & Ferreira AJM (2011) Uniaxial mechanical behavior of the human female bladder. 991–995
- Mattana S, Caponi S, Tamagnini F, Fioretto D & Palombo F (2017) Viscoelasticity of amyloid plaques in transgenic mouse brain studied by Brillouin microspectroscopy and correlative Raman analysis. 10: 1–14
- McCawley LJ & Matrisian LM (2001) Matrix metalloproteinases: They're not just for matrix anymore! *Curr Opin Cell Biol* 13: 534–540
- Mierke CT (2018) The Matrix Environmental and Cell Mechanical Properties regulate Cell Migration and contribute to the Invasive Phenotype of Cancer Cells. *Reports Prog Phys*: 0–23
- Mohan V, Das A & Sagi I (2020a) Emerging roles of ECM remodeling processes in cancer. *Semin Cancer Biol* 62: 192–200
- Mohan V, Das A & Sagi I (2020b) Emerging roles of ECM remodeling processes in cancer. *Semin Cancer Biol* 62: 192–200
- Morgante D & Southgate J (2022) Bladder tissue regeneration. *Tissue Eng Using Ceram Polym*:

- Mostowy S, Janel S, Forestier C, Roduit C, Kasas S, Pizarro-Cerdá J, Cossart P & Lafont F (2011) A role for septins in the interaction between the *Listeria monocytogenes* invasion protein InlB and the Met receptor. *Biophys J* 100: 1949–1959
- Murawaki Y, Kusakabe Y & Hirayama C (1991) Serum lysyl oxidase activity in chronic liver disease in comparison with serum levels of prolyl hydroxylase and laminin. *Hepatology* 14: 1167–1173
- Murphy MC, Huston J, Jack CR, Glaser KJ, Senjem ML, Chen J, Manduca A, Felmlee JP & Ehman RL (2013) Measuring the characteristic topography of brain stiffness with magnetic resonance elastography. *PLoS One* 8: 1–14
- Murray PJ & Wynn TA (2011) Protective and pathogenic functions of macrophage subsets. *Nat Rev Immunol* 11: 723–737
- Nagy N, De La Zerda A, Kaber G, Johnson PY, Hu KH, Kratochvil MJ, Yadava K, Zhao W, Cui Y, Navarro G, *et al* (2018) Hyaluronan content governs tissue stiffness in pancreatic islet inflammation. *J Biol Chem* 293: 567–578
- Nakao T, Ushigome H, Nakamura T, Harada S, Koshino K, Suzuki T, Ito T, Nobori S & Yoshimura N (2015) Evaluation of renal allograft fibrosis by transient elastography (fibro scan). *Transplant Proc* 47: 640–643
- Naruse K (2018) Mechanomedicine: Applications of mechanobiology to medical sciences and next-generation medical technologies. *J Smooth Muscle Res* 54: 83–90
- Nebuloni M, Albarello L, Andolfo A, Magagnotti C, Genovese L, Locatelli I, Tonon G, Longhi E, Zerbi P, Allevi R, *et al* (2016) Insight On Colorectal Carcinoma Infiltration by Studying Perilesional Extracellular Matrix. *Nat Publ Gr*: 1–13
- Nenadic I, Mynderse L, Husmann D, Mehrmohammadi M, Bayat M, Singh A, Denis M, Urban M, Alizad A & Fatemi M (2016) Noninvasive evaluation of bladder wall mechanical properties as a function of filling volume: Potential application in bladder compliance assessment. *PLoS One* 11: 1–14
- Nia HT, Munn LL & Jain RK (2020) Physical traits of cancer. *Science (80-)* 370
- Nikos K, Karamanos, Achilleas D, Theocaris, Thomas Neill RVI (2019) Matrix modeling and remodeling: a biological interplay regulating tissue homeostasis and diseases. *Matrix Biol* 72: 1–11

- Nilsson M, Hägglöf C, Hammarsten P, Thysell E, Stattin P, Egevad L, Granfors T, Jernberg E, Wikstrom P, Halin Bergström S, *et al* (2015) High Lysyl oxidase (LOX) in the non-malignant prostate epithelium predicts a poor outcome in prostate cancer patient managed by watchful waiting. *PLoS One* 10: 1–14
- Noguchi S, Saito A & Nagase T (2018) YAP/TAZ signaling as a molecular link between fibrosis and cancer. *Int J Mol Sci* 19
- Northey JJ, Barrett AS, Acerbi I, Hayward MK, Talamantes S, Dean IS, Mouw JK, Ponik SM, Lakins JN, Huang PJ, *et al* (2020) Stiff stroma increases breast cancer risk by inducing the oncogene ZNF217. *J Clin Invest* 130: 5721–5737
- Orabi H, Bouhout S, Morissette A, Rousseau A, Chabaud S & Bolduc S (2013) Tissue engineering of urinary bladder and urethra: Advances from bench to patients. *Sci World J* 2013
- Osmulski P, Mahalingam D, Gaczynska ME, Liu J, Horning AM, Wang C, Thompson IM, Huang TH & Chen C (2015) Nanomechanical biomarkers of single circulating tumor cells for detection of castration resistant prostate cancer. *Prostate* 74: 1297–1307
- Oudin MJ & Weaver VM (2016) Physical and chemical gradients in the tumor microenvironment regulate tumor cell invasion, migration, and metastasis. *Cold Spring Harb Symp Quant Biol* 81: 189–205
- Paolillo M & Schinelli S (2019) Extracellular matrix alterations in metastatic processes. *Int J Mol Sci* 20
- Park D, Wershof E, Boeing S, Labernadie A, Jenkins RP, George S, Trepas X, Bates PA & Sahai E Extracellular matrix anisotropy is determined by TFAP2C-dependent regulation of cell collisions. *Nat Mater*
- Paszek MJ, Zahir N, Johnson KR, Lakins JN, Rozenberg GI, Gefen A, Reinhart-King CA, Margulies SS, Dembo M, Boettiger D, *et al* (2005) Tensional homeostasis and the malignant phenotype. *Cancer Cell* 8: 241–254
- Pathria P, Louis TL & Varner JA (2019) Targeting Tumor-Associated Macrophages in Cancer. *Trends Immunol* 40: 310–327
- Paul Kennedy, Octavia Bane, Stefanie J Hectors, Sonja Gordic, Mark Berger, Veronica Delaney, Fadi Salem, Sara Lewis, Madhav Menon BT (2020) Magnetic resonance elastography vs. point shear wave ultrasound elastography for the assessment of renal allograft dysfunction. *Eur J Radiol* 126: 139–148

- Pedersen M, Møller H, Osther P, Vedsted P, Holst R & Rafaelsen S (2017) Comparison of Tissue Stiffness Using Shear Wave Elastography in Men with Normal Testicular Tissue, Testicular Microlithiasis and Testicular Cancer. *Ultrasound Int Open* 03: E150–E155
- Pedersen MR, Sloth Osther PJ, Nissen HD, Vedsted P, Møller H & Rafaelsen SR (2019) Elastography and diffusion-weighted MRI in patients with testicular microlithiasis, normal testicular tissue, and testicular cancer: an observational study. *Acta radiol* 60: 535–541
- Peinado H, Alečković M, Lavotshkin S, Matei I, Costa-Silva B, Moreno-Bueno G, Hergueta-Redondo M, Williams C, García-Santos G, Ghajar CM, *et al* (2012) Melanoma exosomes educate bone marrow progenitor cells toward a pro-metastatic phenotype through MET. *Nat Med* 18: 883–891
- Peinado H, Lavotshkin S & Lyden D (2011) The secreted factors responsible for pre-metastatic niche formation: Old sayings and new thoughts. *Semin Cancer Biol* 21: 139–146
- Peinado H, Zhang H, Matei IR, Costa-Silva B, Hoshino A, Rodrigues G, Psaila B, Kaplan RN, Bromberg JF, Kang Y, *et al* (2017) Pre-metastatic niches: Organ-specific homes for metastases. *Nat Rev Cancer* 17: 302–317
- Pierre Parot, Yves F. Dufrene, Peter Hinterdorfer, Christian Le Grimellec, Daniel Navajas J-LP and SS (2007) Past, present and future of atomic force microscopy in life sciences and medicine. *Mol Recogn* 6: 418–431
- Plodinec M, Loparic M, Monnier CA, Obermann EC, Zanetti-Dallenbach R, Oertle P, Hyotyla JT, Aebi U, Bentires-Alj M, Lim RYH, *et al* (2012) The nanomechanical signature of breast cancer. *Nat Nanotechnol* 7: 757–765
- Prabhune M, Belge G, Dotzauer A, Bullerdiek J & Radmacher M (2012) Comparison of mechanical properties of normal and malignant thyroid cells. *Micron* 43: 1267–1272
- Prevedel R, Diz-muñoz A, Ruocco G & Antonacci G (2019) Brillouin microscopy: an emerging tool for mechanobiology. *Nat Methods* 16: 969–977
- Provenzano PP, Eliceiri KW, Campbell JM, Inman DR, White JG & Keely PJ (2006) Collagen reorganization at the tumor-stromal interface facilitates local invasion. *BMC Med* 4: 1–15
- Provenzano PP, Inman DR, Eliceiri KW, Knittel JG, Yan L, Rueden CT, White JG & Keely PJ (2008) Collagen density promotes mammary tumor initiation and progression. *BMC Med* 6: 1–15
- Pupa SM, Ménard S, Forti S & Tagliabue E (2002) New insights into the role of extracellular matrix

- during tumor onset and progression. *J Cell Physiol* 192: 259–267
- Puricelli L, Galluzzi M, Schulte C, Podestà A & Milani P (2015a) Nanomechanical and topographical imaging of living cells by atomic force microscopy with colloidal probes. *Rev Sci Instrum* 86: 1–18
- Radmacher M (2007) Studying the Mechanics of Cellular Processes by Atomic Force Microscopy. *Methods Cell Biol* 83: 347–372
- Raghu Kalluri RAW (2010) The basics of epithelial-mesenchymal transition. *J Clin Invest* To be subm: 1420–1428
- Ramos JR, Pabijan J, Garcia R & Lekka M (2014) The softening of human bladder cancer cells happens at an early stage of the malignancy process. *Beilstein J Nanotechnol* 5: 447–457
- Raposo G & Stoorvogel W (2013) Extracellular vesicles: Exosomes, microvesicles, and friends. *J Cell Biol* 200: 373–383
- Reiß S, Burau G, Stachs O, Guthoff R & Stolz H (2011) Spatially resolved Brillouin spectroscopy to determine the rheological properties of the eye lens. 2: 341–348
- Romani P, Valcarcel-Jimenez L, Frezza C & Dupont S (2021) Crosstalk between mechanotransduction and metabolism. *Nat Rev Mol Cell Biol* 22: 22–38
- Rouvière O, Melodelima C, Hoang Dinh A, Bratan F, Pagnoux G, Sanzalone T, Crouzet S, Colombel M, Mège-Lechevallier F & Souchon R (2017) Stiffness of benign and malignant prostate tissue measured by shear-wave elastography: a preliminary study. *Eur Radiol* 27: 1858–1866
- Royce PM, Camakaris J & Danks DM (1980) Reduced lysyl oxidase activity in skin fibroblasts from patients with Menkes' syndrome. *Biochem J* 192: 579–586
- Ryu S, Martino N, Kwok SJJ, Bernstein L & Yun S-H (2021) Label-free histological imaging of tissues using Brillouin light scattering contrast. *Biomed Opt Express* 12: 1437
- Sanli O, Dobruch J, Knowles MA, Burger M, Alemozaffar M, Nielsen ME & Lotan Y (2017b) Bladder cancer. *Nat Rev Dis Prim* 3: 1–19
- Scarcelli G, Polacheck WJ, Nia HT, Patel K, Grodzinsky AJ, Kamm RD & Yun SH (2015) Noncontact three-dimensional mapping of intracellular hydromechanical properties by Brillouin microscopy. *Nat Methods* 12: 1132–1134
- Schachar RA, Chan RW & Fu M (2011) Viscoelastic properties of fresh human lenses under 40 years of age: Implications for the aetiology of presbyopia. *Br J Ophthalmol* 95: 1010–1013

- Schillers H, Rianna C, Schäpe J, Luque T, Doschke H, Wälte M, Uriarte JJ, Campillo N, Michanetzis GPA, Bobrowska J, *et al* (2017) Standardized Nanomechanical Atomic Force Microscopy Procedure (SNAP) for Measuring Soft and Biological Samples. *Sci Rep* 7: 1–9
- Schneider A, Richert L, Francius G, Voegel JC & Picart C (2007) Elasticity, biodegradability and cell adhesive properties of chitosan/hyaluronan multilayer films. *Biomed Mater* 2
- Sergei Kusmartsev DIG (2006) Effect of tumor-derived cytokines and growth factors on differentiation and immune suppressive features of myeloid cells in cancer. *Cancer Metastasis* 25: 323–331
- Shellard A & Mayor R (2021) Durotaxis: The Hard Path from In Vitro to In Vivo. *Dev Cell* 56: 227–239
- Shen J, Xie Y, Liu Z, Zhang S, Wang Y, Jia L, Wang Y, Cai Z, Ma H & Xiang M (2018) Increased myocardial stiffness activates cardiac microvascular endothelial cell via VEGF paracrine signaling in cardiac hypertrophy. *J Mol Cell Cardiol* 122: 140–151
- Shen Y, Wang X, Lu J, Salfenmoser M, Wirsik NM, Schleussner N, Imle A, Freire Valls A, Radhakrishnan P, Liang J, *et al* (2020) Reduction of Liver Metastasis Stiffness Improves Response to Bevacizumab in Metastatic Colorectal Cancer. *Cancer Cell* 37: 800-817.e7
- Sherratt MJ (2009) Tissue elasticity and the ageing elastic fibre. *Age (Omaha)* 31: 305–325
- Shi Y, Glaser KJ, Venkatesh SK, Ben-Abraham EI & Ehman RL (2015) Feasibility of using 3D MR elastography to determine pancreatic stiffness in healthy volunteers. *J Magn Reson Imaging* 41: 369–375
- Spinelli AE, Bresolin A, Zuppone S, Perani L, Fallara G, Di Muzio N, Vago R, Fiorino C & Cozzarini C (2020) A non-invasive ultrasound imaging method to measure acute radiation-induced bladder wall thickening in rats. *Radiat Oncol* 15: 1–10
- Stegg PS (2006) Tumor metastasis: Mechanistic insights and clinical challenges. *Nat Med* 12: 895–904
- Swaminathan V, Mythreye K, Tim O'Brien E, Berchuck A, Blobe GC & Superfine R (2011) Mechanical Stiffness grades metastatic potential in patient tumor cells and in cancer cell lines. *Cancer Res* 71: 5075–5080
- Sylvester RJ, Brausi MA, Kirkels WJ, Hoeltl W, Calais Da Silva F, Powell PH, Prescott S, Kirkali Z, van de Beek C, Gorlia T, *et al* (2010) Long-Term Efficacy Results of EORTC Genito-Urinary Group Randomized Phase 3 Study 30911 Comparing Intravesical Instillations of

- Epirubicin, Bacillus Calmette-Guérin, and Bacillus Calmette-Guérin plus Isoniazid in Patients with Intermediate- and High-Risk . *Eur Urol* 57: 766–773
- Sylvester RJ, Van Der Meijden APM, Oosterlinck W, Witjes JA, Bouffoux C, Denis L, Newling DWW & Kurth K (2006) Predicting recurrence and progression in individual patients with stage Ta T1 bladder cancer using EORTC risk tables: A combined analysis of 2596 patients from seven EORTC trials. *Eur Urol* 49: 466–477
- Taljanovic MS, Gimber LH, Becker GW, Latt LD, Klauser AS, Melville DM, Gao L & Witte RS (2017) Shear-wave elastography: Basic physics and musculoskeletal applications. *Radiographics* 37: 855–870
- Thiery JP & Sleeman JP (2006) Complex networks orchestrate epithelial-mesenchymal transitions. *Nat Rev Mol Cell Biol* 7: 131–142
- Thomas A. Wynn LB (2010) Macrophages: master regulators of inflammation and fibrosis. *Semin Liver Dis* 30: 245–257
- Tian M, Li Y & Weiren Liu, Lei Jina, Xifei Jianga, Xinyan Wangd, Zhenbin Dinga, Yuanfei Penga, Jian Zhoua, b, Jia Fana, b, Yi Cao, Wei Wangc YS (2013) The Nanomechanical Signature of Liver Cancer Tissues and its Molecular Origin. *R Soc Chem* 20xx 47: 7634–7639
- Troyanova-Wood M, Meng Z & Yakovlev V V. (2019) Differentiating melanoma and healthy tissues based on elasticity-specific Brillouin microspectroscopy. *Biomed Opt Express* 10: 1774
- Tschumperlin DJ & Lagares D (2020) Mechano-therapeutics: Targeting Mechanical Signaling in Fibrosis and Tumor Stroma. *Pharmacol Ther* 212: 107575
- Tsvirkun D, Revilloud J, Giannetti A & Verdier C (2022) The intriguing role of collagen on the rheology of cancer cell spheroids. *J Biomech* 141: 111229
- Tuttle TG, Lujan HL, Tykocki NR, DiCarlo SE & Roccabianca S (2022) Remodeling of extracellular matrix in the urinary bladder of paraplegic rats results in increased compliance and delayed fiber recruitment 16 weeks after spinal cord injury. *Acta Biomater* 141: 280–289
- Tyson MD & Barocas DA (2017) Quality of Life After Radical Cystectomy. *Uro Clin N Am*
- Uriarte JJ, Meirelles T, Del Blanco DG, Nonaka PN, Campillo N, Sarri E, Navajas D, Egea G & Farré R (2016) Early impairment of lung mechanics in a murine model of marfan syndrome. *PLoS One* 11: 1–19
- Usukura E, Narita A, Yagi A, Sakai N, Uekusa Y, Imaoka Y, Ito S & Usukura J (2017) A Cryosectioning Technique for the Observation of Intracellular Structures and

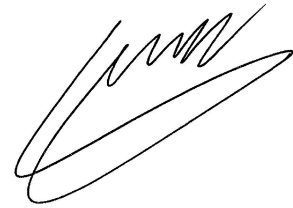
- Immunocytochemistry of Tissues in Atomic Force Microscopy (AFM). *Sci Rep* 7: 1–10
- Uvelius B, Persson L & Mattiasson A (1984) Smooth muscle cell hypertrophy and hyperplasia in the rat detrusor after short-time infravesical outflow obstruction. *J Urol* 131: 173–176
- Varinelli L, Guaglio M, Brich S, Zanutto S, Belfiore A, Zanardi F, Iannelli F, Oldani A, Costa E, Chighizola M, *et al* (2022) Decellularized Normal and Tumor Extracellular Matrix as Scaffold for Cancer Organoid Cultures of Colorectal Peritoneal Metastases Short title : Engineered 3D-models of the peritoneal metastatic niche Abstract. www.biorxiv.org
- Vartak D & Gemeinhart R (2007) Matrix metalloproteases: Underutilized targets for drug delivery. *J Drug Target* 15: 1–20
- Venugopal B, Mogha P, Dhawan J & Majumder A (2018) Cell density overrides the effect of substrate stiffness on human mesenchymal stem cells' morphology and proliferation. *Biomater Sci* 6: 1109–1119
- Véronique Masson, Laura Rodriguez de la Ballina, Carine Munaut, Ben Wielockx, Maud Jost, Catherine Maillard, Silvia Blacher, Khalid Bajou, Takeshi Itoh S & Itohara, Zena Werb, Claude Libert, Jean-Michel Foidart and AN (2005) Contribution of host MMP-2 and MMP-9 to promote tumor vascularization and invasion of malignant keratinocytes. *FASEB J* 19: 234–236
- Virues Delgado JO, Delorme S, El-Ayoubi R, DiRaddo R & Hatzikiriakos SG (2010) Effect of freezing on the passive mechanical properties of arterial samples. *J Biomed Sci Eng* 03: 645–652
- Volikova AI, Marshall BJ, Yin JMA, Goodwin R, Ee-Pan Chow P & Wise MJ (2019) Structural, biomechanical and hemodynamic assessment of the bladder wall in healthy subjects. *Res Reports Urol* 11: 233–245
- Wang TH, Hsia SM & Shieh TM (2017) Lysyl oxidase and the tumor microenvironment. *Int J Mol Sci* 18: 1–12
- Wei B, Zhou X, Liang C, Zheng X, Lei P, Fang J, Han X, Wang L, Qi C & Wei H (2017) Human colorectal cancer progression correlates with LOX-induced ECM stiffening. *Int J Biol Sci* 13: 1450–1457
- Wei C, Li C, Szewczyk-Bieda M, Upreti D, Lang S, Huang Z & Nabi G (2018) Performance Characteristics of Transrectal Shear Wave Elastography Imaging in the Evaluation of Clinically Localized Prostate Cancer: A Prospective Study. *J Urol* 200: 549–558

- Wei C, Zhang Y, Malik H, Zhang X, Alqahtani S, Upreti D, Szewczyk-Bieda M, Lang S & Nabi G (2019) Prediction of Postprostatectomy Biochemical Recurrence Using Quantitative Ultrasound Shear Wave Elastography Imaging. *Front Oncol* 9: 1–10
- Weigelin B, Bakker G-J & Friedl P (2012) Intravital third harmonic generation microscopy of collective melanoma cell invasion: Principles of interface guidance and microvesicle dynamics. *IntraVital* 1: 9–20
- Weis SM & Cheresch DA (2011) Tumor angiogenesis: Molecular pathways and therapeutic targets. *Nat Med* 17: 1359–1370
- Whitcott CJ, Diep CH, Jiang P, Watanabe A, Lobello J, Sima C, Hostetter G, Shepard HM & Hoff DD Von (2015) Desmoplasia in primary tumors and metastatic lesions of pancreatic cancer. *Clin Cancer Res* 21: 3561–3568
- Whitehead B, Wu LP, Hvam ML, Aslan H, Dong M, Dyrskjøt L, Ostensfeld MS, Moghimi SM & Howard KA (2015) Tumour exosomes display differential mechanical and complement activation properties dependent on malignant state: Implications in endothelial leakiness. *J Extracell Vesicles* 4: 1–11
- Whiteside TL (2017) Tumor-derived exosomes and their role in cancer progression. *Adv Clin Chem* 176: 139–148
- Wolf K, te Lindert M, Krause M, Alexander S, te Riet J, Willis AL, Hoffman RM, Figdor CG, Weiss SJ & Friedl P (2013) Physical limits of cell migration: Control by ECM space and nuclear deformation and tuning by proteolysis and traction force. *J Cell Biol* 201: 1069–1084
- Wolf K, Wu YI, Liu Y, Geiger J, Tam E, Overall C, Stack MS & Friedl P (2007) Multi-step pericellular proteolysis controls the transition from individual to collective cancer cell invasion. *Nat Cell Biol* 9: 893–904
- Woo S, Kim SY, Cho JY & Kim SH (2014) Shear wave elastography for detection of prostate cancer: A preliminary study. *Korean J Radiol* 15: 346–355
- Wu PH, Aroush DR Ben, Asnacios A, Chen WC, Dokukin ME, Doss BL, Durand-Smet P, Ekpenyong A, Guck J, Guz N V., *et al* (2018) A comparison of methods to assess cell mechanical properties. *Nat Methods* 15
- Wu PJ, Masouleh MI, Dini D, Paterson C, Török P, Overby DR KI (2019) Detection of proteoglycan loss from articular cartilage using Brillouin microscopy , with applications to osteoarthritis. 10: 2457–2466

- Xing Zhi Huang, Ai Yun Zhou, Min Wei Liu, Yan Zhang PX (2020) Shear wave elasticity differentiation between low- and high-grade bladder urothelial carcinoma and correlation with collagen fiber content. *Am Inst Ultrasound Med*: 40:113-122
- Yang Y, Zhao X, Shi J & Huang Y (2019) Value of shear wave elastography for diagnosis of primary prostate cancer: A systematic review and meta-analysis. *Med Ultrason* 21: 382–388
- Yavuz A, Yokus A, Taken K, Batur A, Ozigokce M & Arslan H (2018) Reliability of testicular stiffness quantification using shear wave elastography in predicting male fertility: A preliminary prospective study. *Med Ultrason* 20: 141–147
- Yaxin Guo, Xiang Ji, Jinbo Liu, Dandan Fan, Quanbo Zhou, Chen Chen, Weiwei Wang, Guixian Wang, Haijiang Wang, Weitang Yuan, Zhenyu Ji ZS (2019) Effects of exosomes on the Pre-metastatic Niche Formation in Tumors. *Mol Cancer* 8: 1–11
- Ye M, Song Y, Pan S, Chu M, Wang ZW & Zhu X (2020) Evolving roles of lysyl oxidase family in tumorigenesis and cancer therapy. *Pharmacol Ther* 215: 107633
- Yoo L, Gupta V, Lee C, Kavehpore P & Demer JL (2011) Viscoelastic properties of bovine orbital connective tissue and fat: Constitutive models. *Biomech Model Mechanobiol* 10: 901–914
- Yoshida K, Tsuda M, Matsumoto R, Semba S, Wang L, Sugino H, Tanino M, Kondo T, Tanabe K & Tanaka S (2019) Exosomes containing ErbB2/CRK induce vascular growth in premetastatic niches and promote metastasis of bladder cancer. *Cancer Sci* 110: 2119–2132
- Yu Q & Stamenkovic I (2000) Cell surface-localized matrix metalloproteinase-9 proteolytically activates TGF- β and promotes tumor invasion and angiogenesis. *Genes Dev* 14: 163–176
- Zemła J, Danilkiewicz J, Orzechowska B, Pabijan J, Seweryn S & Lekka M (2018a) Atomic force microscopy as a tool for assessing the cellular elasticity and adhesiveness to identify cancer cells and tissues. *Semin Cell Dev Biol* 73: 115–124
- Zemła J, Stachura T, Gross-Sondej I, Górka K, Okoń K, Pyka-Fościk G, Soja J, Sładek K & Lekka M (2018b) AFM-based nanomechanical characterization of bronchoscopic samples in asthma patients. *J Mol Recognit* 31: 1–9
- Zhang J & Reinhart-King CA (2020) Targeting Tissue Stiffness in Metastasis: Mechanomedicine Improves Cancer Therapy. *Cancer Cell* 37: 754–755
- Zhu H, Chen H, Wang J, Zhou L & Liu S (2019) Collagen stiffness promoted non-muscle-invasive bladder cancer progression to muscle-invasive bladder cancer. *Oncotargets Ther* 12: 3441–3457

Zwaans BMM, Grobbel M, Carabulea AL, Lamb LE & Roccabianca S (2022) Increased extracellular matrix stiffness accompanies compromised bladder function in a murine model of radiation cystitis. *Acta Biomater* 144: 221–229

Zwaans BMM, Wegner KA, Bartolone SN, Vezina CM, Chancellor MB & Lamb LE (2020) Radiation cystitis modeling: A comparative study of bladder fibrosis radio-sensitivity in C57BL/6, C3H, and BALB/c mice. *Physiol Rep* 8: 1–14

A handwritten signature in black ink, consisting of several overlapping loops and a final flourish.